GEOPHYSICAL STUDIES OF BADIN BLOCK, LOWER INDUS BASIN, PAKISTAN

MAHMOOD SULTAN

01-262162-006

A thesis is submitted in the fulfillment of the

requirements for the award of the degree of

Master of Science (Geophysics)

Department of Earth and Environmental Sciences

Bahria University, Islamabad

2020

APPROVAL FOR EXAMINATION

Scholar's Name: Mahmood Sultan

Enrollment No. 01-262162-006

Programme of Study: MS (Geophysics)

Thesis Title: **Geophysical Studies Of Badin Block, Lower Indus Basin, Pakistan**

It is to certify that the above scholar's thesis has been completed to my satisfaction and, to my belief, its standard is appropriate for submission for examination. I have also conducted plagiarism test of this thesis using HEC prescribed software and found similarity index 14 % that is within the permissible limit set by the HEC for the PhD degree thesis. I have also found the thesis in a format recognized by the BU for the PhD thesis.

Principal Supervisor's Signature: _____

Date: _____

Name: Dr. Muhammad Fahad Mahmood

AUTHOR'S DECLARATION

I, Mahmood Sultan hereby state that my PhD thesis titled "**Geophysical Studies Of Badin Block, Lower Indus Basin, Pakistan** " is my own work and has not been submitted previously by me for taking any degree from Bahria University, Islamabad Campus, Islamabad or anywhere else in the country/world.

At any time if my statement is found to be incorrect even after my graduation, the University has the right to withdraw/cancel my PhD degree.

Name of scholar: Mahmood Sultan

Date: _____

PLAGIARISM UNDERTAKING

I, solemnly declare that research work presented in the thesis titled "**Geophysical Studies Of Badin Block, Lower Indus Basin, Pakistan**" is solely my research work with no significant contribution from any other person. Small contribution / help wherever taken has been duly acknowledged and that complete thesis has been written by me.

I understand the zero tolerance policy of the HEC and Bahria University towards plagiarism. Therefore I as an Author of the above titled thesis declare that no portion of my thesis has been plagiarized and any material used as reference is properly referred / cited.

I undertake that if I am found guilty of any formal plagiarism in the above titled thesis even after award of MS degree, the university reserves the right to withdraw / revoke my MS degree and that HEC and the University has the right to publish my name on the HEC / University website on which names of scholars are placed who submitted plagiarized thesis.

Scholar / Author's Sign: _____

Name of the Scholar: Mahmood Sultan

ACKNOWLEDGEMENTS

First of all, I would like to offer my gratitude to my supervisor, Dr. M. Fahad Mahmood (Assistant Professor, Department of Earth & Environment Studies, Bahria University, Islamabad) for his advice and support throughout the work and help in the analysis. My sincere appreciation goes to Dr. Fahad Mahmood, Mr. Muhammad Maqsood (Consultant, Geophysics) and Dr. Farhan Javed (ICTP, Italy) for their great technical knowledge, guidance, suggestions and idea to complete my thesis. The Department of Earth and Environmental Sciences, Bahria University, Islamabad campus has provided the support, I have needed to complete my thesis. Last but not least, I am thankful to my parents and my wife for the inspirations, motivation and support to study and to continue acquiring knowledge after long break.

ABSTRACT

The Lower Indus Basin is one of the best case studies of extensional tectonic regime of Pakistan with respect to the structural and sedimentary architecture. The Sembar Formation is source in the study area. The producing reservoir in Badin block is Lower Goru Formation. Upper Goru Formation is cap rock in the study area. The Lower Goru Formation in particular is important for seismic and well log interpretation and cover most of the basin. Badin block is one of the important block in Lower Indus Basin because of number of discoveries associated with this block. Four main reflectors (Khadro, Upper Goru, Lower Goru and Sembar formations) had been interpreted using 2D seismic reflection data in order to investigate in detail the normal fault system with horst and graben architecture. Therefore, extensional normal fault system is considered a key control on the geological structures and sedimentary architecture of the Lower Indus Basin as presently seen. Seismic attributes were applied on 2D seismic line GPK-92-1686 for character identification of Sembar Formation. Petrophysics and rock physics studies are carried out for Sember Formation for source rock characteristics analysis. Total organic carbon analysis also showed the Sembar Formation source rock potential characteristics for shale gas. The crustal deformation phenomenon of subsidence was observed through the application of Interferometric Synthetic Aperture Radar technique. It demarcated the continual of subsidence in 4mm/yr with over pumping of hydrocarbons in the area of study.

TABLE OF CONTENTS

LIST OF TABLES

LIST OF FIGURES

CHAPTER 1

INTRODUCTION

This research project is carried out for the different geophysical applications over the area of Badin Block of Lower Indus Basin, Pakistan. The objective of this geophysical study is to highlight the geological features of Sembar Formation, its characteristics and its potential as source rock for shale gas. Along with this surface crustal deformation studies are carried out.

The focus of study is structural modeling of the area. Lower Indus Basin has extensional structural trend with normal faulting and horst and graben structures. This structure is to be modeled from six 2D seismic line data. Seismic data is the worth base of information as it makes available broad area study as compare to wireline logs and core data. Although it present meandering information with less resolution but it is commonly utilized for subsurface modeling. Integration of geophysical data is shaping the industry standard performing for reservoir classification for validity and reliability of results. Each class of data has its own distinctiveness in provisions of its accuracy, coverage, scale and the degree of significance. Therefore, other tools are also applied, which include attribute analysis on 2D seismic line GPK-92-1686 to study Sembar Formation characteristics, because, seismic attributes are commanding aide to seismic interpretation. They present information to interpret faults, distinguish the depositional settings, and geological lithology classification for validation of seismic model.

Petrophysical studies are quite close to realness of rock characteristics. For demarcation of Sembar Formation properties the petrophysical studies are carried out. Particularly, for shale gas probable of Sembar Formation Passey technique is opted. Therefore, this study is an incorporated investigation of seismic interpretation, rock physics, shale gas identification and seismic attributes analysis (spectral decomposition, instantaneous frequency, instantaneous phase etc) for identification of

Sembar Formation characteristics in Badin block. One well i.e. Raj-01 depicted the shale gas potential while other two well i.e., Raj East-01 and Nereri-01 have organic carbon immaturity for unconventional shale gas production according to results obtained through Passey method.

Lower Indus Basin is one of major hydrocarbon source for Pakistan hydrocarbon reserves. Due to over exploitation and pumping the area is facing the crustal deformation i.e. subsidence phenomenon. This is continuous process and can cause the enduring loss of porosity and permeability of subsurface. If the balance in hydrocarbon extraction and recharge of reservoir from source is practiced, this will mitigate this subsidence. The surface subsidence is measured with application of Interferometric Synthetic Aperture Radar technique. From this technique subsidence rate of 4mm per year is found.

1.1.Introduction to the study area

Area for study is located in the Badin district, Sindh, southern part of Pakistan. It is positioned in the southwestern periphery of the subcontinent plate, i.e. lower indus basin. It was part of the supercontinent Gondwana during the Permian to Middle Jurassic times, it passed through multiple phases of extension culminating during the separation of the subcontinent plate in the Late Jurassic to Early Cretaceous (Ahmad et al., 2014; Robison et al., 1999; Zaigham and Mallick, 2000). Disjointing of the Madagascar in the Late Cretaceous to Paleogene led to further extension and the development of conventional structural traps which have been the focus of petroleum exploration (Naeem et al., 2016). The petroleum source and reservoir rocks of the Sembar and Lower Goru formations were deposited along the west-facing passive margin during the Early Cretaceous. At the beginning of Eocene, the subcontinent plate collided with Eurasia plate as a result, Kirthar fold belt was formed along with adjacent foreland basin .

Geographically, Badin block is bordered in the Hyderabad district north, in the east by Tharparkar districts, whereas Thatta district is adjacent in its west side and Arabian Sea in its southern side as in figure. 1.

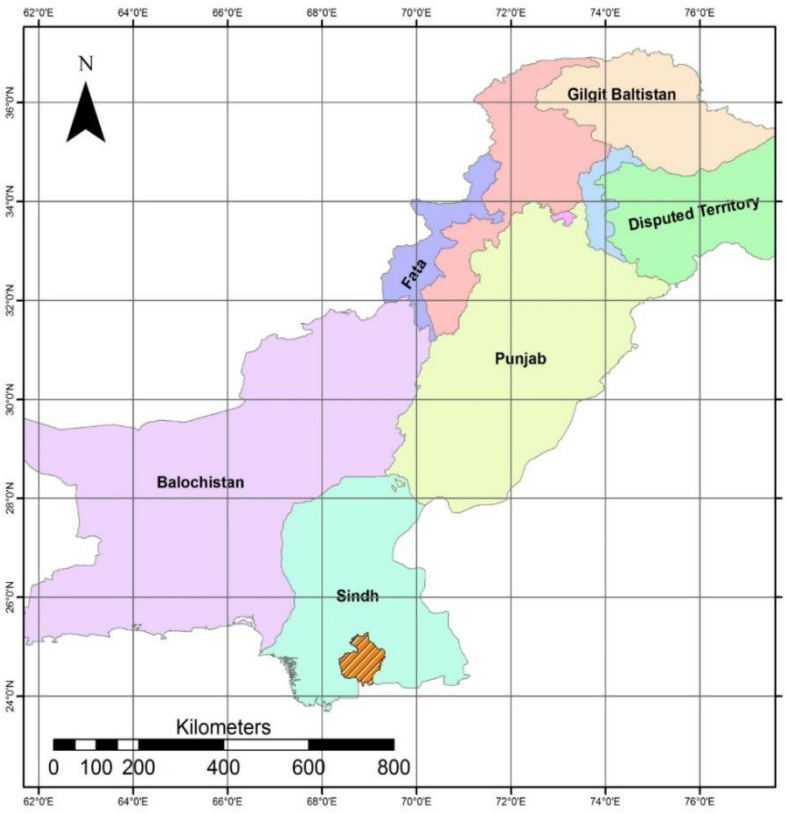

Figure 1.1 Geographical location of study area (Mozaffar et al., 2002).

1.2. Objectives

Following are the objective of this geophysical study

1) To interpret the sub-surface structure of the study area using 2D seismic data.
2) Seismic attributes study of Sembar Formation
3) Petrophysical studies of Sembar Formation.
4) Sembar Formation potential as source rock for shale gas with application of Passey method.
5) Surface crustal deformation studies with InSAR technique.

1.3. Data Set

1) Six 2D seismic line data.
2) Well logs of three wells which include Raj-01, Raj East-01 and Nereri-01.
3) ENVISAT satellite InSAR data down loaded from European Space Agency site.

1.4 Base map of the study area

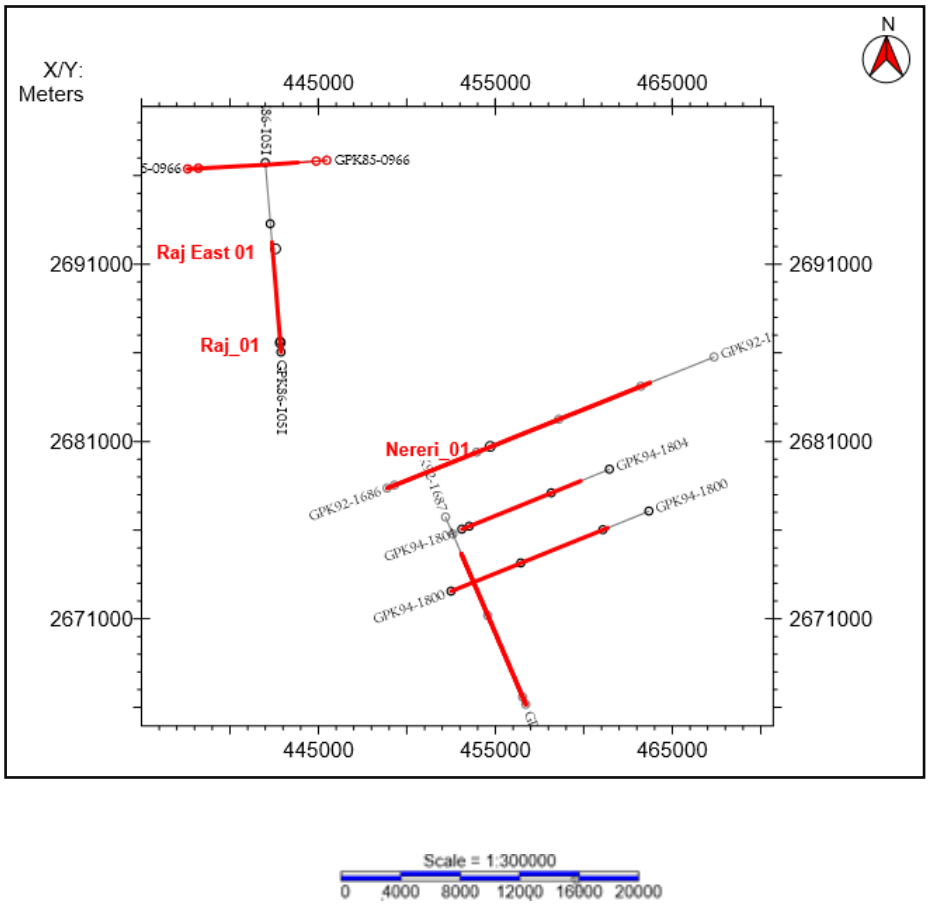

Figure 1.2 Base map of study area.

CHAPTER 2

GEOLOGY OF THE STUDY AREA

2.1 Tectonic setting and geology

Tectonic evolution of the Indus Basin starts along the rifting and breakup of Gondwana in Middle Jurassic (approximately 166 ma). Indian Plate drifting apart Gondwanaland (Jurassic or Early Cretaceous) possibly generated tectonic episodes shaping the tectonic structure in the Badin. Beginning of Cretaceous is responsible for NE-SW to N-S drifting systems, isostatic uplift at the margins of the newly formed ocean probable sourced uplift and eastwards tilting. The partitioning of Madagascar and Indian plates in the Middle to Late Cretaceous is the probably basis for sinistral strike-slip faulting. Early to Middle Cretaceous time, the Lower Goru and Upper Goru formations syn-rift and post rift depositions are progressed. It is obserable from existence of thin Upper Goru Formation on the top of the horst blocks whereas it thickens in the graben blocks. The faults direction in the study area are NW-SE, the main play is due to the extensional rifting with some strike slip movement (Zaigham and Mallick, 2000).

Due to extensional tectonics tilted fault blocks traps hydrocarbons are formed. In Early Cretaceous the deposition of organic rich Sembar Formation was formed. Rifting was continued at that time. Structural traps in the block are the result of constant drifting (Ahmad et al., 2014; Bannert and Raza, 1992).

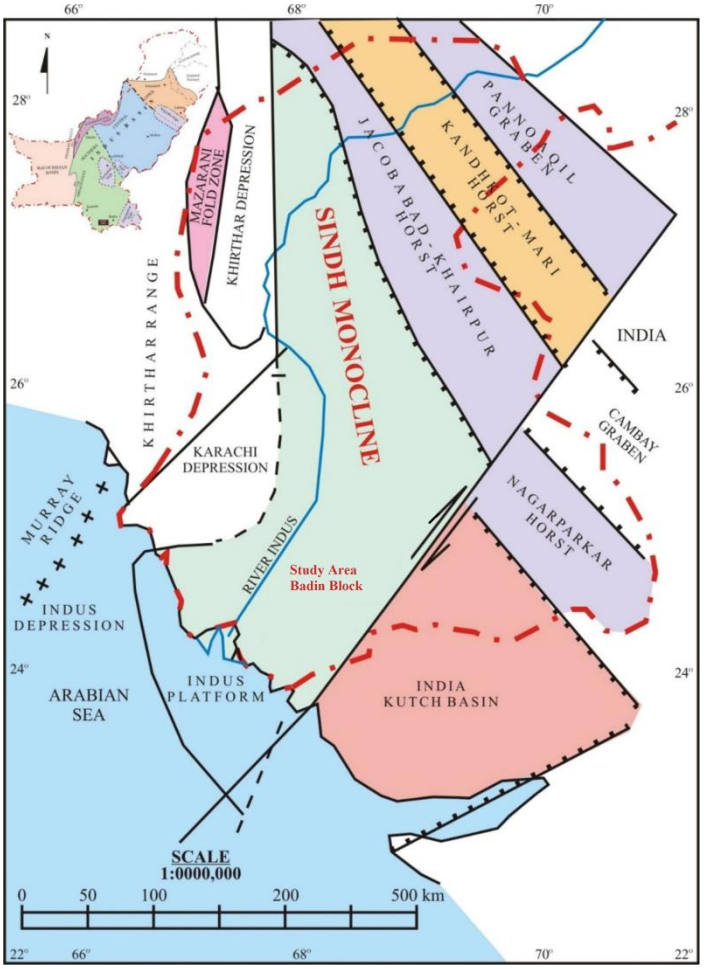

Figure 2.1 Generalized tectonic map (Raza et al., 1990).

2.2 Stratigraphy

The generalized stratigraphy of the Badin block is shown figure 2.3. which is displaying the distribution, age and lithology of the study area.

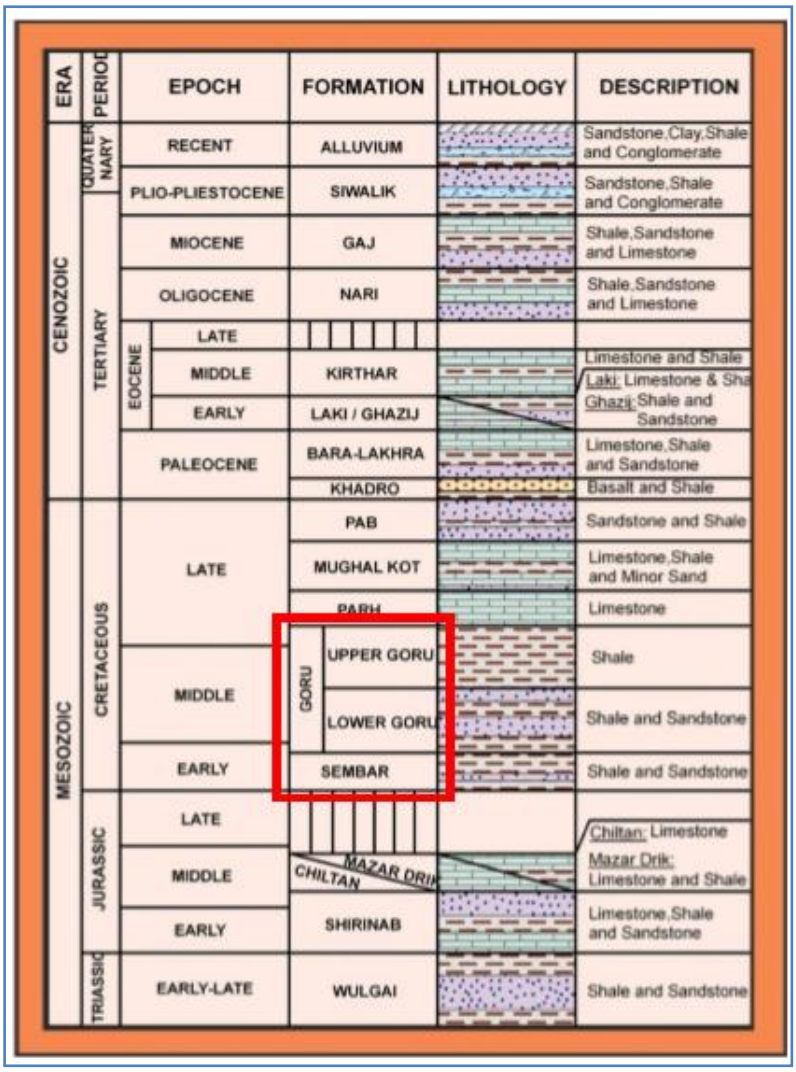

Figure 2.2 Generalized stratigraphic sequence of Southern Indus Basin (Raza et al., 1990).

The stratigraphic succession of the study area is as follows

2.2.1 Chiltan Formation

The oldest formation penetrated in Badin is the Jurassic Chiltan Formation (Alam et al., 2002). It consists of Limestone, which is enormous, thick bedded, and dark in color. It was deposited on a wide carbonate shelf on the Pangean supercontinent prior to rift and drift of the Indian plate in the Late Jurassic. Its contact with the Sembar Formation is gradational in the Lower Indus Basin representing the unconformity (Sheikh et al., 2002).

2.2.2 Sembar Formation

It consists of black shale with interbeded siltstone, argillaceous limestone with glauconite which is of greenish color. It is also of Cretaceous age, with deep marine environment of deposition (Memon et al., 1999; Alam et al., 2002).

2.2.3 Lower Goru Formation

It is of early Cretaceous age and consists of interbeds of limestone, siltstone and shale. Deposition setting is shelf to shallow marine. Its sand act as reservoir for the area. Therefore, it is the main reservoir rock within the block and it overlies the Sembar Formation (Alam et al., 2002).

2.2.4 Upper Goru Formation

The Upper Goru Formation composes of marl and calcareous claystone sporadically with inter bedded of silt and limestone. (Alam et al., 2002). The lithology color changes from black to grey and rarely maroon. The depositional environment is marine (Memon et al., 1999).

2.2.5 Parh Formation

The Parh Formation is primarily limestone. Typically, it is hard, thin to medium bedded. Color changes from light grey to white, cream, and at different places olive green. Intercalations of calcareous shale and marl are also exit. The depositional setting is shallow to deep marine (Memon et al., 1999).

2.2.6 Mughal Kot Formation

It compose of light grey calcareous sandstone and is underlain by calcareous claystone and sandy limestone. The limestone is grey and argillaceous (Cheema et al., 1977).

2.2.7 Pab Formation

The Pab Formation compose of quartzose sandstone mainly medium to coarse grained. Color changes from white, cream or brown, while yellow brown weathered color thick bedded to massive. The depositional setting is fluvio-deltaic to shelf marine environment (Cheema et al., 1977).

2.2.8 Ranikot Formation

The Ranikot Formation largely composes of sandstone and shale. Medium to coarse grained sandstone is present with shape of sub angular to sub rounded. Color changes from light grey, white, and translucent. Shale is light to dark grey, slightly calcareous. The depositional setting is shallow marine (Cheema et al., 1977).

2.2.9 Laki Formation

Laki Formation was proposed as part of Kirthar series (Blanford, 1876). Later Hunting Survey Corporation (1960), redefine unit as Laki group and divided into two groups. Basal member named Sohnari and upper as Meting limestone and shale (Jones, 1960). It consists of mainly cream colored to grey limestone, chalk and calcareous shale (Memon et al., 1999). Laki Formation is comprised of the alluvial fans also contains clastic sediments of marl, with subordinate sandstone and conglomerate (Nabi et al., 2018). It is early Eocene age (Kureshy, 1984). It is unconformable by underlained Ranikot group (Paleoacene) and upper conformable with Kirthar Formation (Kureshy, 1984).

2.2.10 Kirthar Formation

It constitutes of intercalation limestone and shale having slight marl. The limestone sorts by light grey, cream colored or chalky white. It is thick bedded to enormous, plentifully fossiliferous. The depositional setting is shelf to shallow aquatic (Cheema et al., 1977).

2.3 Petroleum system

Exploration target in Badin area lies between Sembar-Goru play, (Wandrey et al., 2004). The Lower Goru Formation sand is the major reservoirs and Sembar Formation is considered as the source rock as shown in figure 2.3.

2.3.1 Source

The established primary source rocks in Lower Indus Basin Sembar Formation, which is organic rich shales (Zaigham and Mallick, 2000). The age of Sembar Formation is Early Cretaceous. Due to major composition of organic matter, oil and gas prone kerogen (type 2 and 3) and ample thermal maturity this shale is

considered as source rock in Badin block. It's composition is of siltstone and shale (Zaigham and Mallick, 2000). The average thickness of Sembar Formation is 610m.

2.3.2 Reservoir

Lower Goru Formation Cretaceous age sands, which over lies the Sembar Formation are the major reservoir of the region (Kazmi and Jan, 1997).

2.3.3 Seal

In Lower Indus Basin Upper Goru Formation is composes of impervious marls and calcareous clay stone with interstratified silt and limestone considered as cap rockl (Zaigham and Mallick, 2000; Wandrey et al., 2004).

2.3.4 Trapping mechanism

The tilted normal fault blocks provide the trapping mechanism in the Badin block. In the study area, horst structures act as traps for hydrocarbon accumulation. These traps were developed during Late Cretaceous and Early Paleocene rift phase (Shah, 2009; Wandrey et al., 2004).

2.3.5 Migration pathway

From the Sembar Formation source rock, hydrocarbon migrate and charge the reservoir through normal faults present within the area, provide career medium to the Lower Goru Formation (Ahmad et al., 2014).

2.3.6 Overburden rocks

The Tertiary sequence i.e. Ranikot group, Laki, Kirther and recent clastics of Nari, and Gaj formations formed the overloaded pressure (Ahmad et al., 2014).

2.3.7 Geothermal gradient

The geothermal gradient in the region ranges from 2.0 c/100m to 4.0 c/100m (Khan and Raza, 1986). The gas window is in the range of 2625m to 5250m, compatible with depth range of Sembar and Lower Goru Formation.

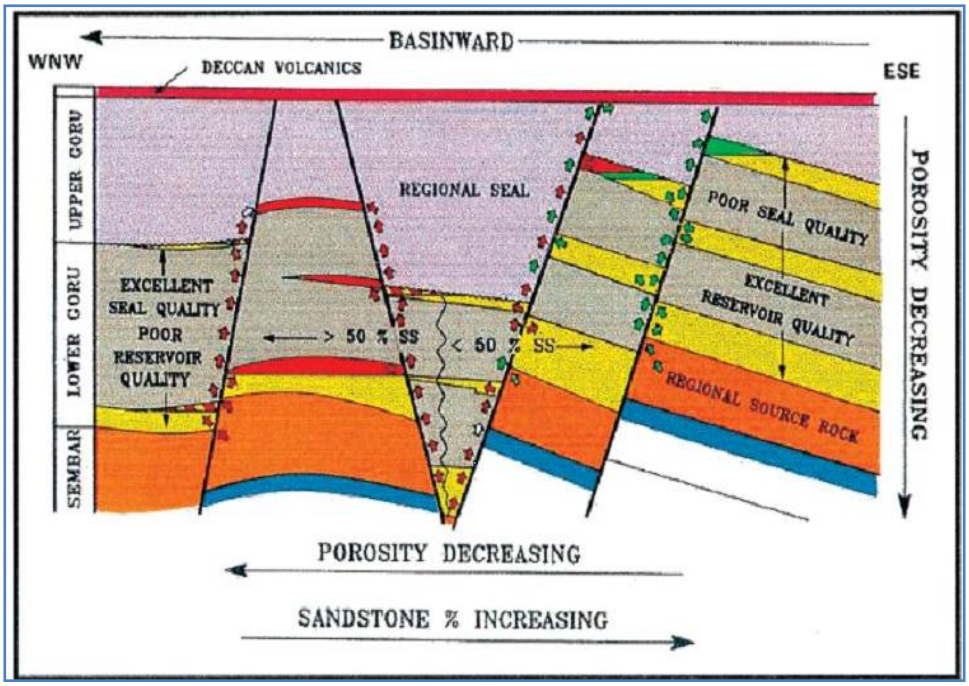

Figure 2.3. Petroleum system of Badin block, southern Indus basin (Alam et al., 2002).

CHAPTER 3

SEISMIC DATA INTERPRETATION

3.1 Introduction

Structural Interpretation of 2D seismic data of Badin block was carried out for the study of geological structural trends of the subsurface. Total six 2D seismic lines and well logs data of three wells were utilized in the study. Horizons of the four formations i.e. Khadro, Upper Goru, Lower Goru and Sembar formations were picked by identifying their character with the help of synthetic seismogram. The faults were also demarcated by identifying the structural trends and discontinuities. The demarcated fault trend revealed the normal faulting in the area of interest. The fault polygons were also generated. Time structure maps and depth maps were produced to identify the structures, especially the faults in the study area. The extensional regime structural trend was modeled with normal faulting with horst and graben structural geometry.

Seismic interpretation involves picking and tracking laterally continuing horizons to study subsurface structural architecture. *Therefore, t*he transformation of seismic data into geological information is the core objective of the seismic interpretation. The reflectors or horizons are marked according to changes in acoustic impedance (AI) across the boundaries. Greater is the amplitude of reflection when there is a greater contrast in the acoustic impedance. In seismic data interpretation, important objective is to distinguish formations on the basis of reflection, which may be lithological or structural. Well data and known geology of the area is correlated with the seismic data to achieve this purpose. There are two methods for seismic data interpretation which are stratigraphic interpretation and structural interpretation. In current study, structural interpretation technique is opted. Corrections, time-depth conversion and time-depth maps the seismic to well tie and structural interpretation are the main processes for the transformation of seismic reflection data into a

structural image. This interpretation and integrating with the available geological information can give a picture closer to the real (Dobrin and Savit, 1988). The more refined 2D seismic images were interpreted to permit closer insight for this geophysical study of area.

The structural interpretation was carried out on 2D seismic data of Badin area. The primary structure of area of interest is of extensional nature due to rifting phases experienced by the subcontinent plate during Cretaceous episode. Therefore, normal faulting and horst and graben geological structures because of extensional tectonics during Cretaceous time are present in the study area. Grabens are main sites for generation of hydrocarbons. The grabens with normal faults generate the trapping mechanism in the lower indus basin. Six 2D seismic lines with three wells are utilized for this study. These seismic lines along with wells are displayed in fig. 3.1. Seismic reflectors, displaying Cretaceous and older layers, are resulted by a normal dipping faults system. Contour maps present faults with northwest to southeast drift in the area of study.

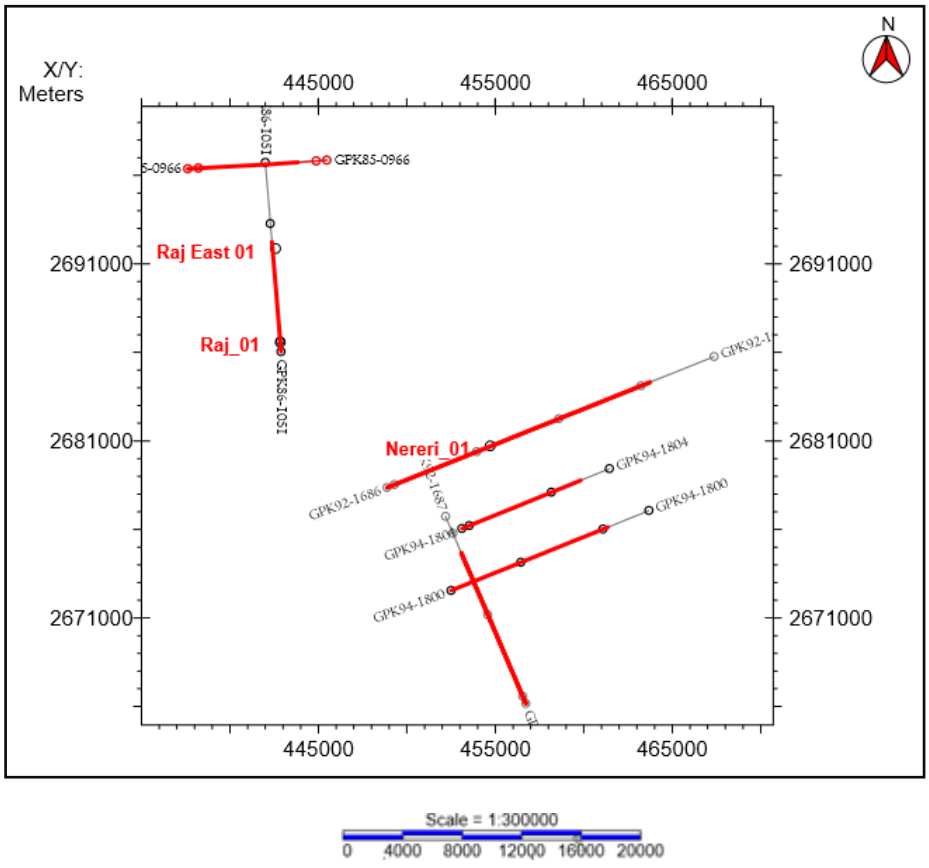

Figure 3.1 Base Map of the Study Area.

3.2 Methodology

The core task in the interpretational analysis was to identify horizons. This step involved the subsurface structural interpretation of the study area. For this study, the published geophysical and geological work of Badin was also utilized to understand subsurface geological trends. Data of Six 2D seismic lines and three wells are loaded in the project generated in the Kingdom software and basemap is generated as displayed in figure 3.1. The adopted methodology is displayed in figure 3.2. The well logs data is utilized to perform seismic to well tie utilizing synthetic seismogram. The well tops correlated with the synthetic seismogram. Synthetic seismogram is the tool utilized for horizon identification and for correlating deep bore well data to that of seismic data in time. The synthetic seismogram is generated by utilizing sonic log velocity data and density data from density log. Synthetic seismograms from wells data are generated as the initial stage of interpretation. Total four horizons have been marked after confirming well tops with synthetic seismogram. These were named as R1 of Khadro Formation, R2 as Upper Goru Formation, R3 as Lower Goru Formation and R4 as Sembar Formation. Interpretation is carried out after marking of horizons and fault identification by examining the discontinuity in the wavelets. Therefore, faults are picked on dip lines. All the major faults are demarcated and assigned a specified color in order to correlate fault and generation of fault polygons for mapping. After fault demarcation, the second step is marking of horizons on all seismic sections. The horizons are picked on seismic lines after removing all the misties. The horizon picking is based on event correlation because only two lines are intersecting from data provided. The value of mistie is <5 milliseconds, which is adjusted. Because the events representing the same subsurface point must tie at intersecting lines. The main objective of tying seismic lines is to develop relationship between the traces in subsurface on seismic lines and other is having better control over the area under study.

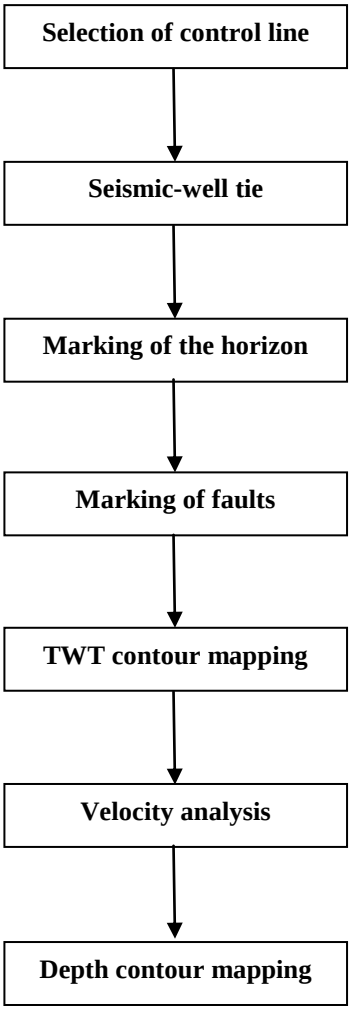

Figure 3.2 2D Seismic interpretation steps.

3.3 Analysis and Discussion

Extensional tectonic environment is present in Badin area that resulted in formation of horst and graben structures with normal faulting. Although the main horizon of interest is Sembar Formation. Upper Goru, Lower Goru and Khadro formations are also demarcated for the modeling of the subsurface structural trends of Badin block. It is found that Lower Goru Formation had almost same variations as present at the level of formation.

Faults were demarcated on the dip lines and linked across the strike lines for tectonic structure mapping throughout the area. Interpreted main faults were F1, F2, F3, F4, F5 and F6 were marked. F2 and F3 are forming the horst structure on the dip lines. This seismic interpretation confirms horst and graben geometry in the study

area. Faults are dipping in north-west and south-east direction. Two way time (TWT) maps are developed utilising time values and correlated fault polygons for presenting the structural inclination at different levels. Velocity versus depth values are plotted, where we have the depth and velocities of Khadro, Upper Goru, Lower Goru and Sembar formations are demarcated 630m, 760m, 1550m 2800m and 2180m/s, 2350m/s, 2800m/s, 3600m/s respectively as in Fig. 3.14. Depth contour maps of all four horizons of interest are prepared.

First step is generation of synthetic seismogram for Badin block. For synthetic seismogram generation, sonic and density logs from well data are utilized to produce the acoustic impedance in shape of reflection coefficient. Wavelet is extracted from seismic traces and T-D chart is prepared by utilizing velocity functions. Source wavelet is convolved with the reflection coefficients to form a synthetic seismogram of Raj-01 well as shown in figure 3.3. This synthetic seismogram is evaulated with the real seismic trace of line number --.

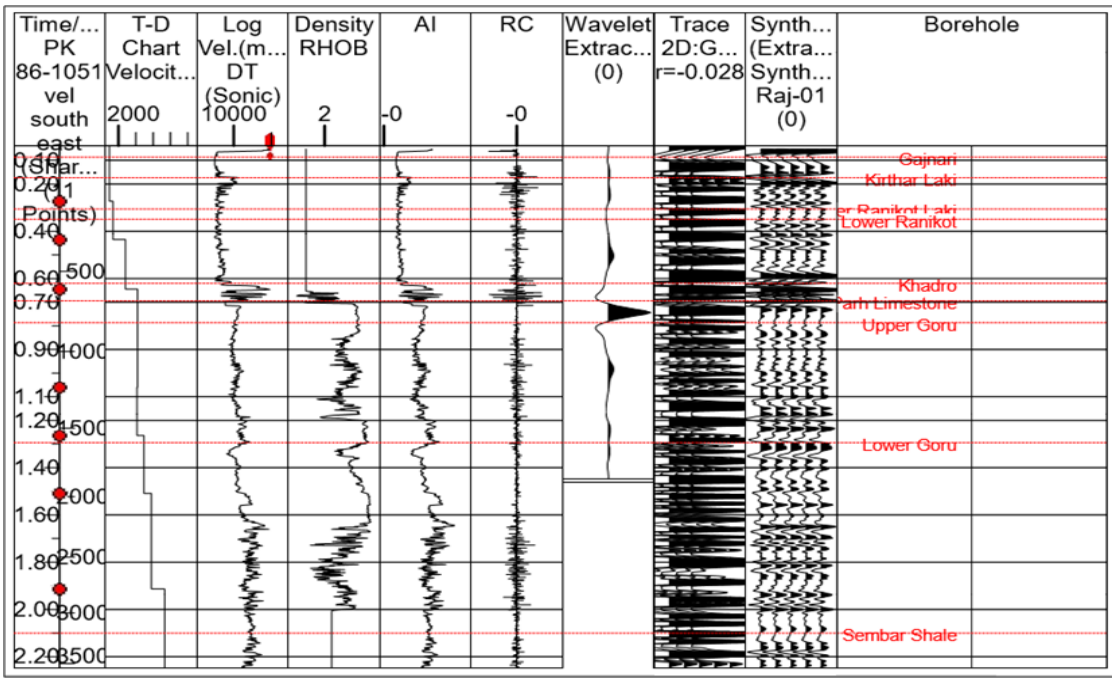

Figure 3.3 Synthetic seismogram of Raj-01 well.

Total four horizons are Interpreted with marking on peak, which are as

1. Horizon 1 : Khadro Formation shown by yellow color
2. Horizon 2 : Upper Goru Formation shown by green color
3. Horizon 3 : Lower Goru Formation by blue color
4. Horizon 4 : Sembar Formation shown by magenta pink color

The 2D seismic sections of have been interpreted and horizons of interested are marked, that is Khadro, Upper Goru, Lower Goru and Sembar formations, to delineate the extent and structural trends. These horizons on other seismic lines are marked on the basis of event correlation technique with respect to seismic line GPK92-1686, as shown in figure 3.4. Each reflector is demarcated with unique color so that they can be easily identified. By using the faults and horizons information structural trend model for the study area is developed.

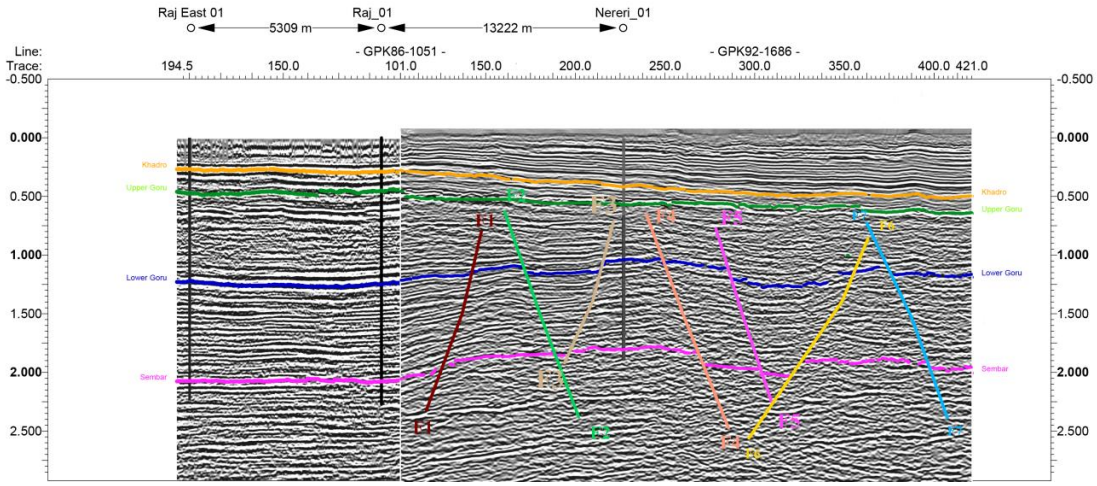

Figure 3.4 Event correlation based demarking of seismic horizons.

Faults are also marked and correlated along all the seismic sections. Khadro Formation had no indication of faults. The magnitude of extensional forces at the time of deposition of Khadro Formation was weaken and resulted in the generation of minor faults which are not visible as seismic section due to limited seismic resolution. Interpretation below the level of Khadro Formation indicated tilted fault blocks, normal faults north-south direction with significant throw, producing the horst and

graben structures. All these events correlated with the regional geology of the area which indicates the authenticity of the interpretation. The faults are characteristically demarcated at the break in continuity of the reflectors. Six normal faults F1, F2, F3, F4, F5 and F6 were demarcated at the breaks in the continuity of reflectors. The faults are dipping in north south direction. The negative flower structure has been developed because of normal faulting. Fault linked structural closures are source for trapping and transportation of hydrocarbon in the reservoir rocks.

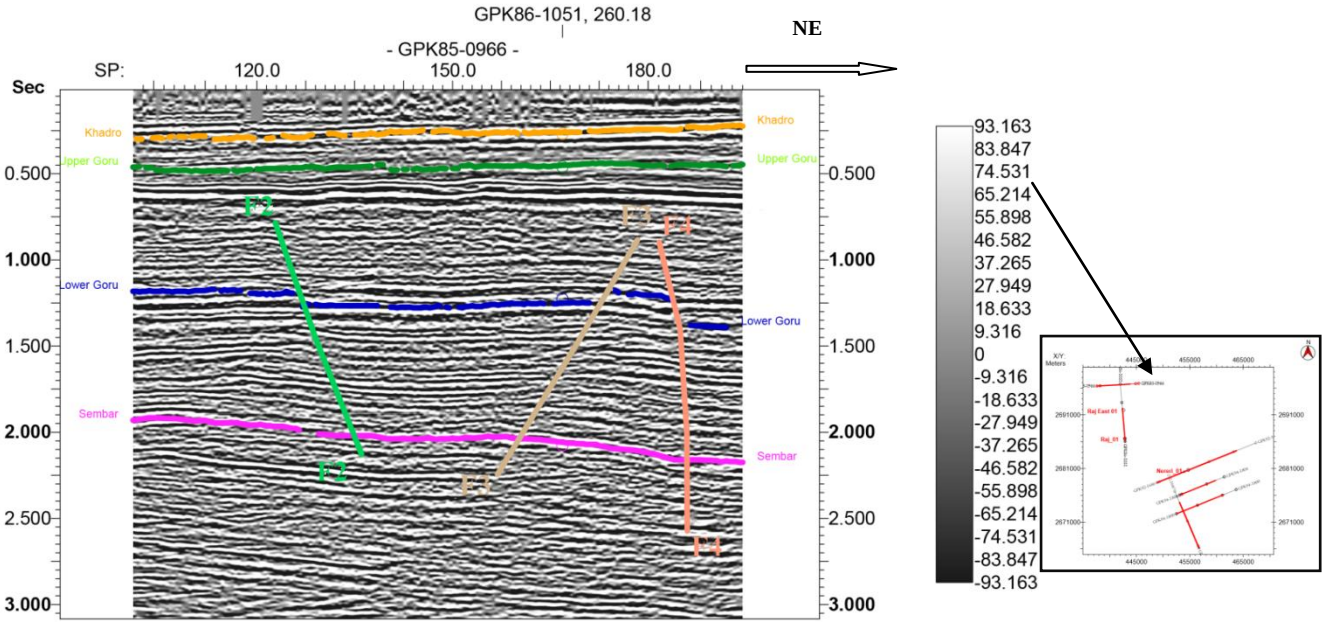

Figure 3.5 Interpreted seismic line GPK85-966.

The interpretation of line GPK-85-966 is shown in Fig. 3.4. The events on this line are marked on the basis of event correlation technique. The Khadro and Upper Goru formations have a continues trend with little or no deformation. While the structural faults are present at Lower Goru and Sembar formations. The faults are marked on this seismic line, which are normal faults in nature. These normal faults are basis for the formation of horst and graben structure at lower Goru and Sembar formations level. These normal faults generate from Sembar Formation. Significant throw of normal faults are observed at Lower Goru Formation level.

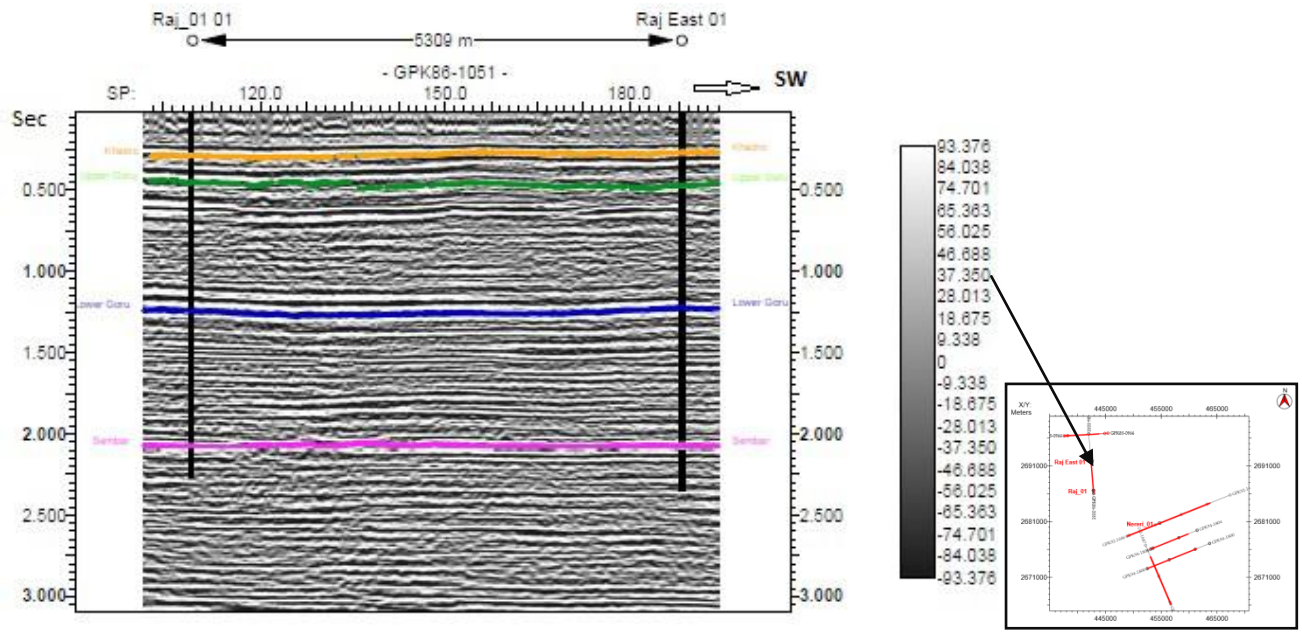

Figure 3.6 Interpreted seismic line GPK86-1051.

The interpreted strike line is shown in Fig 3.5. No structural deformation is present at Khadro and Upper Goru formations level. Slight structural deformation can be observed at Lower Goru and Sembar formations level, while formations are of horst and graben structures.

The structural interpretation of all dip lines shows the extensional tectonics with the formation of horst and graben structures. These horst and graben structures are trending in north south direction. No structural deformation is present at Khadro Formation level. The structural closures are present at the level of Lower Goru and Sembar formations due to the bounding faults. These fault bounded traps are responsible for hydrocarbon accumulation in the study area.

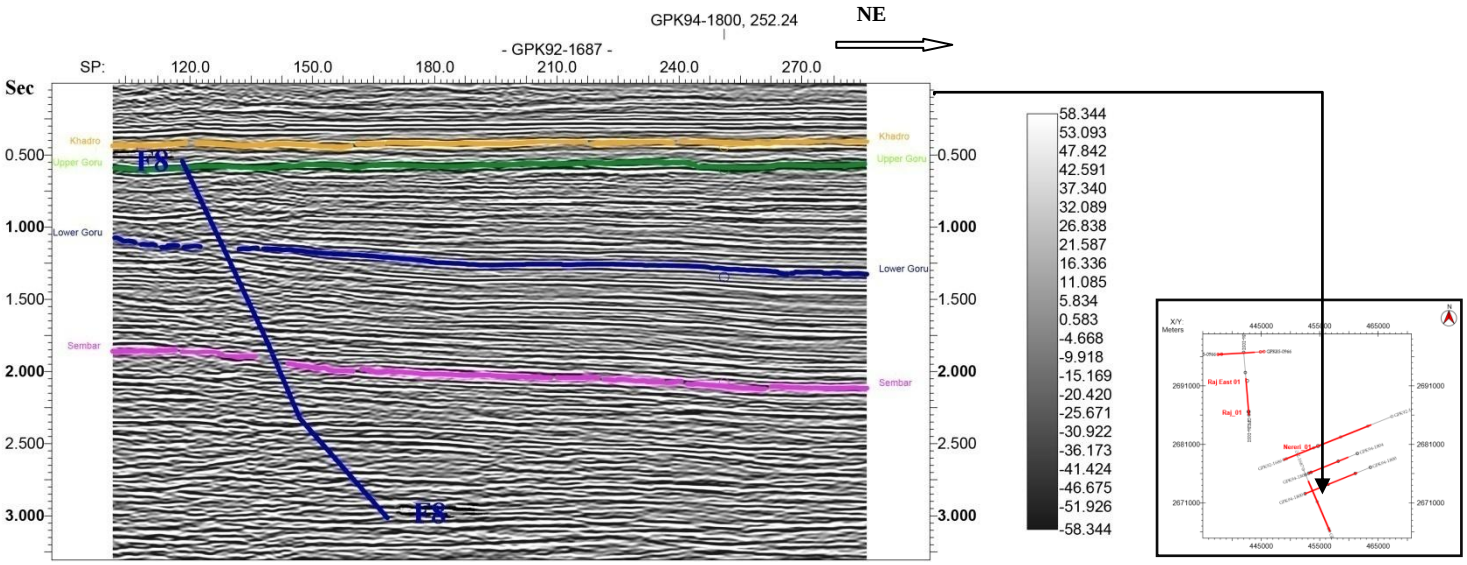

Figure 3.7 Interpreted seismic line GPK92-1687.

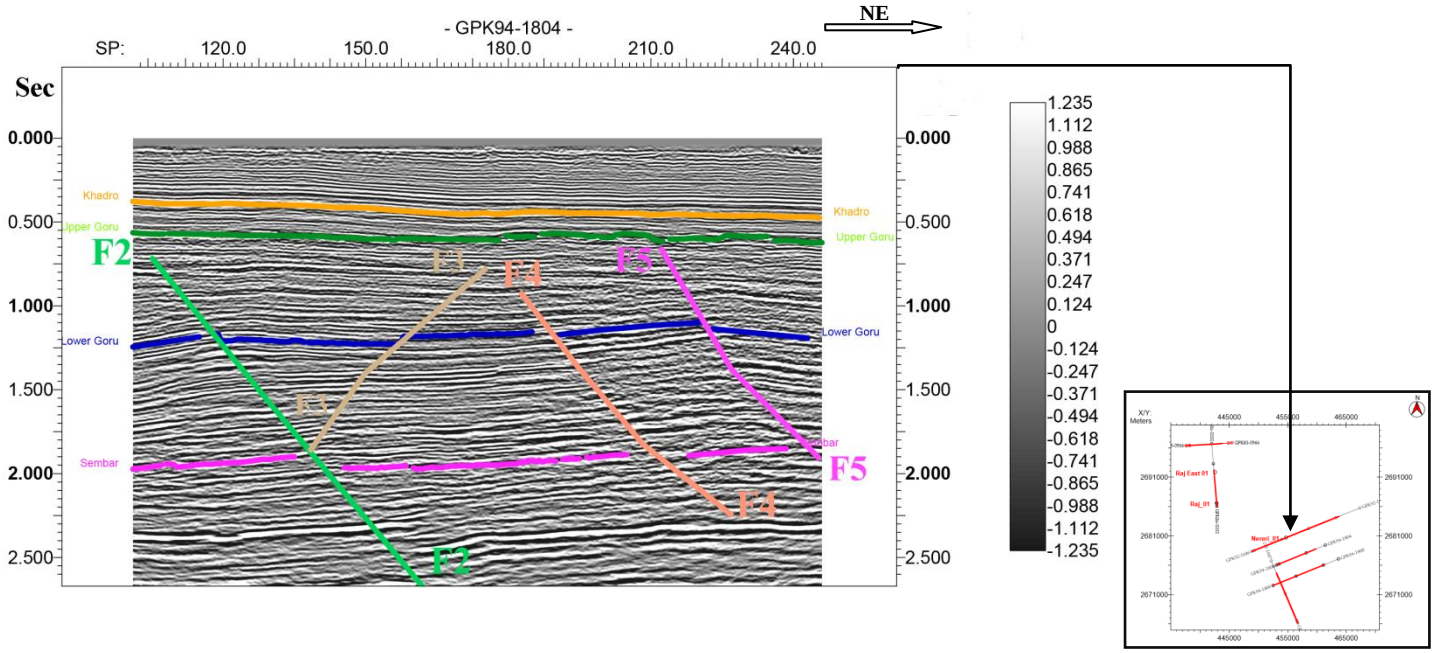

Figure 3.8 Interpreted seismic line GPK94-1804.

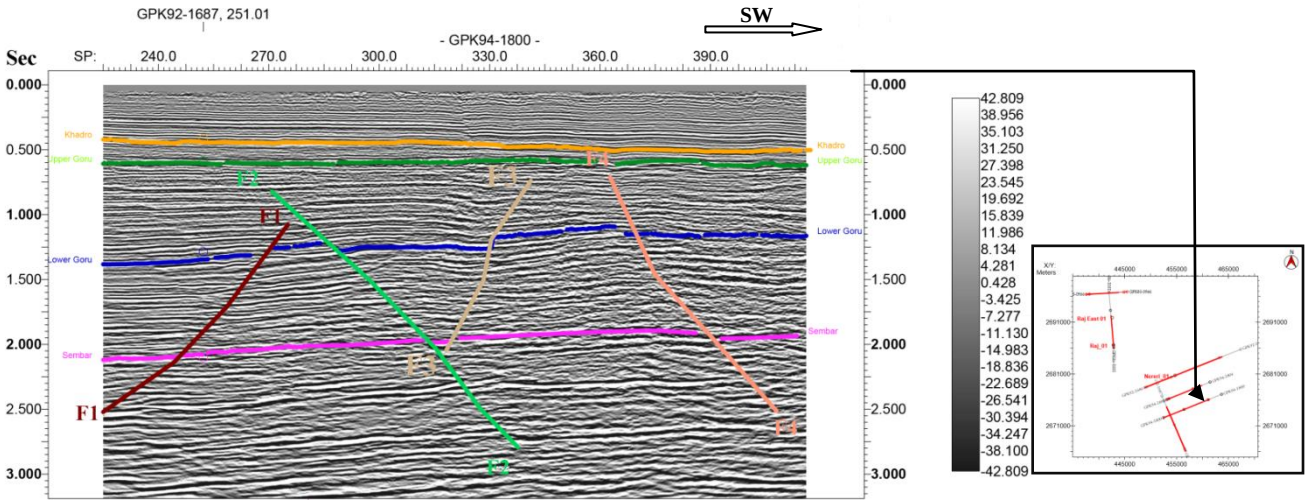

Figure 3.9 Interpreted seismic line GPK 90-1800.

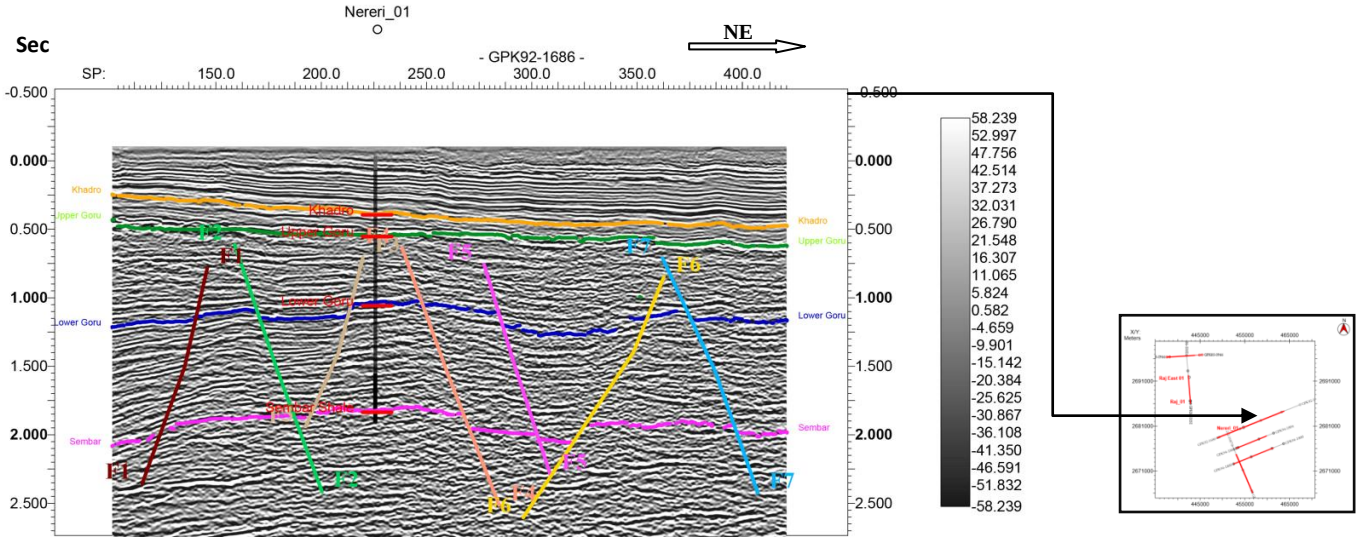

Figure 3.10 Interpreted seismic line GPK92-1686.

3.3.1 Two Way Time Contour maps

Two way time (TWT) contour maps by using the interpretation method, time grids and time contour maps of all the horizons are generated for time contour maps. The contour interval is 0.1 second. From TWT contour maps, it is evident that contour are enclosing against the faults, thus making a trap against the faults, which is feasible for future well locations as well. The time contour maps are generated by making time grids and correlating the fault polygons across the dip lines. Extent of these polygons depicted the heave and closure on both ends.

TWT contour maps of all horizons which are Khadro, Upper Goru, Lower Goru and Sembar formations are shown in fig. 3.10, 3,11, 3.12 and 3.13. In case of Khadro Formation the color bar is showing time variations from 0.35 to 0.65sec for the Khadro Formation as displayed in Fig. 3.10. The contours are closing and showing shallower values of time along seismic lines near to Nereri-01 well. The contours near to Raj-01 well and Raj East-01 well is relatively showing high value of time.

For Upper Goru Formation, TWT values are lying between 0.536 sec and 0.816 sec. The contour pattern is similar to Khadro Formation. At Nereri-01 shallow time values contours with closure is present near seismic lines 1687 and 1686. Higher time value is present near seismic lines 1800 and 1804. On the south western side near to Raj-01 and Raj East-01 wells, the higher time values are observed.

Similarly the TWT contours values are ranged between values from 1.038 to 1.425 sec for Lower Goru Formation and from 1.85 to 2.18 sec for Sembar Formation. Horst and graben structure can be observed along these formations. The extensional tectonics is source for the formation of horst and graben structure. Higher values of time can be observed along graben while low value along the horst part. The abrupt changes in time value are due to presence of faults and strata displacement. Both the formations depict higher time values on the south western side of Badin block.

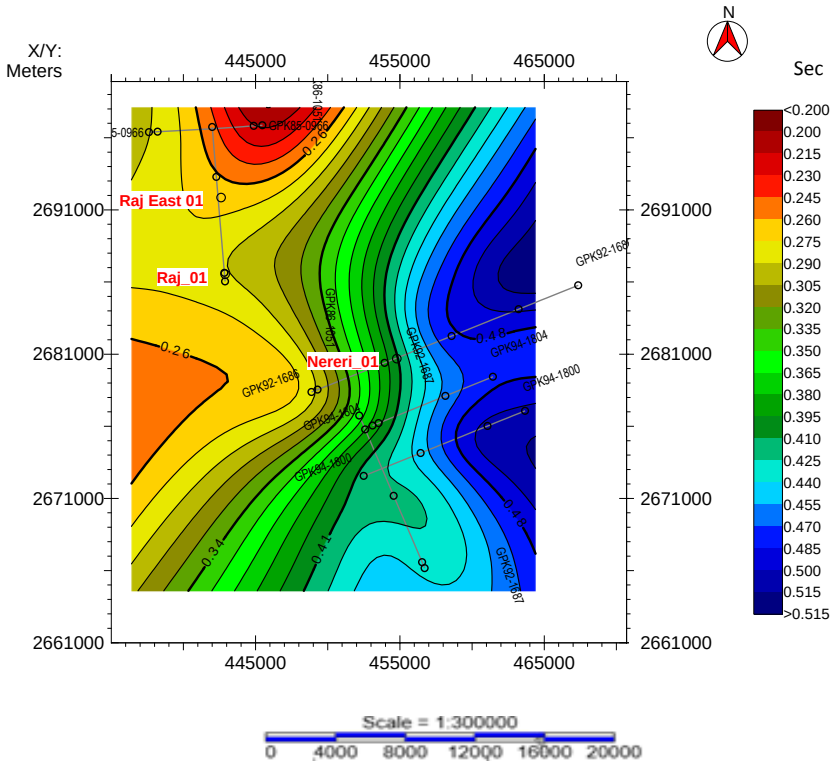

Figure 3.11 TWT contour interval map of Khadro Formation.

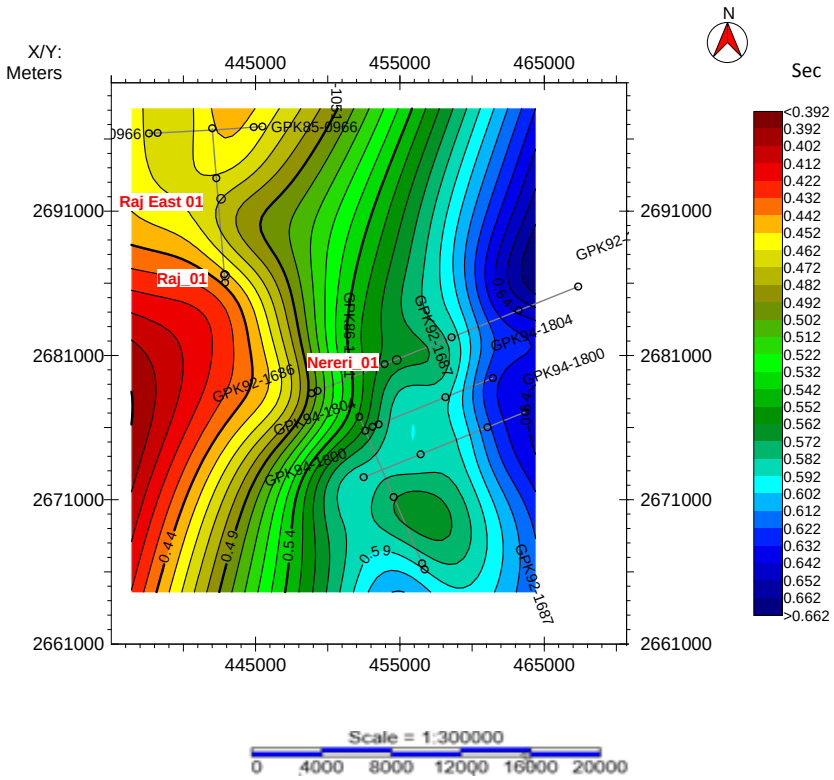

Figure 3.12 TWT contour interval map of Upper Goru Formation.

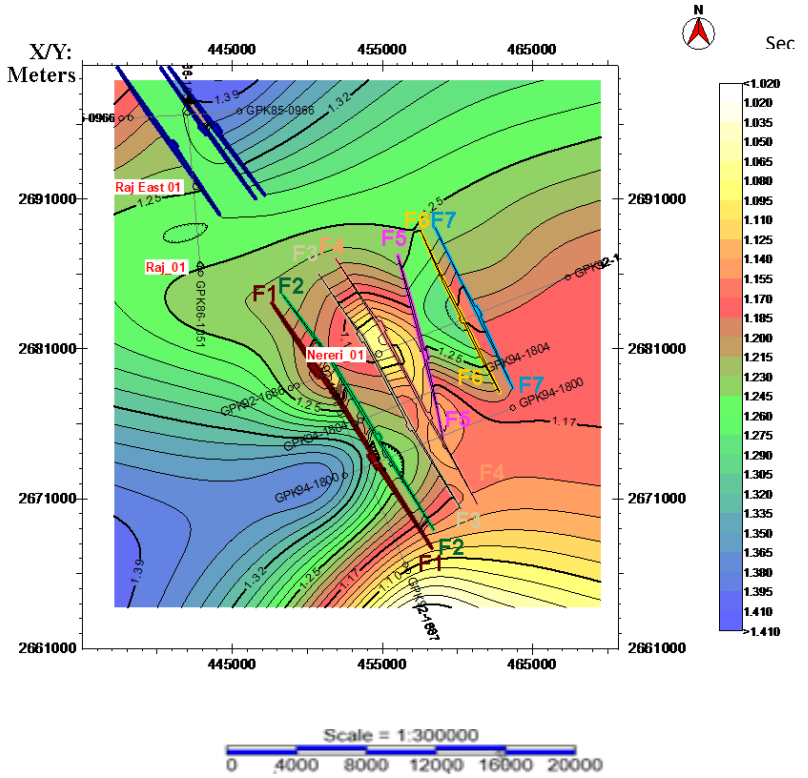

Figure 3.13 TWT contour interval map of Lower Goru Formation.

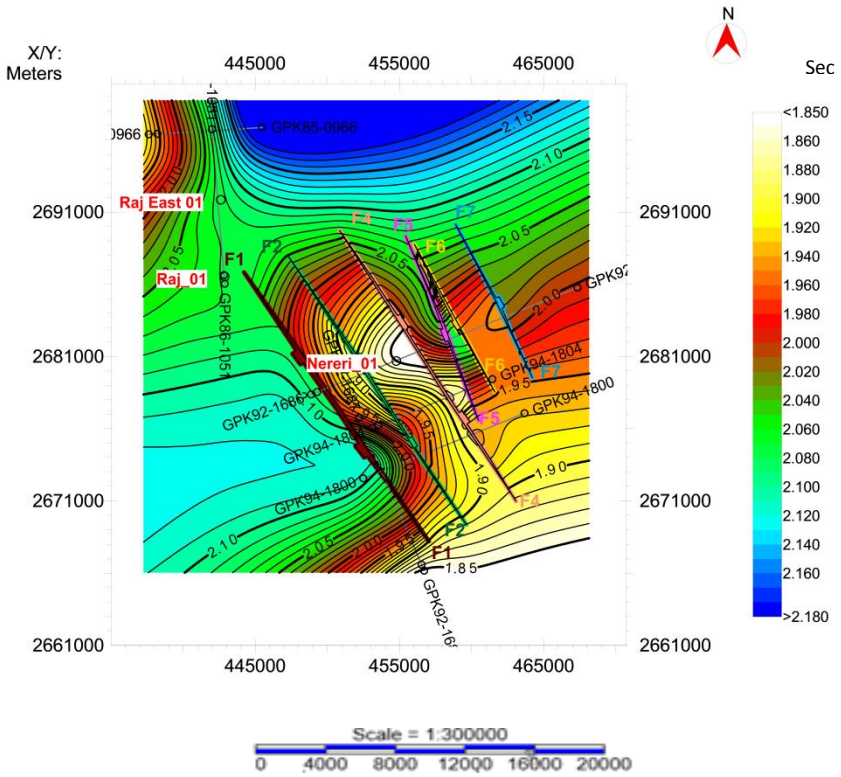

Figure 3.14 TWT contour interval map of Sembar Formation.

3.3.2 Depth and Velocity relationship

The objective of seismic data interpretation is conversion of seismic section into a geological structural model which presents a realistic subsurface picture. To calculate the depth of target, the time values must be converted into depth domain with the help of velocity analysis (Coffeen, 1984). The velocity analysis is one of the most important steps in depth conversion. Therefore, this time domain information can be transformed into depth domain by utilizing velocity information as shown in following formula

$$\text{Depth} = V_{av} * T/2$$

Where, V_{av} = Average velocity of respective horizon (meter/sec) and T = Two way travel time of the horizon (second).

For depth and velocity relationship, the Khadro Formation depth approximates to 635 meters with velocity value of 2200 m/sec, the values of depth and velocity for Upper Goru Formation calculated are 750 meters and 2300 m/sec respectively. Similarly depicted depth and velocity values of Lower Goru are 1550 meters and 2780 m/sec. The Sembar shale values are 3081 meters of depth with velocity value of 3600 m/sec. These values are utilized in generation of depth contours maps of these four formations from TWT contour maps.

3.3.3 Depth Contour maps

The outcome of the seismic analysis is conversion of seismic data into geological model, which is the representation of structure in the shape of depth contour maps. The depth conversion is carried out by utilizing a single velocity. These single velocity functions are utilized for depth conversion. The color bar is displayed with the contour maps which displayed with the contour maps which is displaying the minimum and maximum values of contours. The depth contour maps are depicting the existence of horst and graben structure formed due to extensional tectonics. The fault bounded closures are prominent. Deeper values of depth are present in the graben part while shallower values of depth can be observed in the horst part. The contour interval for depth contour maps 20m.

The depth contour map of Khadro Formation is displayed in Fig. 3.15, showing maximum and minimum contour values of 470m and 850m. The shallower depth values are present in the central part of structure while deepening outwards. The shallower contour values is showing the presence of horst structure on western side of Nereri-01 well and graben part is present adjacent right to Nereri-01 well. The contours are showing the narrower trend towards East-western side near the Raj-01 and Raj East-01 wells.

In the depth contour map of Upper Goru Formation minimum and maximum contour values are 610m and 925m respectively as displayed in fig 3.16. The contour trends for Upper Goru Formation are similar to Khadro Formation.

Lower Goru Formation is considered as major reservoir Formation of Lower Indus Basin. The depth range of contours of Lower Goru Formation varies between 1395m and 1995m as shown in Fig. 3.17. For shale gas potential, shale of Sembar Formation is considered in this study. The depth contour map of Sembar Formation is displayed in Fig. 3.18. The depth range of contours varies between 2775m and 3300m. These contour maps of Lower Goru and Sembar formations are showing abrupt shift of depth values on both sides of faults, which is a clear indication of presence of horst and graben structures formed by normal faulting.

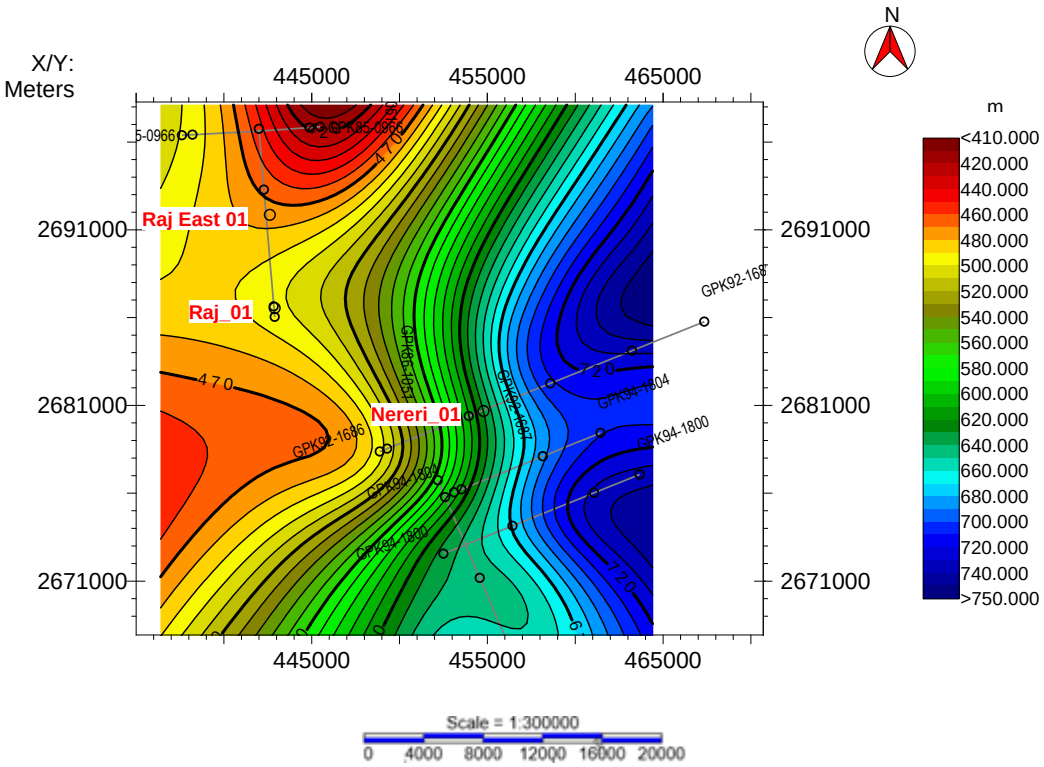

Figure 3.15 Depth contour map for Khadro Formation.

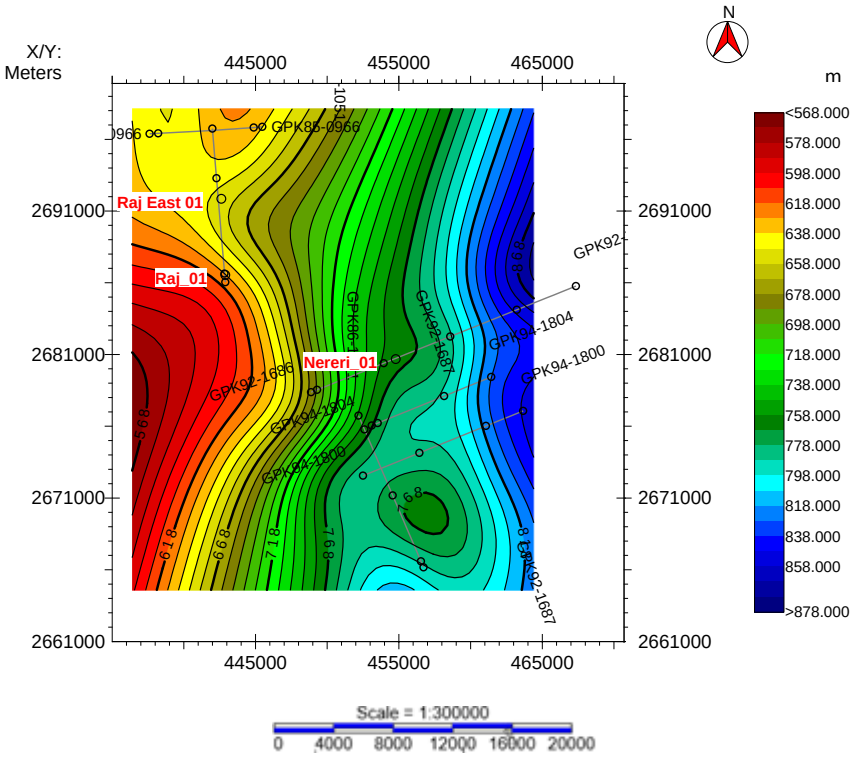

Figure 3.16 Depth Contour map for Upper Goru Formation .

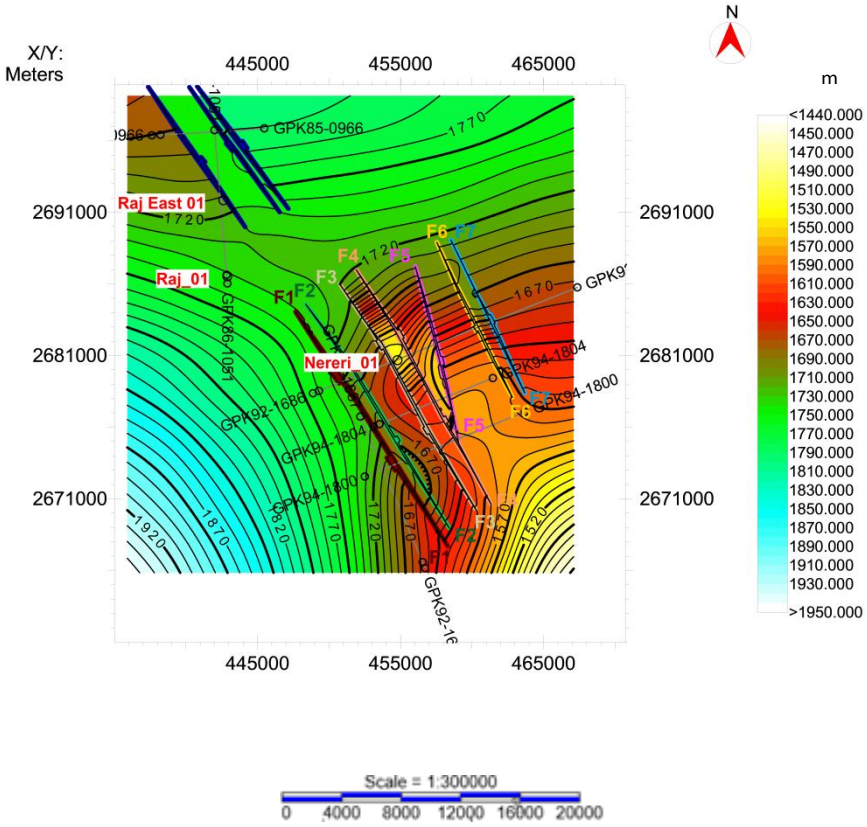

Figure 3.17 Depth contour map for Lower Goru Formation.

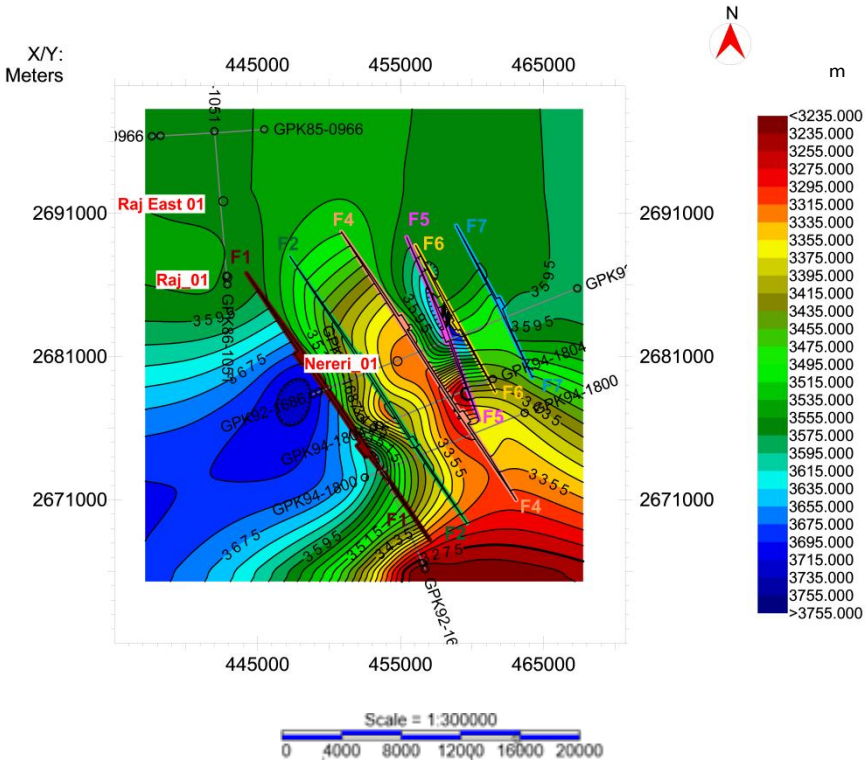

Figure 3.18 Depth contour map for Sembar Formation.

3.4 Discussions

The presence of geological structure is an important element along with the Petroleum system of the area. The interpretation and mapping of 2D seismic data revealed that Badin area underwent through extensive extensional tectonic activites forming horst and graben structures at Sembar Formation and Lower Goru Formation level of Cretaceous age whereas Khadro Formation of Eocene age remained undisturbed. These horst and graben structure are the result of early Cretaceous rifting in Badin area. The grabens in the Badin block are serving as sites for accumulation and generation of hydrocarbons. The normal faults are acting as transporting pathway for hydrocarbon movement from source rock i.e. Sembar Formation to reservoir rocks i.e. Lower Goru Formation. Faults are acting as trapping mechanism for hydrocarbons. The major components of petroleum system are existing in Badin block as established by number oil and gas discoveries in the Lower Indus Basin. These structural patterns were modeled through 2D seimic lines interpretation.

CHAPTER 4

ATTRIBUTE ANALYSIS

4.1 Introduction

Quantity which is computed through seismic data can be quantified as an attribute. There are many types of attributes such as, pre-stack, post-stack, inversion, velocity, horizon and multi-component. The core of seismic data is amplitude.

Seismic attributes are necessary unit of qualitative interpretative method that aids structural and stratigraphic (channels, pinch out, meanders, etc) interpretation and predict the lithology type and fluid content with a advantage of comprehensive reservoir characterization (Strecker et al., 2004). In this study post stack attributes are applied on 2D seismic line GPK-92-1686 to classify potential source rock and unconventional shale gas potential in Sembar Formation. This line is selected because of its full length with well on this line. The applied post stack attributes include Amplitude, Spectral Decomposition, Instantaneous Phase and Frequency, Sweetness and Shale Indicator. Most of them showed positive correlation with demarcated Sembar Formation.

Attributes are being applied by geoscientists to map subsurface features on micro-level scale to 2D seismic line to macro-level on entire basins. All sort of information can be derived from seismic data by applying seismic attributes, which can be extracted with direct measurements or with logical or experience based analysis (Taner, 2001). The information extracted from seismic data by applying attributes includes amplitude, phase or frequency of the waveform. The amplitude part of the seismic data determines the physical parameters, such as the velocities, reflection coefficient and acoustic impedance. The phase content determines the shape of the reflectors and their geometrical configurations. Analysis of amplitude can indicate hydrocarbon properties by identifying lithofacies and porosities. Instantaneous attributes like instantaneous phase and instantaneous frequency can

help in tracking of horizons of interest on seismic data (Chopra and Marfurt, 2008). Spectral decomposition can aid in recognizing geologic feature at any frequency (Subrahmanyam and Rao, 2008). These subsurface signatures help in measuring characteristics of interest in the formation of interest (Chopra and Marfurt, 2005).

More than seventy distinct seismic attributes can be analyzed and calculated from seismic data and can be related with geologic features. With increase in number and variety, seismic attributes are classified into families for better application. Common classification divides seismic attributes into general and specific classifications. General attributes computes geometric, kinematic, dynamic, or statistical characters from seismic data which include amplitude, dip and azimuth, Hilbert attributes, coherence, AVO, and spectral decomposition. These are based on morphological character of lithology of the subsurface generically. Specific attributes may correlate to a geologic characteristic in a specific basin, but these correlations cannot be applied throughout the Earth. Therefore, these attributes are basin specific (Chopra and Marfurt, 2005).

Utilization of seismic attributes has been increasing to improve workflows by applying these well-established attributes for exploring unrecognized or overlooked geologic features (Chopra and Marfurt, 2008) from seismic data. Seismic attributes have several applications:

(a) To measure a particular property (e.g., porosity prediction, bright spot identification)

(b) For features identification, isolate and visualize a seismic characteristic (e.g., faults).

This study is intended to determine the response of basic post stack seismic attributes from 2D seismic section of Badin block particularly Sembar Formation. Sembar Formation is proven source rock in Lower Indus Basin.

Seismic attributes are the quantitative measurements of properties of seismic for area. The attributes are used to mark subtle features which cannot be observed on normal seismic data. A seismic attribute is employed to increase understanding that might not be extracted in a specific seismic image, which help to produce an better

geological or geophysical interpretation. Computed time, amplitude and frequency are some of examples of seismic attributes.

4.2 Methodology, Analysis and Results

Seismic attributes are applied on seismic line GPK-92-1686. Applied attributes are geometrical, instantaneous, coherency and spectral decomposition applied on seismic line to characterize structural, and petrophysical aspects of the Sembar Formation. These attributes have given the information about lateral changes, continuity, structural and lithological characteristics of Sembar Formation.

Seismic attributes are applied and correlated with the geological data computed from the bore hole. Sembar Formation was drilled in Nereri-01 well. Sembar Formation has weaker and non-consistent character. By applying the seismic attributes, Sembar Formation was characterized for detailed study of its character.

The attribute analysis help to overcome the problems associated with seismic amplitudes. Post-stacks seismic attributes are extracted and applied to mark Sembar Formation. The results of attributes analysis revealed that average instantaneous frequency, instantaneous phase, average energy and trace envelope are effective attributes to identify probable source rock i.e. Sembar Formation (Bodine, 1984; Chopra and Marfurt, 2005; Taner, 2001). The variance attribute typifies the trace-to-trace not consistent with a particular sample interval and generate an interpretable lateral changes in acoustic impedance. Similar traces result low variance values while faults and channels may cause discontinuity in the adjoining lithologies generating discontinuities with high values.

4.2.1 Amplitude Attribute

Amplitude defines the strength of the seismic trace envelope. Amplitude is simply the height of a wave. It is positive, independent of the polarity or phase of trace. It is default attribute and analyzed as the cosine of instantaneous phase angle which emphasize lateral continuity of the event. Its major types are reflection

strength, rms amplitude, maximum amplitude, average absolute amplitude, and total energy etc.

Reflection strength is the measure of suitable amplitude, which is computed through complex seismic trace analysis and is synonymous with trace envelope and instantaneous amplitude. The strength of the trace is the amplitude of the reflection and is dependent on the difference in velocities between the adjacent rock layers. The greater the change is, more be the strength of the reflection. These attributes reveal bright spots and dim spots caused by presences of gas, or porosity changes and hence can be correlated with porosity and fluid saturation. When lithology or fluid components of one of the rock layers changes, the velocity difference is probable to change, creating a contrast in the reflection amplitude. Amplitude is measured in unit of decibel, denoted by dB (Robison, 2010).

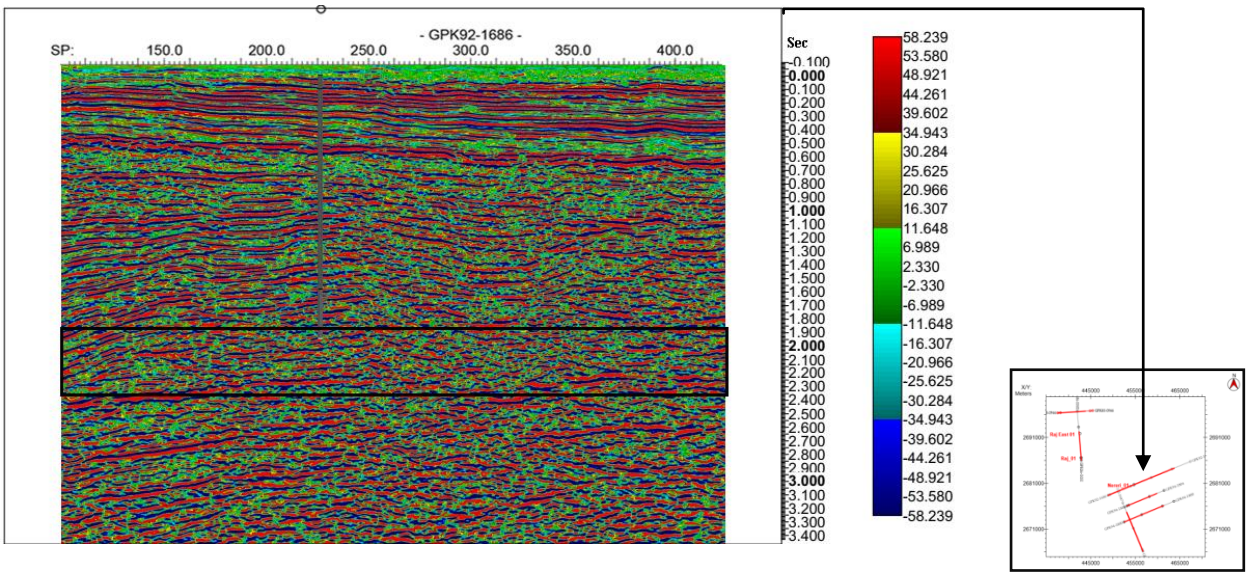

Figure 4.1 Amplitude attribute applied on seismic line GPK92-1686.

Calculated values of amplitude lies in range of 17 to 26 at Nereri-1 location as displayed in figure 4.1. These values indicate very less chance of the occurrence of hydrocarbons in the source rock. The amplitude map for Sembar Formation indicates same amplitude value along GPK92-1686.

4.2.2 Spectral Decomposition

It is basically frequency attribute, which reveal seismic signal into its constituent frequencies i.e. spectral sub-bands. Utilization of spectral decomposition is the substitution of the single input trace with a gather of traces. The input for spectral decomposition is a seismic line while the output consists of several lines representing individual frequency sub-bands. Spectral decomposition permits the structures with various frequency bands tuned to specific wavelengths to be highlighted to deserve if a particular frequency band gives better resolution (Chopra and Marfurt, 2008). This attribute is also utilized for detection of bright spots. It can be utilized for identifying DHI (direct hydrocarbon indicators) specifies and analyzed fluid types and lithologies.

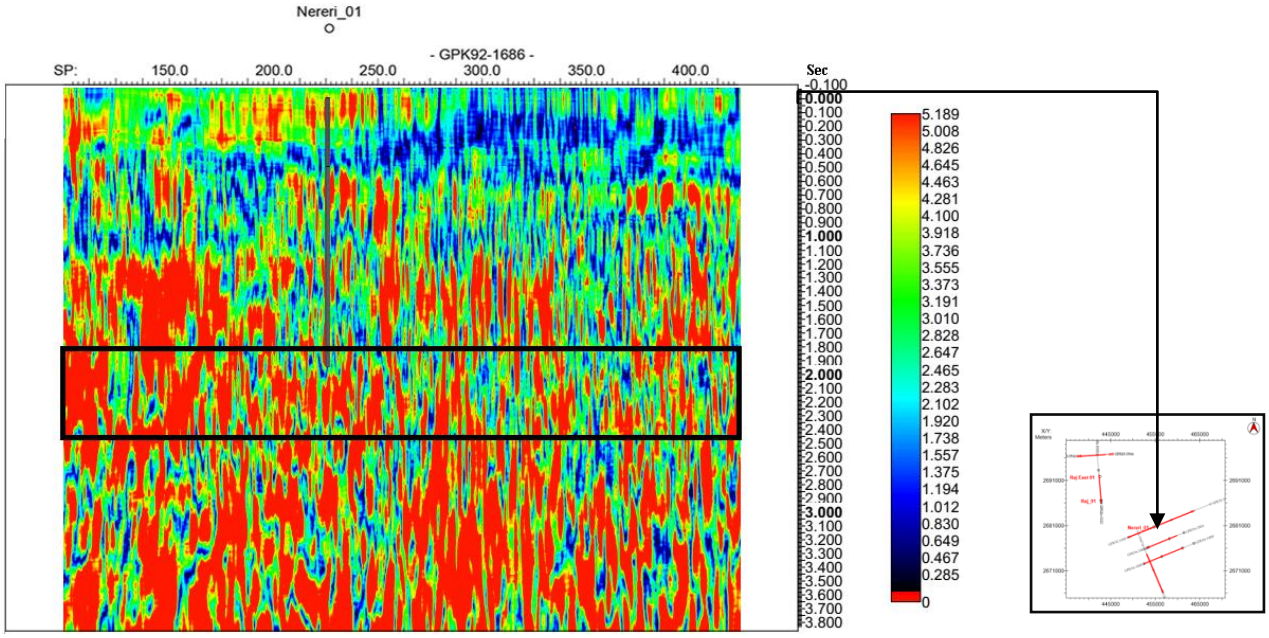

Figure 4.2 Spectral Decomposition Envelope Sub Band 8 Hz.

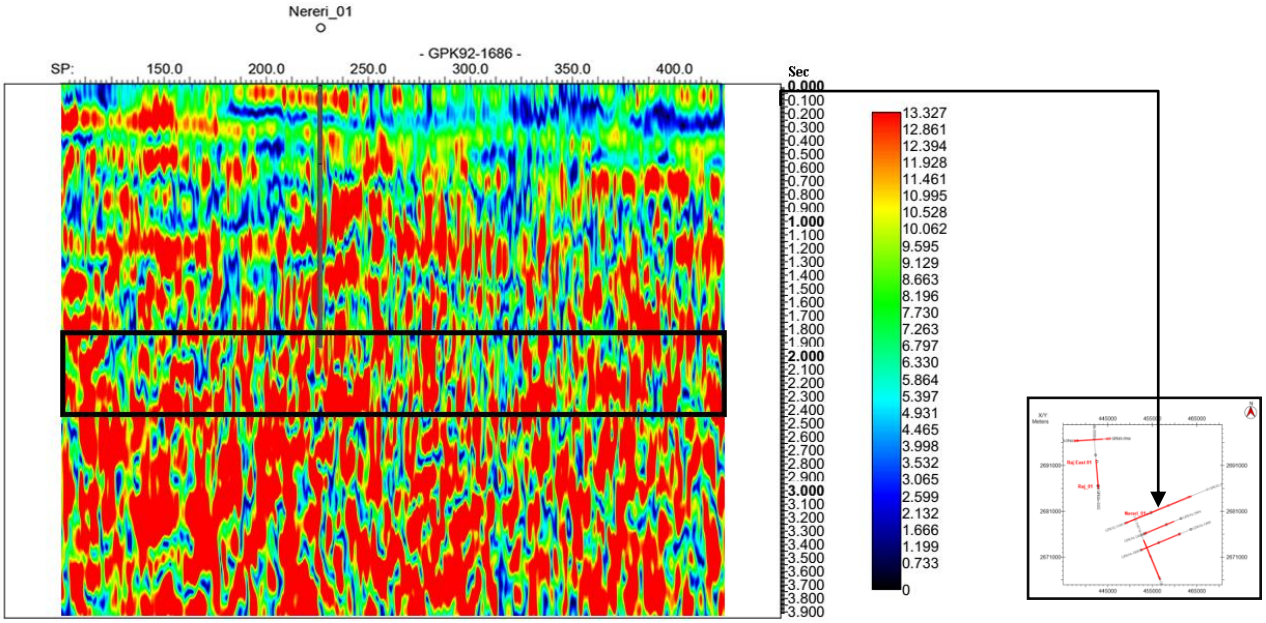

Figure 4.3 Spectral Decomposition Envelope Sub Band 10.3 Hz.

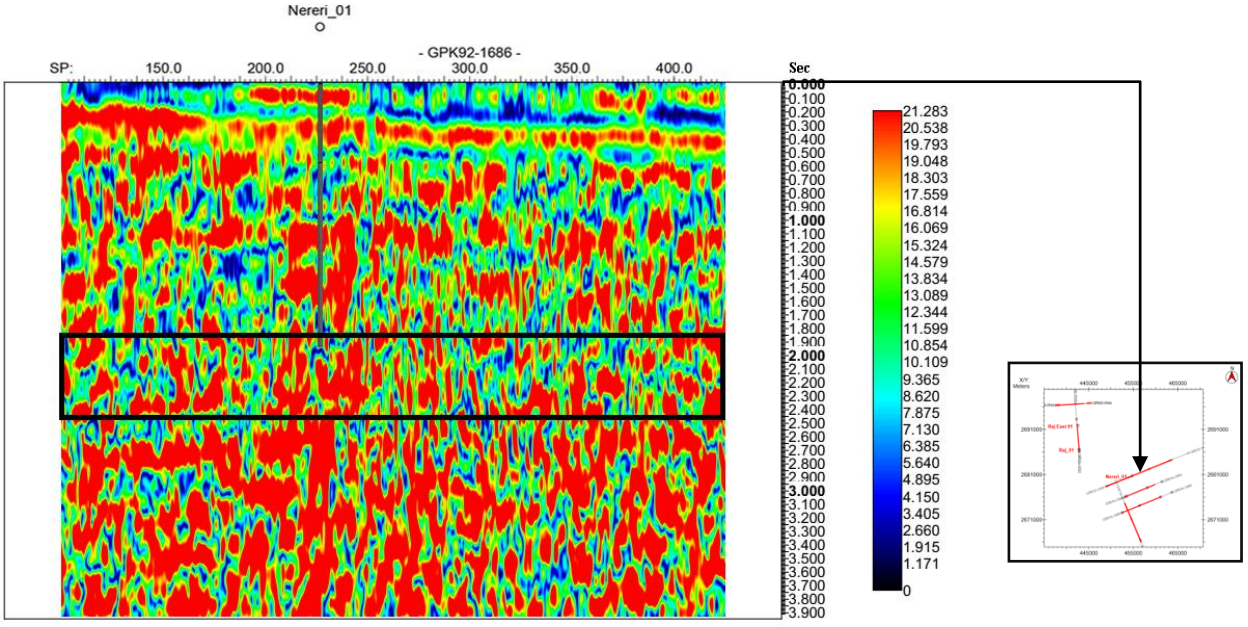

Figure 4.4 Spectral Decomposition Envelope Sub Band 13.3 Hz.

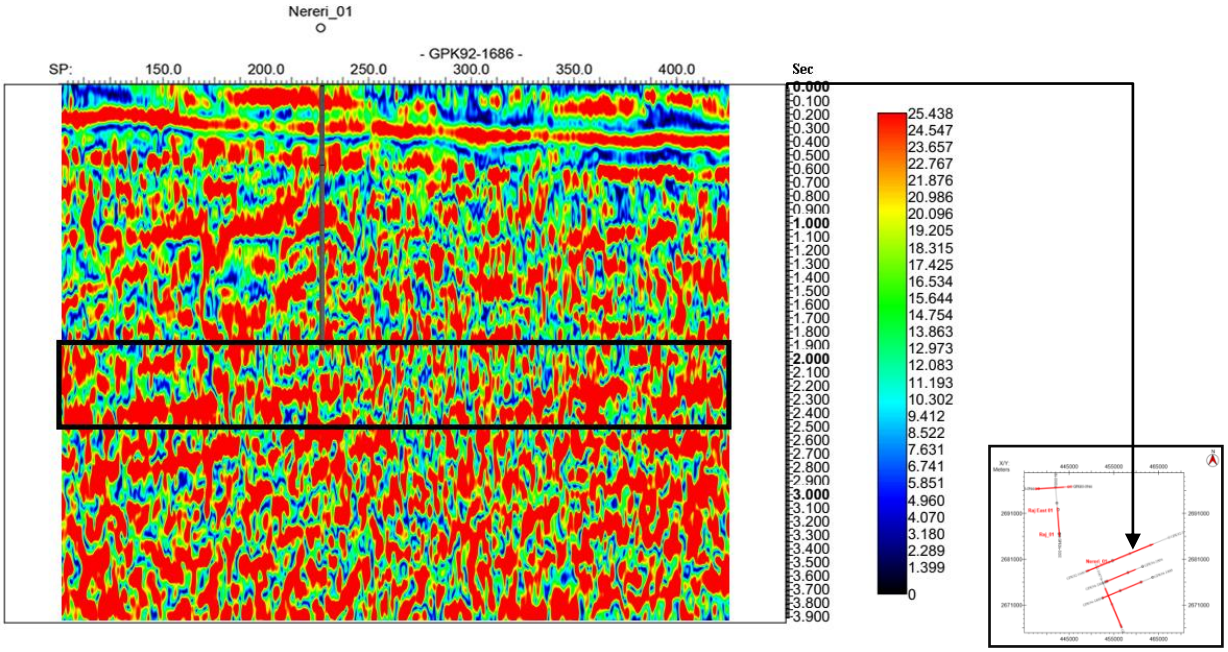

Figure 4.5 Spectral Decomposition Envelope Sub Band 17.2 Hz.

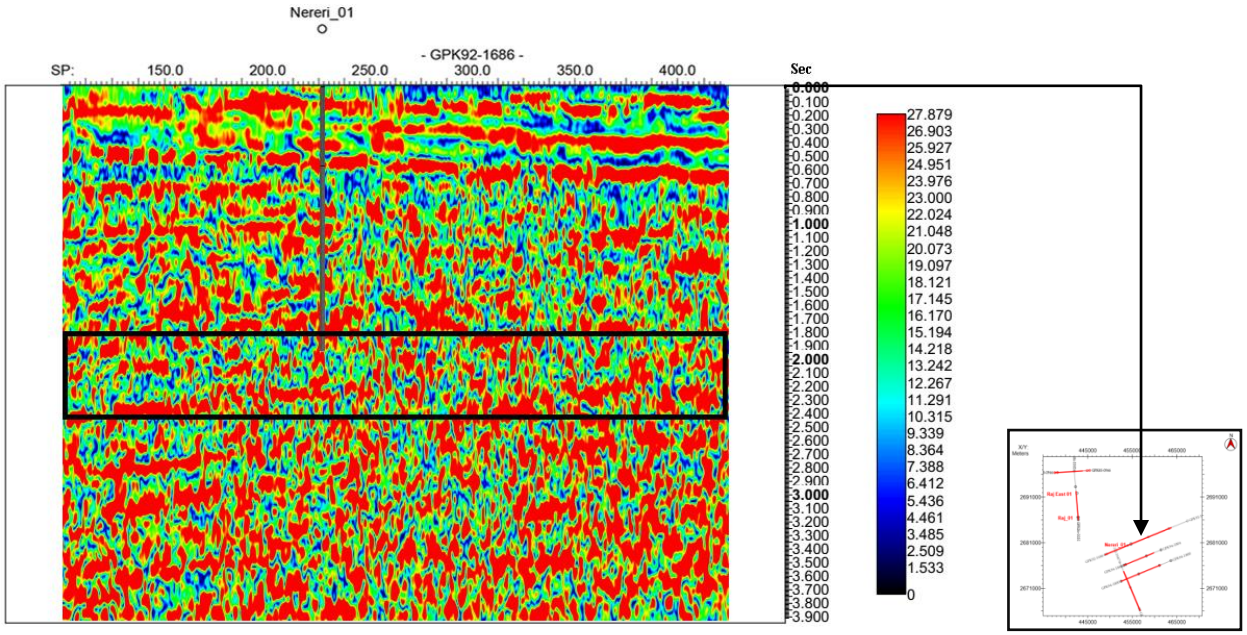

Figure 4.6 Spectral Decomposition Envelope Sub Band 22.3 Hz.

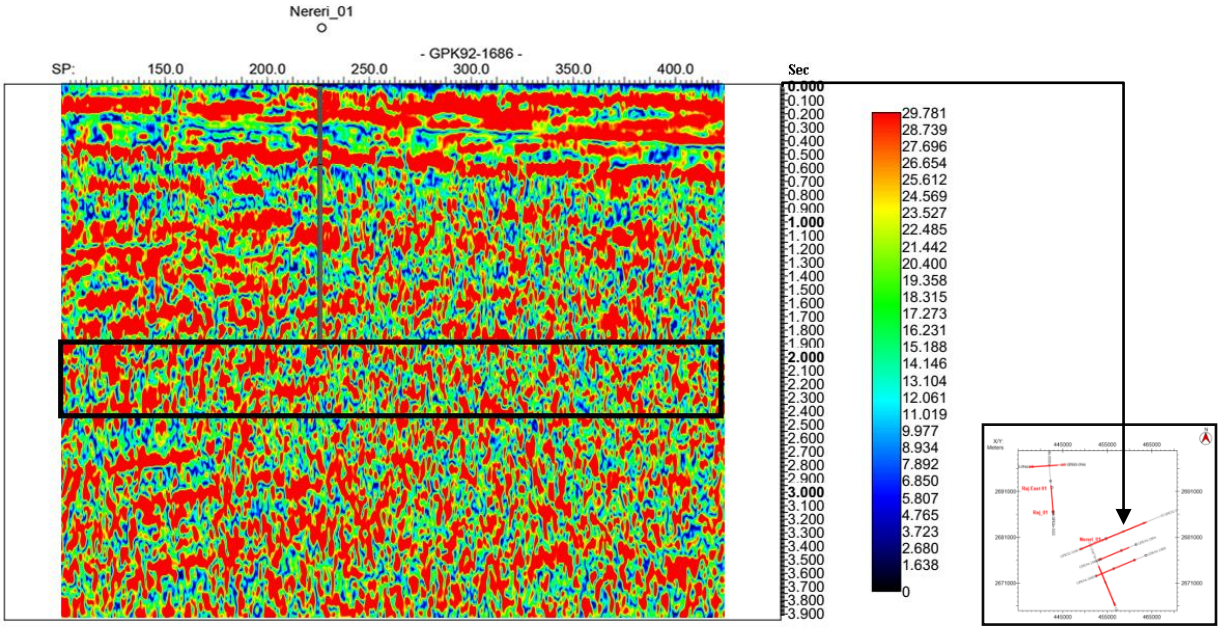

Figure 4.7 Spectral Decomposition Envelope Sub Band 28.8 Hz.

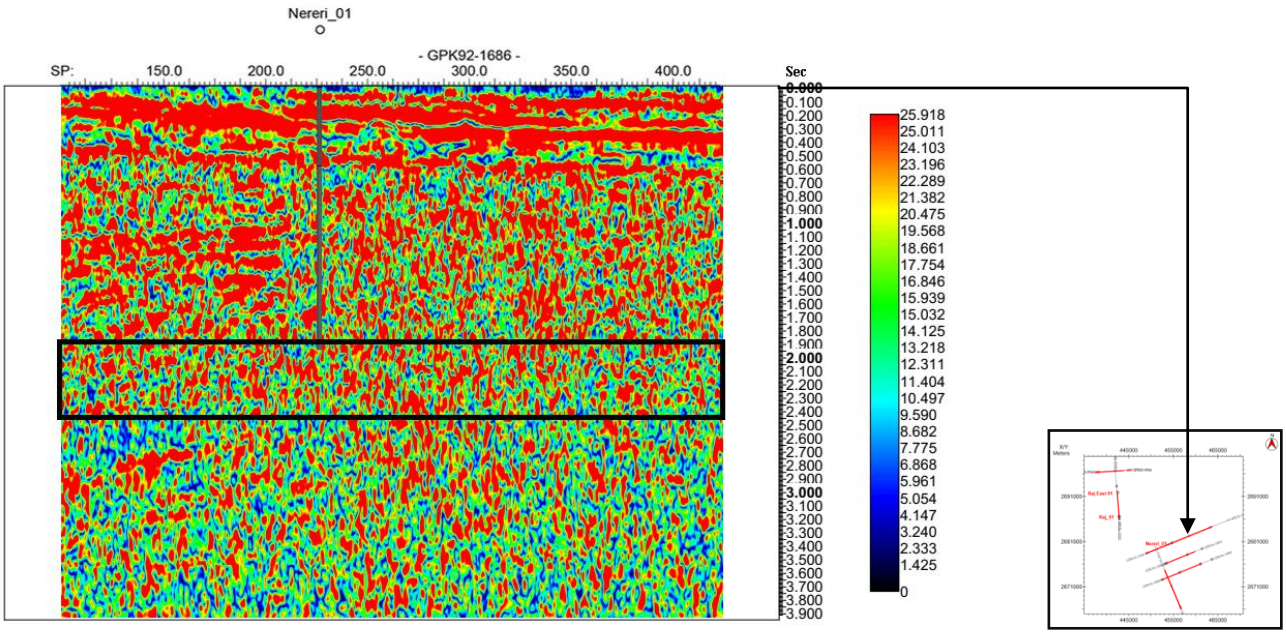

Figure 4.8 Spectral Decomposition Envelope Sub Band 37.1 Hz.

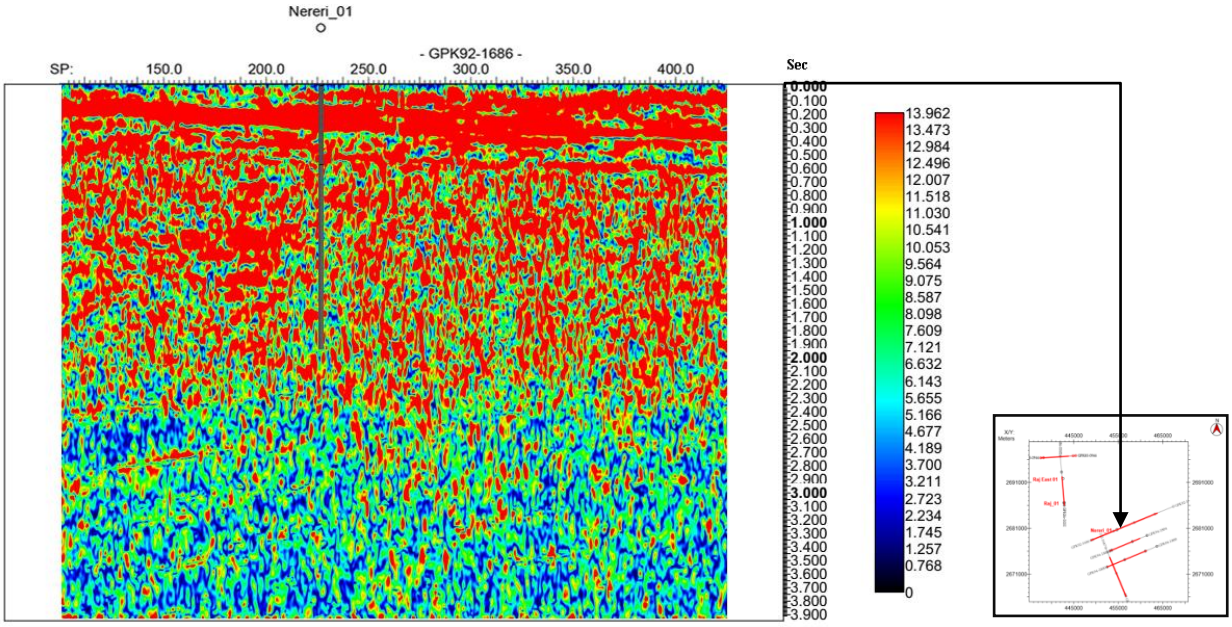

Figure 4.9 Spectral Decomposition Envelope Sub Band 48 Hz.

From sepctral decomostion attribute, uses of wavelet transform is carried out to decomse broad band seismic singnal into discreet sub-bands. Therefore, the spectral decomposition envelop sub-bands are computed at different sub-bands values which are 8, 10.3, 13.3, 17.2, 22.3, 28.8, 37.1, 48 Hz as displayed in figures 4.2, 4.3, 4.4,4.5, 4.6, 4.7, 4.8, and 4.9 respectively. This attribute is utlised to decomse seismic data into time frequency domain in order to find the sembar layer thickness estimation with better resolution. After comparison of results it can be observed that best results are obtained for spectral decomposition envelope sub band 17.2 Hz at Sembar Formation level on seismic line GPK-92-1686 as depicted sub band for Sembar Formation in figure 4.4. Therefore, it is evident that at 17.2 Hz the Sembar Formation event display its highest amplitude. It gives the better understanding and quantification of temporal extent of Sembar thickness and energy information of sembar region. At this band we have maximum amplitude and energy band information for Sembar Formation. From 17.2 Hz band Semabr rock mass characteristic can be mapped in the study area.

4.2.3 Instantaneous phase

The phase information is not dependent of trace amplitudes and links to the propagation of phase of the seismic wave front. It is utilized for lithological and

reservoir characterization (Taner, 2001). It presents the phase of the resultant vector of individual harmonic motion. Instantaneous phase attribute computes the instantaneous phase at the point of sample, it highlights spatial continuity or break of reflections by giving opportunity for weak and strong events to emerge with equal strength. It effectively highlights discontinuities of reflectors, faults, angularities and bed interfaces (Taner and Sheriff, 1977). It is independent of amplitude. It is computed from real and imaginary traces as given in equation below

$$\theta\,(t) = \tan{-}1[f\,(t){+}h\;\;(t)]$$

Instantaneous phase is the best indicator of, lateral continuity, fluid content, pinchouts, depositional environment, which narrates to the phase component of the wave propagation. Figure 4.10.shows the instantaneous phase attribute of Sembar Shale which showed week coherence in amplitude but depicted the coherent based on consistent phase angel. Therefore, the Sembar Shale horizon lied over the zero phase region. In figure, at the Sembar Formation, uneven phase variation values are seen, which is the indication of discontinuity of bedding with low fluid contents, and lithology contrast with above Lower Goru. The discontinued indication also demark the good porosity in Sembar Formation.

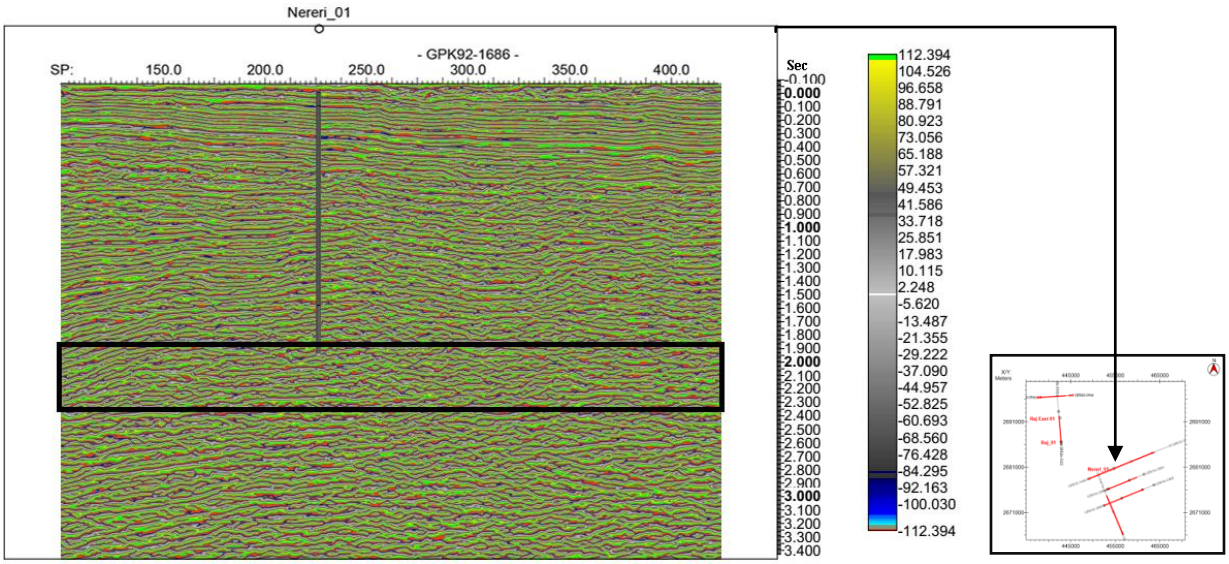

Figure 4.10. Instantanous Phase applied on seismic line GPK92-1686.

4.2.4 Instantaneous frequency (Hz)

It is defined as the phase changes rate over time. It is time derivative of instantaneous phase. Depositional environments can be linked to instantaneous frequencies e.g. thin beds, tuning thicknesses. It may be indicator of hydrocarbon saturation with low frequency (Raef, 2001). Massive beds such as sandstone have low frequencies. Sharp interfaces like thinly laminated shale are specified by higher frequencies. Limestone shows high frequencies. This attribute can also be used for presenting fracture zone (fractures may appear as lower frequency zones) and presenting bed thickness. Instantaneous frequency is computed by the following equation:

$$w(t) = \boldsymbol{d}|\boldsymbol{\Phi}(\boldsymbol{t})| / \boldsymbol{dt}$$

Where Φ (t) is instantaneous phase and t is time (or depth)

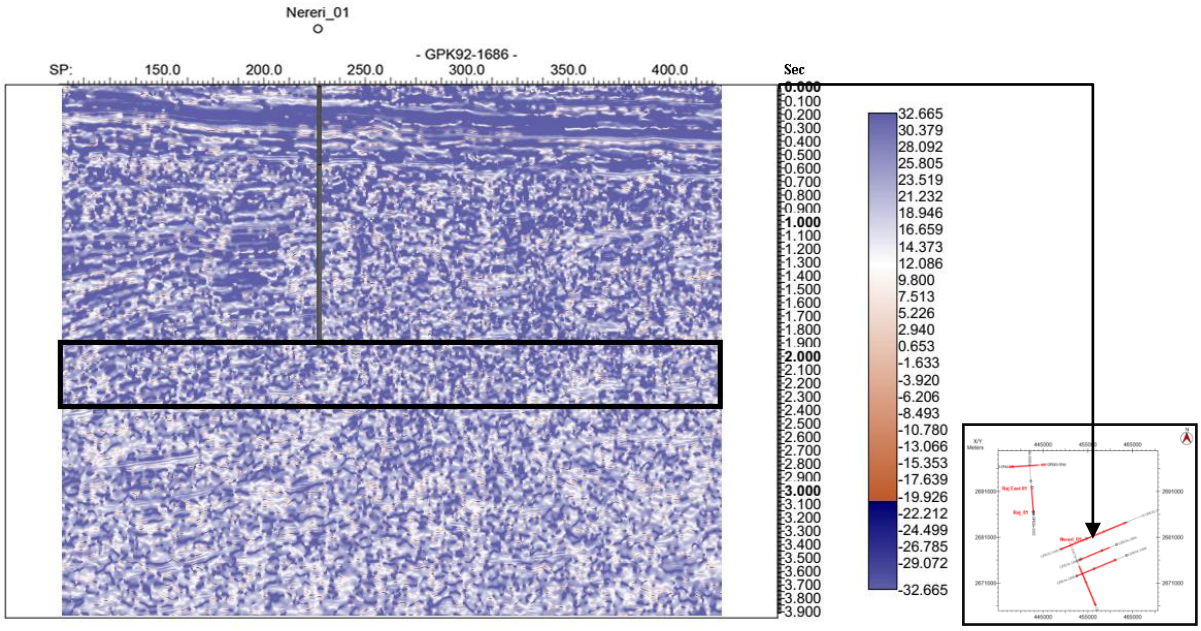

Figure 4.11 Instantaneous frequency with color change.

Instantaneous frequency attribute applied to seismic line GPK-92-1686 as displayed in figure 4.11. This attribute is confirming the fault and horizon interpretation at Sembar Formation level due to lithology contrast and bedding

discontinuity. The high value of instantaneous frequency is showing shales of Sembar Formation but with stratigraphical small thickness. Higher frequency values are observed at the source rock level i.e., Sembar Formation with low level of saturated gas zone with thin extent of bedding.

4.2.5 Sweetness

Sweetness is an observed attribute developed to distinguish "sweet spots," which are prone sites for oil and gas resources and usually are direct hydrocarbon indicators. Sweetness is particularly helpful for channel detection. Sweetness $s_r(t)$ is defined as below,

$$s_r(t) = a_r(t)/\sqrt{f_r(t)}$$

Response amplitude is denoted by $a_r(t)$ and is the value at the envelope peak, and response frequency is donated by $f_r(t)$. Sweetness closely resembles reflection strength. Sweetness anomalies of interest are those that are more pronounced than the corresponding reflection strength anomalies (Hart, 2008). In this case study, Sembar Formation, sweetness attribute show value that range between 8 and 12 according to color bar scale. These range of values show the presence of hydrocarbons in Sembar Formation as displayed in figure 4.12. The sweetness value for Sembar Formation lied between 8 and 12, which is low channel continuity and low level hydrocarbon reservoir, with low level of acoustic impedance contrast because of shale prone clastic environment.

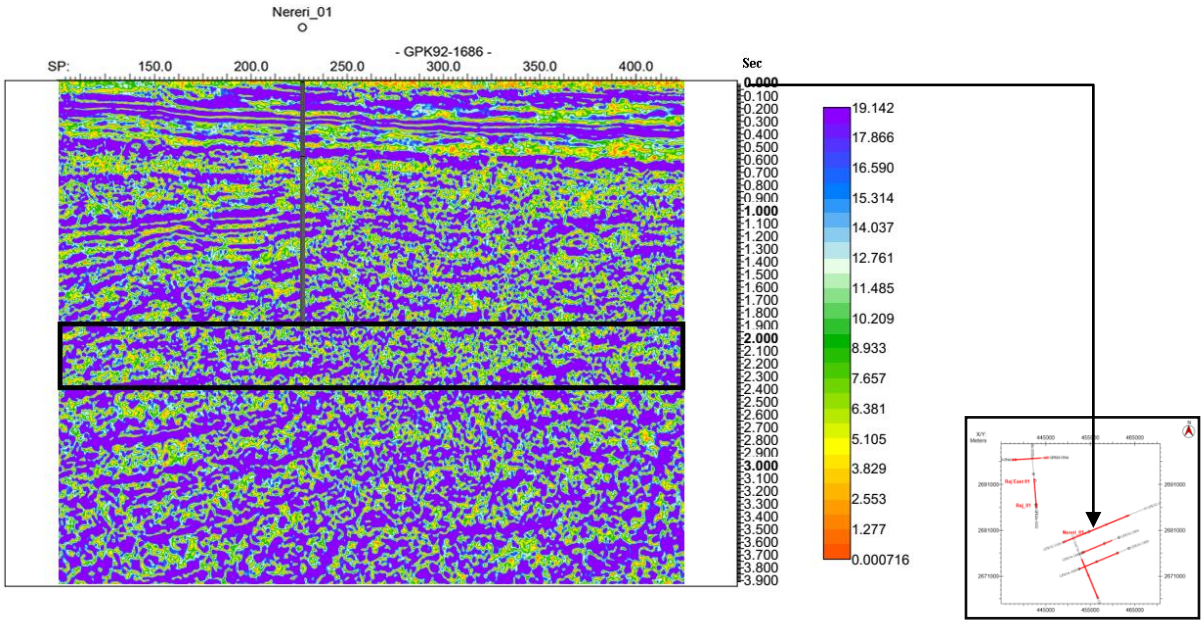

Figure 4.12 Sweetness attribute.

4.2.6 Average Energy

It classifies reflection strength and lateral continuity of reflector. Energy of the horizon is based on the reflection strength. It also identifies the porosity and lithological variations. Compact lithology shows high energy where as loose lithology has low energy value. It also demarcates the reservoir quality and continuity of reflectors. Average energy is particular window with the square root of the sum of squared amplitudes and divided by their number of samples. It is calculated at the crest of the envelope, which shows the attribute of the wavelets in the distinct zone with the trace envelope minima. This attribute indicates spatial variation of the wavelet and relates to the response of the composite group of individual interfaces below the seismic resolution. The attribute has compact response and highlight the Sembar Formation as shown in figure 4.13. Sembar Formation has low average energy as compare to overlying Lower Goru Formation.

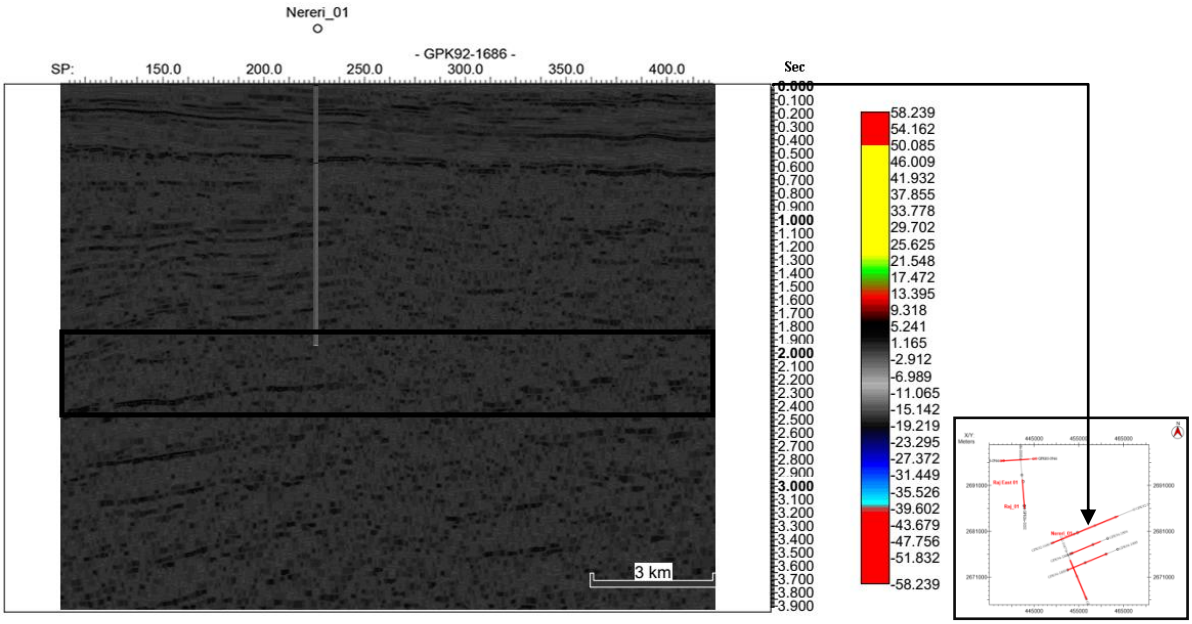

Figure 4.13 Average energy attribute.

4.2.7 Event Continuity

Event Continuity is calculated for highlighting continuous events. The program outputs values of +1 at the location of each peak's maximum, and –1 at the location of each trough's minimum. The remaining of the trace samples are set to 0. The attribute of event continuity applied on seismic line PK92-1686 is displayed in figure 4.14.

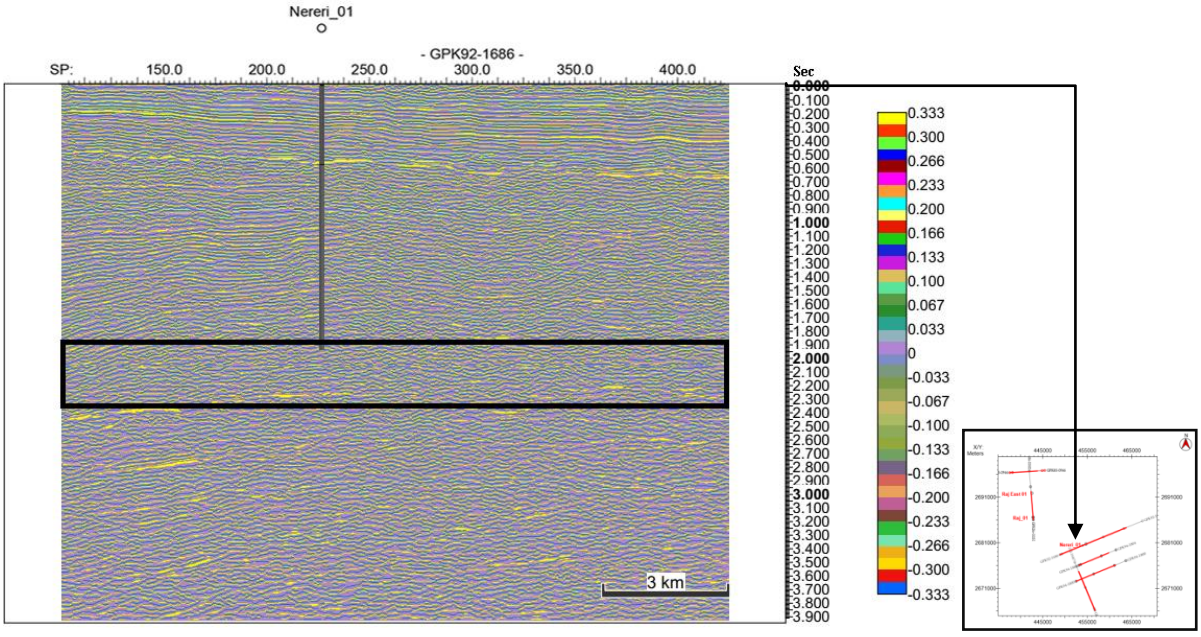

Figure 4.14 Event Continuity attribute.

4.2.8 Shale Indicator

It is a hybrid attributes, with combination of several attributes which is used for shale zone detection in a clastic environment. Shale lithology may be classified by its geometrical configuration and thin, parallel beds with lateral continuity. This attribute applies instantaneous frequency for the detection of thin bed, and parallel bedding. The higher values of this attribute are indicator of shale occurrence and vice versa.

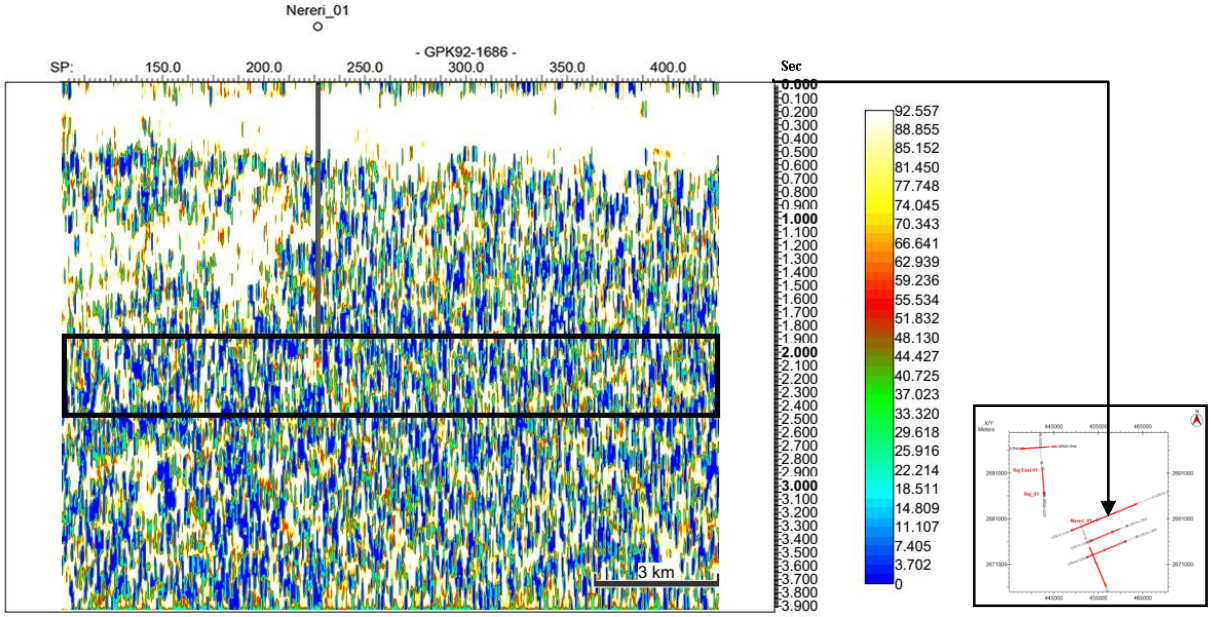

Figure 4.15 Shale indicator attribute.

This attribute is indicating higher output values along the Sembar Formation, which is the possible occurrence of shale lithology. Upper and Lower Goru Formations have consistent low values.

4.2.9 Trace Envelope

Trace Envelope is the total instantaneous energy of the complex trace not dependent on the phase and is calculated as the modulus of the complex trace

$$E(z) = \sqrt{f^2(z) + g^2(z)}$$

Time or depth ranges from top to bottom of the trace. The envelope is directly related to the acoustic impedance difference. It may show the individual interface contrast or, more similar, the collective response of several interfaces, based on the seismic bandwidth. The output is computed with respect to the RMS value of the trace and it is presented as envelop amplitude changing rate.

This attribute is computed for seismic line GPK-92-1686 shown in figure 4.16, to observe the changes in lithology of Sembar Formation. Minimum reflection strength is indicating the package of Sembar Formation. It also showed spatial

patterns representing changes in the thickness of the Formation and breakage due to the faults.

At the level of Sembar Formation, low acoustic impedance contrast can be observed as displayed in figure 4.16. The lower values of the trace envelop shows absorption effects and discontinuities. These changes are clear indicator of shale lithology and also indicating the change of lithology from sand stone to shale.

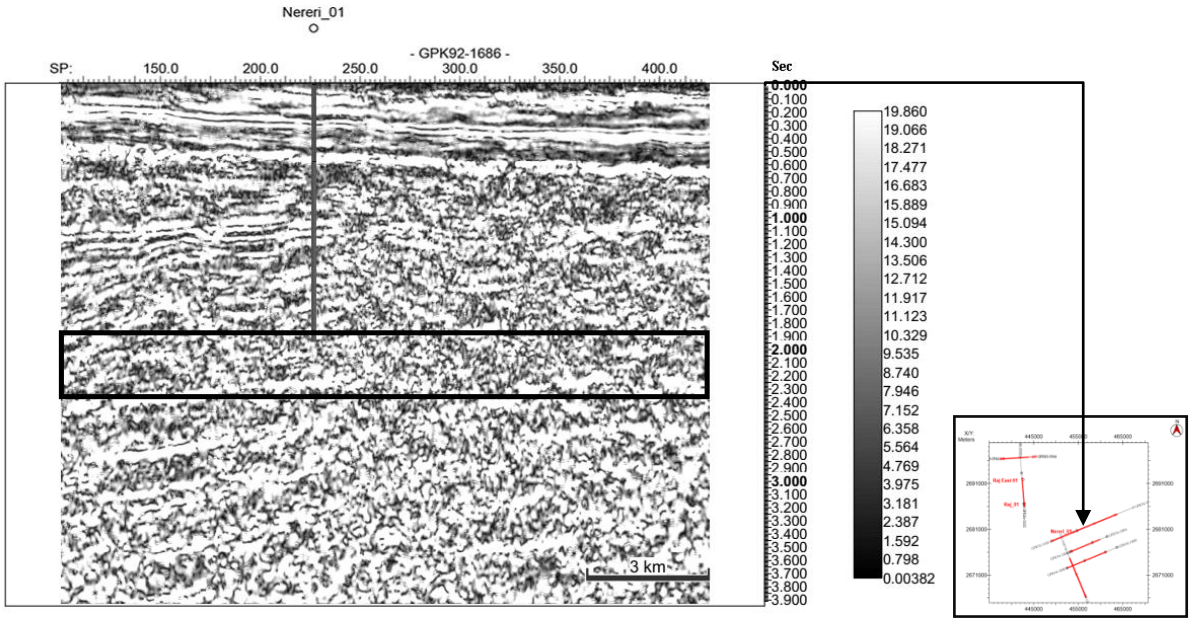

Figure 4.16 Reflection Strength attribute.

4.2.10 Inversion

The post stack seismic inversion is applied to the seismic data of Badin area. It is the technique which extracts information about properties of the subsurface, which includes the prediction of acoustic impedance from stacked seismic data (Keys and Foster, 1998). The basic model is the convolution model which states that the seismic trace is simply the convolution of the wavelet with the reflectivity series of the Earth (Russell, 1988).

Post-stack seismic inversion has been a extensively utized method for the prediction of subsurface geological information (e.g., lithology, porosity) by performing seismic computation tied to well logs data (i.e., sonic and density). The

inverted seismic data is very useful for detailed seismic data interpretation (Buiting and Bacon 1999). Post-stack inversion gives output as P-impedance, because it utilizes normal incidence reflections and involves specifically near-offset stack data to extract geologically consistent results. This method is generally applied to conventional oil and gas reservoirs (Lee et al., 2013). In post-stack inversion, a band-limited estimate of acoustic impedance, is obtained from seismic amplitudes (Latimer et al., 2000). This derived acoustic impedance from seismic inversion can be transcribed into petrophysical parameters, and combined with the structural framework to create a model of the reservoir (Yilmaz, 2001).

Colored Inversion is a fast mean of converting seismic trace data into seismic impedance data. It is band limited and introduced by Lancaster and Whitcombe (2000). It has characteristic of utilizing single operator yielding relative impedence with convolution of reflectivity data. It is based on an integration of the amplitude spectrum, including a -90 degree phase shift and a process that shapes the spectrum to look like the trend of the log data. It is require that the input data should be zero-phase. It enhances the seismic signal, removing the high-frequency noises while honoring the well control and provide more accuracy. This technique integrates well information with the seismic data in an attempt to model the expected response of the strata within the bandwidth of the seismic. The colored inversion is applied where the phase of the data is uncertain, and requires matching events to the well data accurately. Therefore, this method has property to enhance the thin beds and discontnuities (Lancaster and whitcombe, 2000).

Without limitation, there may be numerous outcomes with different low-frequency patterns, all uniformly fulfilling the observation. In figures 4.17 the inverted seismic data is displayed. Figure 4.18 depicts the color inversion with better resolution power. The results of colored inversion are displayed in figures below. From this attribute, we have impedance values of the seismic line, which creates match with response of seismic bandwidth. It characterize higher porous lithological characteristic of Sembar Formation. This may be helpful in identifying hydrocarbon fluid accumulation in Sembar Formation region.

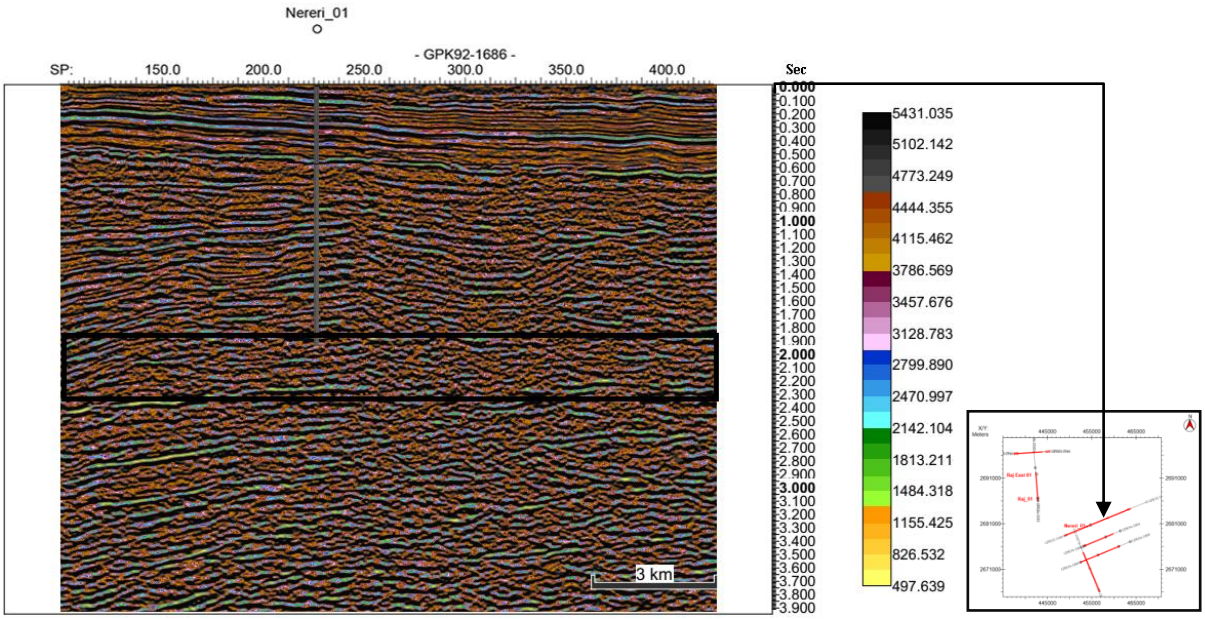

Figure 4.17 Colored inversion.

4.3 Conclusion

This study concludes about application of various post-stack seismic attributes for the detailed interpretation of seismic data. Horizons, faults, major lithological boundaries of Sembar Formation are studied by application of these attributes. Therefore, this attribute analysis acted as validating tool for seismic interpretation and pertophysical studies of Sembar Formation.

From amplitude attribute reflection strength measurements are taken. Sembar Formation, which is shale in lithology, the amplitude or reflection strength, is different from above lying lithology of Lower Goru Formation. The amplitude for Sembar Formation at seismic line GPK92-1686 ranges between 17 to 26 dB which is the indicator of lower chance of mature hydrocarbon. In case of spectral decomposition attribute application on seismic GPK92-1686, the best spectral decomposition envelope for Sembar Formation is sub band 17.Hz. The Sembar Formation has week coherence in amplitude but coherent in phase angel which tells the zero phase region. The phase information is applied for lithological and reservoir characterization. Instantaneous phase attribute is the superior gauge of lateral continuity. Instantaneous phase attribute of Sembar Shale showed week coherence in amplitude but depicted the coherent based on consistent phase angel. Therefore, the

Sembar Shale horizon lied over the zero phase in the study area. Instantaneous frequency (Hz) is the change of phase with the period. On seismic line GPK-92-1686 is confirming the fault and horizon interpretation at Sembar Formation level. The high value of instantaneous frequency is showing shale of Sembar Formation. Sweetness is indicating the bright spot of existence of Hydrocarbons. In Sembar Formation, sweetness attribute shows value of range between 12 and 30. These ranges of values show the presence of hydrocarbons in Sembar Formation.

Average Energy is basically later continuity attribute and highlights the lithology strength. Sembar Formation has low average energy as compare to overlying Lower Goru Formation. Shale Indicator is for shale zone detection, it gives higher values for Sembar Formation region, which is confirming the shale presence, while lower and upper Goru formations giving low values. Trace Envelope is computed for seismic line GPK-92-1686. Minimum reflection strength is indication of the package of Sembar Formation with relative higher porous lithology. It also showed spatial patterns representing changes in the thickness of the Formation and breakage due to the faults. Therefore, this attribute analysis confirms the demarcated Sembar Formation has shale contents.

CHAPTER 5

PETROPHYSICAL AND ROCK PHYSICS ANALYSIS OF SEMBAR FORMATION

5.1 Introduction

Hydrocarbon production from organic rich unconventional shale formations are gaining pace, because of availability of sophisticated and economical techniques of recovery. For formation economical potential, some properties are considered to be critical, which includes hydrocarbon saturation, porosity, and brittleness etc. The well logs data is usually are used to predict these petrophysical and rock properties information.

Rocks are constituted of various minerals and their physical properties based upon their composition, saturation, pores, cementation and textures etc. Rock-physics is the tool to compute and classify the geological properties (lithology, porosity, saturation, etc) of formations at certain physical condition (pressure, temperature) in correspondence with elastic and seismic properties. These approaches can be utilized for rock physics understanding. (Guéguen and Palciauskas, 1994; Mavko et al., 2009). Therefore, main emphasis of this study is the rock physics and petrophysical evaluation of Sembar Formation at Badin block. The ultimate objective of petrophysics and rock physics analysis is to predict physical properties of Sembar shale in the area of interest (AOI) from well logs (Avseth et al., 2010). These log analysis filled the gap between seismic and geology.

For rock physics, the variables P-wave velocity (Vp), S-waves velocity (Vs), Density (ρ), and derivates such as P-impedance, S-impedance are required for attributes calculations for bulk modulus, (K), shear modulus (μ), and young modulus (E). These variables and attributes are used to determine lithology types in the subsurface. The cross plots between calculated attributes and variables from well logs

have been generated. These cross plots could be helpful in interpreting fluid types and rock properties (Omudu et al, 2007).

Rocks with higher bulk density have greater seismic velocities. More density oils have more bulk moduli (lower compressibilities). This result, rocks with more density oils have higher compressional properties and shear impedance, but shear velocity may be less. Shale has characteristic of higher values density and V_P as compare to sand. Higher density oils have more bulk moduli (lower compressibilities). Rocks with large density oils have large compressional properties and shear impedance.

The key technique for producing from unconventional shale formations with low permeability is to hydraulically fracture the tight formation. The more brittle and less ductile formation is easier to fracture due to lesser plastic deformation (Zehnder, 2012). It should be positive by correlated in terms of young modulus and poisson's ratio. Therefore, the brittleness of a shale formation is important property for prospect. The vertical and lateral variation of brittleness is a major factor for selecting a drilling location and a particular zone of interest. Shale containing more quantity of quartz, feldspar and carbonates, have low poisson's ratio, more young's modulus and more brittleness (Ding et al., 2012). Shale formation which composes of higher siliceous and calcareous material is more brittle and prone to natural and induced fracturing, or hydraulic fracturing as well. Lithologies with less siliceous and calcareous contents, and higher clay mineral content, yield a more ductile zone which is proven good seal for hydrocarbon. In literature, brittle index is analyzed from cross plot of poisson's ratio and young's modulus, which give the index of the rock strength to fail under stress (Grieser and Bay, 2007; Rickman et al., 2008). The shale rock with less poisson's ratio and high young's modulus, have better brittleness characteristic.

According to Fertl (1979), utilization of gamma ray for shale differentiation may develop errors because shale radioactivity differs appreciably from one shale to another and not most of the shales are radioactive. Heslop (1974), utilized the gamma-ray (GR) log response as a computation of clay content. The GR log mostly performs good for this objective, but not always. Not all clay minerals are notably radioactive

and which are radioactive can vary significantly in concentration of radioactive elements (Fertl, 1979). On the basis of petrophysical properties of rocks, Katahara (2008) suggested a method for distinguishing shale radioactiveness, which is depend on the differentiation of neutron porosity and density porosity. It is also more suitable for computing clay contents. Neutron logs are porosity logs that compute the hydrogen concentration in a lithology. In clean lithology (shale-free), where the pores are filled with water or oil, therefore, hydrogen is concentrated in the fluid-filled pores. Whenever shale is part of the formation matrix, the neutron porosity may be larger than the actual formation porosity. With the presence of organic content, density decreases. Variation of density specifies porosity changes e.g., low density indicates high porosity (Akinyokun et al., 2009).

5.2 Methodology

For petrophysical analysis, well log data was interpreted. Porosity, Volume of shale, water and hydrocarbon saturation etc, are the variables used to characterize the petrophysical properties of the Sembar Formation. For rock physics cross plot technique was opted.

The main variables of petro physics of Sembar Formation were computed by using available log data of the give three wells. Average porosity defines the average to sum of all porosities in the formation. Average porosity and effective porosity were computed using equation 1

$$\emptyset_A = \frac{\emptyset_D + \emptyset_N}{2} \qquad \text{Eq. 1}$$

$\emptyset_A$ was average porosity, $\emptyset_D$ was density porosity and $\emptyset_N$ was neutron density (Adagunodo et al., 2017).

The higher the porosity of the shale, more amount of water will be in the pore spaces, with low resistivity values. Effective porosity is total porosity minus the clay volume. Equation 2, represent the effective porosity computation.

$$\emptyset_E = \emptyset_A \times (1 - V_{Sh}) \qquad \text{Eq. 2}$$

$Ø_E$ is effective porosity, $Ø_A$ is average porosity and V_{sh} is volume of shale (Adagunodo et al., 2017).

Water saturation is significant component in evaluating a shale prospect. The estimation of water saturation is difficult from log data interpretation for organic rich source formation which has high porosity and low permeability. The water saturation values were calculated using Indonesian equation (Leveaux and Poupon, 1971) developed by field observations in Indonesia, which usually applied to calculate water and brine saturation as a function of resistivity of the shaly formation with high amount of shale. Shale amount must be 30% to 70% in the formation for the Indonesian equation. Indonesian equation is mentioned in equation 3.a and 3.b

$$\frac{1}{R_t} = S_w^{n/2}\left(\frac{V_{sh}^{1-V_{sh}/2}}{\sqrt{R_{sh}}} + \left(\frac{\phi^{m/2}}{\sqrt{a}R_w}\right)\right) \qquad \text{Eq. 3.a}$$

$$S_w = \frac{1}{R_t}\left(\frac{\sqrt{aR_wR_{sh}}}{V_{sh}\sqrt{aR_w} + \phi^{m/2}\sqrt{R_{sh}}}\right)^{n/2} \qquad \text{Eq. 3.b}$$

Where S_w is water saturation, R_t is formation resistivity of un-invaded deep formation, R_{sh} is the average value of the deepest resistivity curve reading in shale, V_{sh} is the volume of shale in the formation (%), Ø is porosity, m is cementation exponent, *a* is value of unity (tortuosity factor), n is saturation exponent and formation brine water resistivity is presented by R_w at formation temperature. In equation 2 exponent V_{sh} is eliminated.

Hydrocarbon saturation can be computed by subtracting water saturation percentage from 100 as given in equation 4

$$\boldsymbol{S_{hc} = 1 - S_w} \qquad \text{Eq. 4}$$

where: S_{hc}= hydrocarbon saturation in %, S_w = water saturation in %.

Therefore, various logs are utilized for computation of different petrophysics variables, for example, sonic log has been used for the calculation of porosity. Density log computes the bulk density of a formation. Typically applied for porosity measurement.

Elastic parameters were utilized to infer the quantitative information for Sembar Formation. In this study cross plot techniques are adopted. Cross-plotting of different factors is a strong mean for illustrative analysis and supportive in highlighting the data clusters in the zones of interest (White 1991). Cross plotting technique is utilized for identifying the formation lithology, fluids type and porosity (Burke et al., 1969). The objective of this analysis is to demark litho-characteristics by utilizing sonic, density, and neutron logs data for Sembar Formation.

Different combination of attributes in form of cross plots had been generated for the study of lithology and fluid properties of Sembar Formation. First cross plot was between Vp and Vs for wells i.e., Nereri-01, Raj East-01, Raj-01 as shown in figure 5.5. Theoretically, shear wave velocities are around half of the primary waves velocities. But this difference depends on the depth and lithology. The relationship of Vp versus Vs in organic shale had been documented by many researchers (Vernik and Liu, 1997). Usually, Vp decrease with declining water saturation (i.e., increasing gas saturation) but Vs increase by about 20%. The cross plots of Vp/Vs versus Vp are generated respectively. Vp/Vs was computed by taking the ratio of Vp shown in figure 5.6.

Plotting the young's modulus versus the poisson's ratio helps in finding the brittleness of the formation. Higher value of young modulus and lower value of poisson's ratio of the formation shows brittleness of lithology with low plastic nature.

The difference between elastic rock properties i.e. acoustic impedance (AI) and shear impedance (SI) may be due to differences in the fundamental mineral properties and variation in elemental composition of the quartz grains, water saturation, TOC, and porosity etc. The directly proportional pattern of acoustic impedance and shear impedance shows water saturated shale lithology i.e., on higher trend dominantly wet shale exists. Vertical increase in trend of shear impedance shows the presence of oil and organic contents in shale. Higher values of acoustic impedance and moderate to high value of shear impedance relationship depict the presence of shale lithology. Compressed rocks have more seismic velocities (compressional and shear impedances) because of connectivity.

Cross plot of neutron porosity and sonic log values is the tool to specify the lithology of the formation and fluid content present in that lithology. The cross plotting between neutron porosity and density porosity is used to compute the clay content (Katahara, 2008). Density-Neutron porosity cross plot is the most effectual mix for lithology characterization. ΦN is plotted on x-axis and ρb is plotted on y-axis.

5.3 Results and Discussions

For the petro-physics and rock physics analysis of Sembar Formation, the log data of three wells, Nereri-01, Raj East-01 and Raj-01, was analyzed and results are presented below in table 5.1.

Table 5.1. Petrophysics calculations for Nereri-01, Rajeast-01 and Raj-01.

Well Name	Sembar Thickness (m)	PHIA (%)	PHIE (%)	PHID (%)	PHIS (%)	V. Sh (%)	V. Sd (%)	Sw (%)	Sh (%)
Nereri_01	31	27	5	16	37	89	11	22	78
Rajeast_01	36	28	7.1	17	39	86	14	23	77
Raj_01	116	34	8.6	19	44.3	83	17	26	74

In Nereri-01 well, average porosity for Sembar Formation ranged is 27% and effective porosity is 5% due to higher shale contents in the formation. The average porosity reading of Sembar Formation at Nereri-01 depicts the characteristic of shale lithology. In nereri-01 volume of shale noted is 89% and low content level of sand which is just 11% of the lithology. Saturation of water is 22% and saturation of hydrocarbon is 78%, which is the good carbon content in the lithology.

For Raj East-01 well of Badin Block, Sembar Formation averages porosity noted values is 28%. The effective porosity for the Raj East-01 is 7.1%. The value of average porosity is bit higher as compared to Nereri-01. Water and hydrocarbon saturation computed results showed 23% and 77% respectively for Rajeast-01. Therefore, Sembar Formation at Raj East-01 well also shows good quantitative values of carbon contents in the lithology.

Evaluation of Sembar Formation of Raj-01 well result the average porosity value 34%. Similarly, effective porosity of Raj-01 well noted is 8.6. Saturation of water and hydrocarbon in Sembar Formation at Raj-01 well are 26% and 74%.

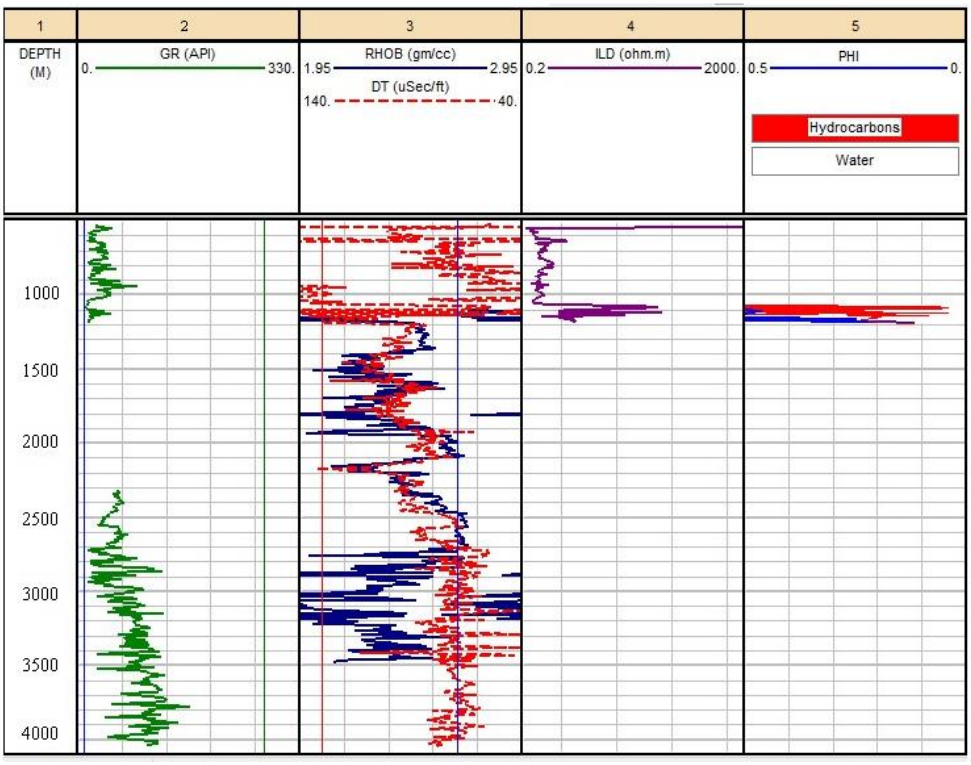

Figure 5.1 Basic Log Analysis of Raj-01 well

Figure 5.2 Clay Volume Analysis for Raj-01 well

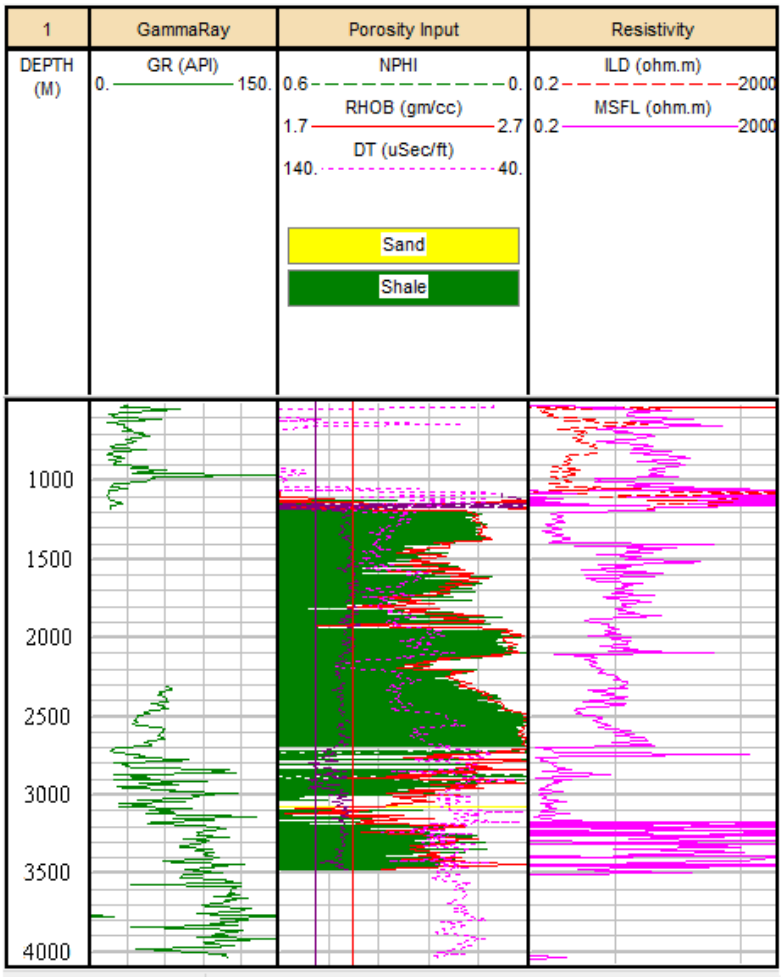

Figure 5.3 Water-Hydrocarbon Saturation of Raj-01

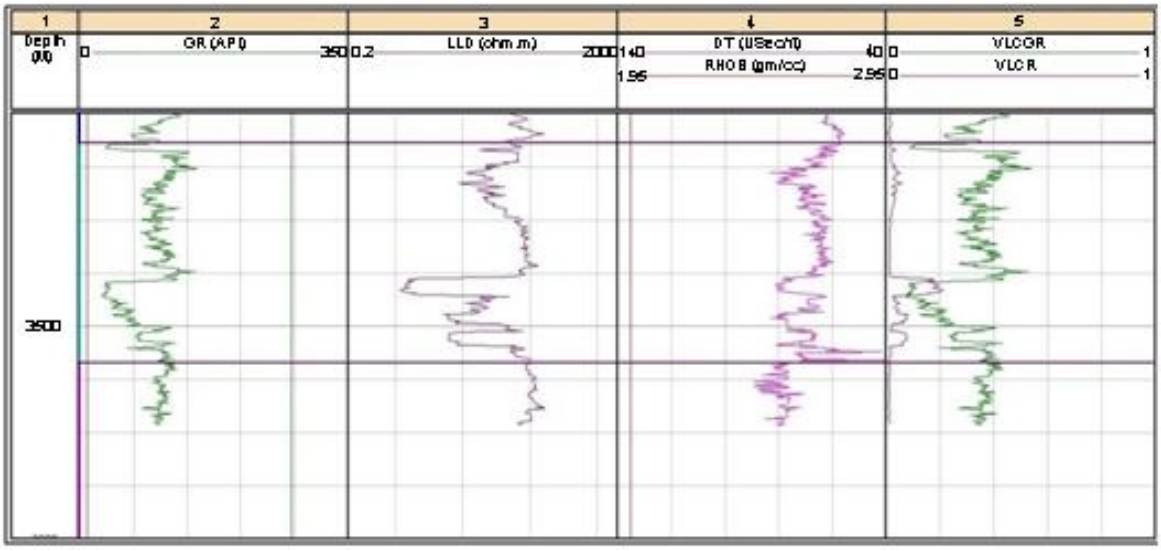

Figure 5.4 Petrophysics of Sembar Formation at Raj-01 well

For Rock physics study for Sembar Formation of all three wells are utilized (Nereri-01, Raj East-01, and Raj-01) for cross plot evaluation and results are presented below.

The results of cross plot of Vp versus Vs in Sembar Formation at Nereri-01, Raj East-01 and Raj-01 wells show linear relationship as displayed in figure 5.5. The results showed the increasing trend of porosity and pore pressure, while reduced velocity ratio was observed. The lower ratio values are due to shale and shaly sand contents in the Sembar Formation. The calculated Vp/Vs ratio values vary between 1.35 and 1.7. The data points showed constant proportional trend despite of saturation, porosity etc. In case of Raj-01 well the values of Vp/Vs ratio range between 1 and 1.35. Reduced velocity ratio usually depict the organic shale containing small amount of kerogen.

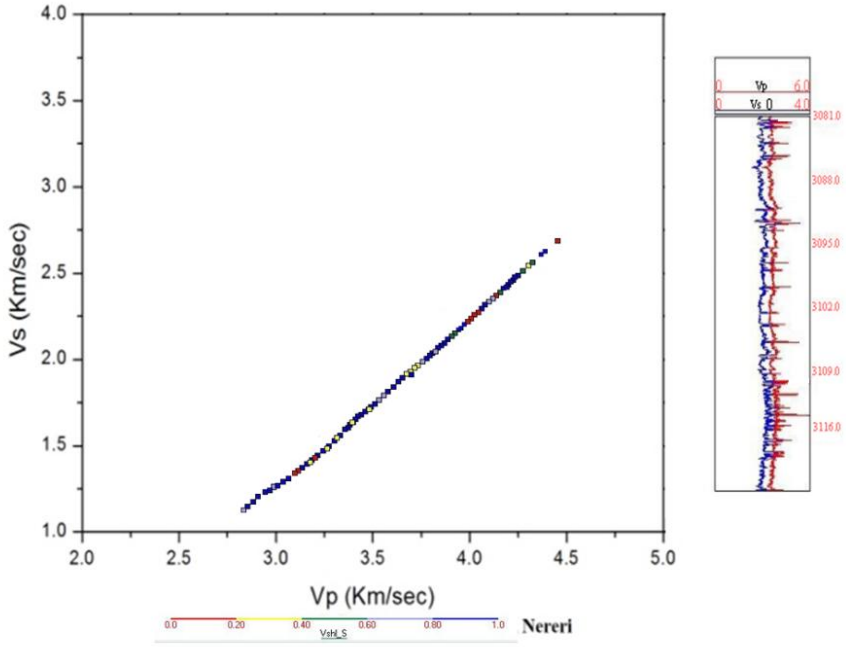

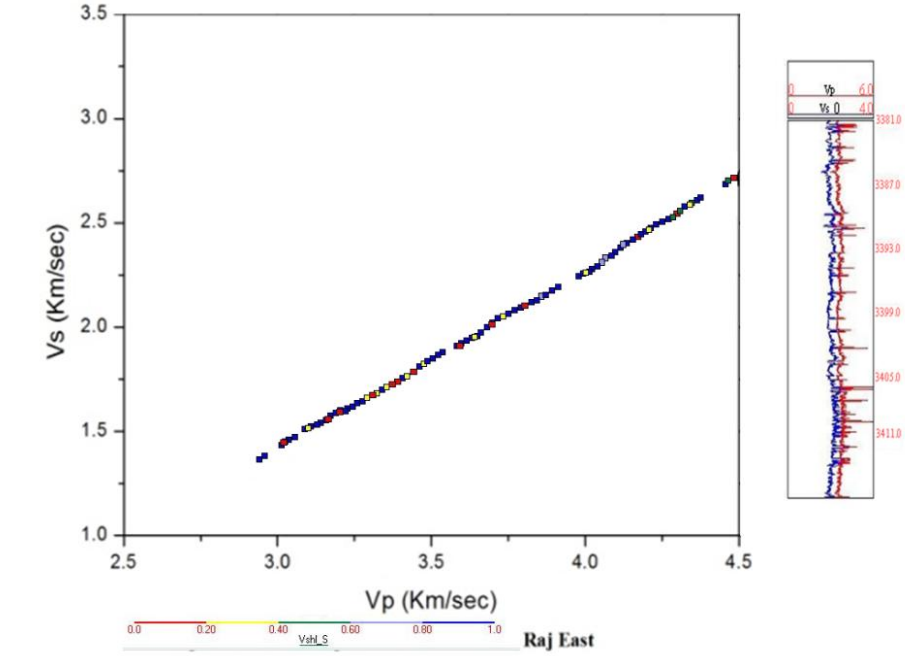

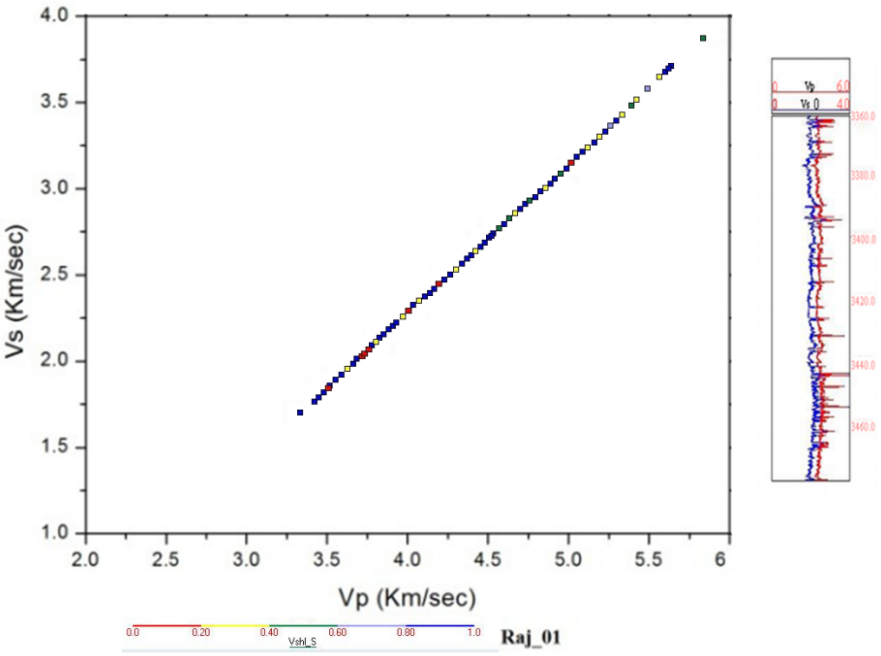

Figure 5.5 Cross plot relationship between Compressional velocity and Shear velocity

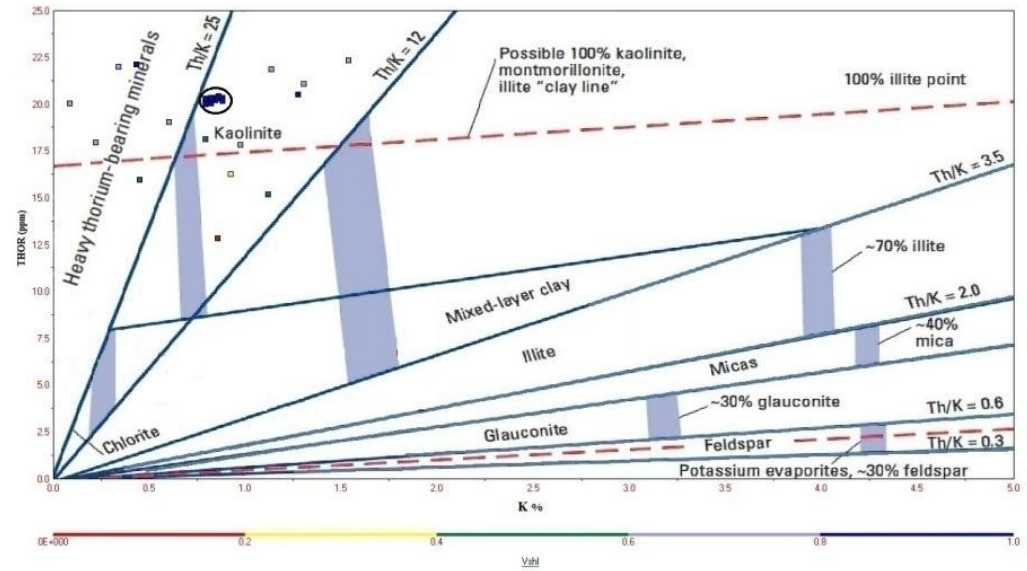
Heavy thorium-bearing minerals
Th/K = 25
Th/K = 12
Possible 100% kaolinite, montmorillonite, illite "clay line"
100% illite point
Kaolinite
Th/K = 3.5
~70% illite
Mixed-layer clay
Illite
Th/K = 2.0
~40% mica
Micas
~30% glauconite
Th/K = 0.6
Glauconite
Feldspar
Th/K = 0.3
Chlorite
Potassium evaporites, ~30% feldspar
THOR (ppm)
K %
Vshl

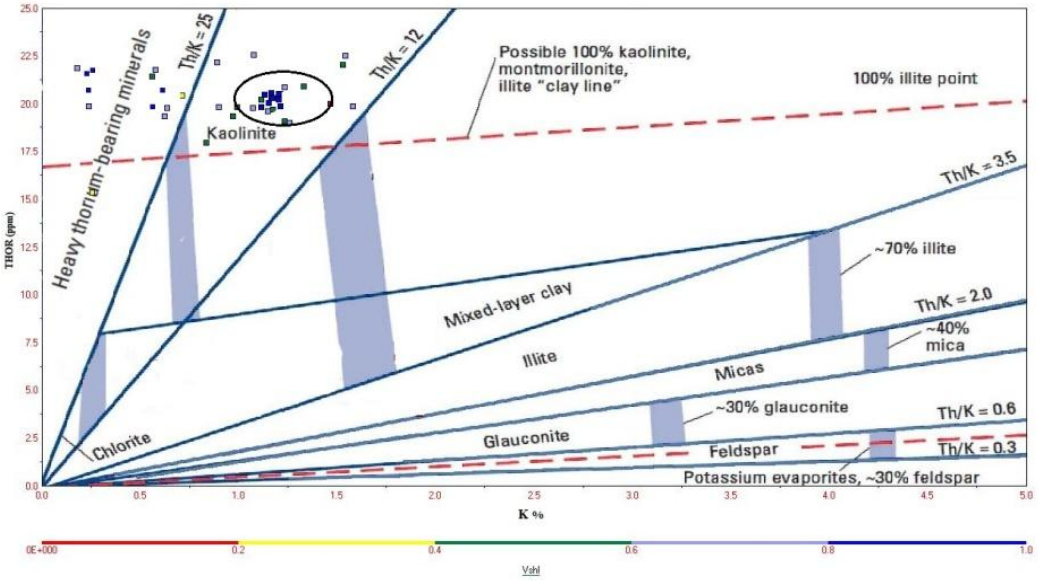
Heavy thorium-bearing minerals
Th/K = 25
Th/K = 12
Possible 100% kaolinite, montmorillonite, illite "clay line"
100% illite point
Kaolinite
Th/K = 3.5
~70% illite
Mixed-layer clay
Illite
Th/K = 2.0
~40% mica
Micas
~30% glauconite
Th/K = 0.6
Glauconite
Feldspar
Th/K = 0.3
Chlorite
Potassium evaporites, ~30% feldspar
THOR (ppm)
K %
Vshl

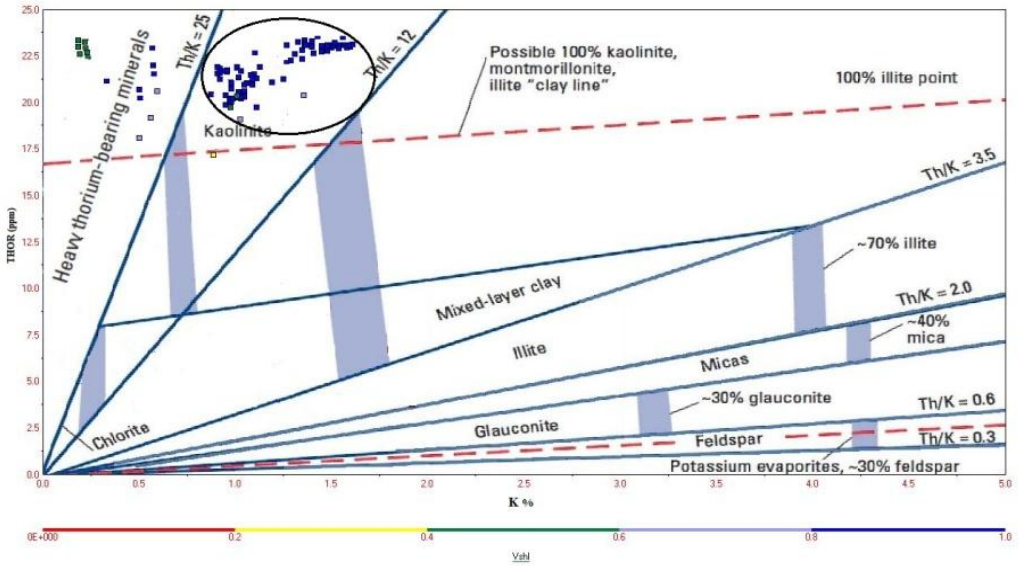

Figure 5.6 Lithology identification plots for the Nereri-01, Rajeast-01 and Raj-01.

Organic materials have a low density (typically 1.1 to 1.4gr/cc) (Passey et al., 2010) consequently increasing the organic material would result in decreasing formation bulk density and decreasing sonic velocity (compressional or shear wave velocity). This decreasing trend of sonic velocity could affect the result of poissons ratio extracted from wave form. The cross plot of youngs modulus and poissons ratio is displayed in figure 5.7. With the increasing TOC content of the rock samples the young's modulus decreases while the poisson's ratio increases. The cross plot of all three wells showed the decreasing trend of young's modulus with increase in poission ratio. Therefore, lower value show brittle nature while higher values depict the ductile nature. In relation to above discussion more brittle be shale, there will be more chances of natural fracturing and could response better to hydraulic fracturing treatment.

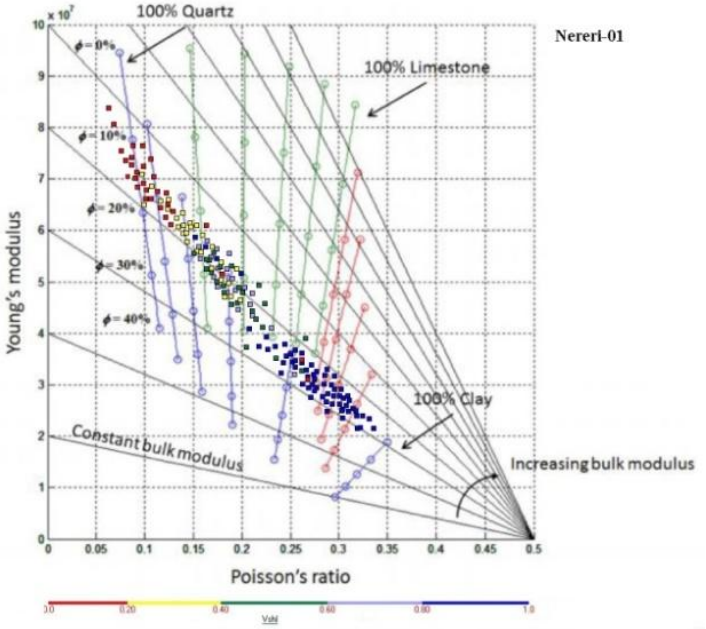
Nereri-01
100% Quartz
100% Limestone
100% Clay
Constant bulk modulus
Increasing bulk modulus
Young's modulus
Poisson's ratio
x 10^7
ϕ = 0%
ϕ = 10%
ϕ = 20%
ϕ = 30%
ϕ = 40%
VsN

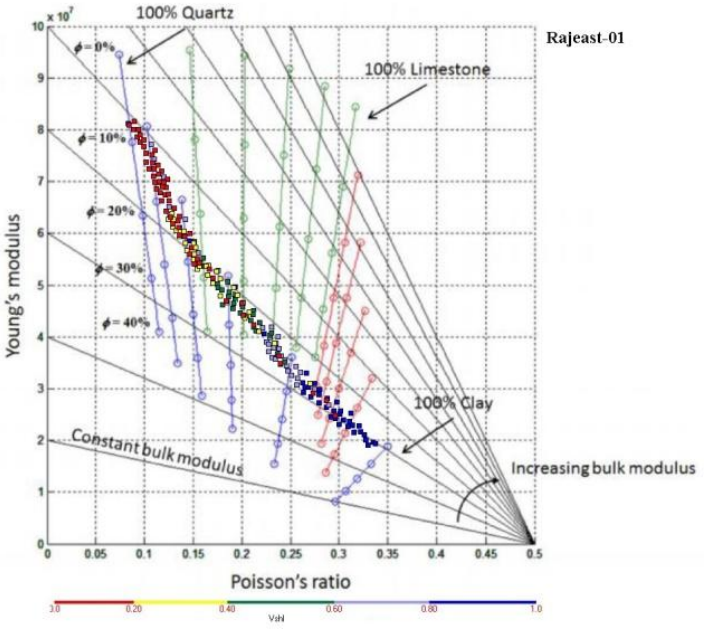
Rajeast-01
100% Quartz
100% Limestone
100% Clay
Constant bulk modulus
Increasing bulk modulus
Young's modulus
Poisson's ratio
x 10^7
ϕ = 0%
ϕ = 10%
ϕ = 20%
ϕ = 30%
ϕ = 40%
VsN

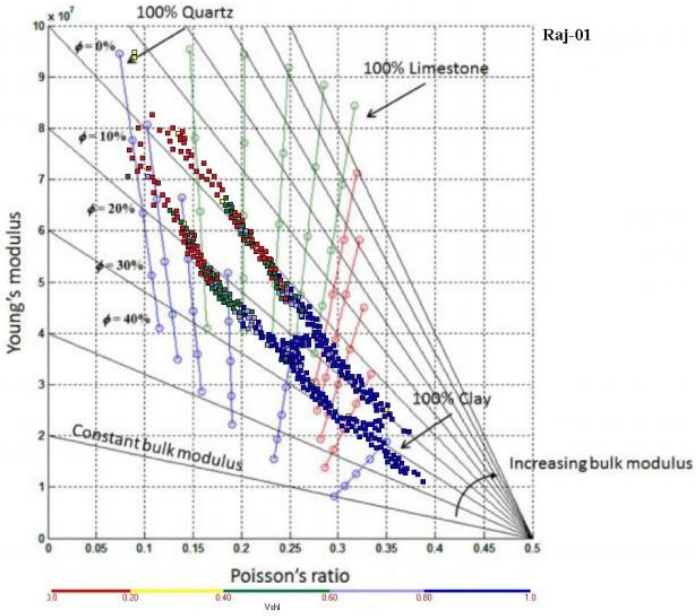

Figure 5.7 Cross plot between poission's ratio and young's modulus of Sembar Formation

The crossplot of acoustic impedance versus shear impedance computed from well-log data is shown in figure 5.8. In the cross plots of three wells, the lower values are due to gas effect and higher values due to water saturation. Therefore, the data with low acoustic impedance show the high porosity and more gas saturation. Lower values of SI, AI are indicators of increasing porosity trend. The directly proportional relation of the AI and SI depicts the presence of shale and shaly sand lithological contents of the Sembar Formation (Chi and Han, 2009).

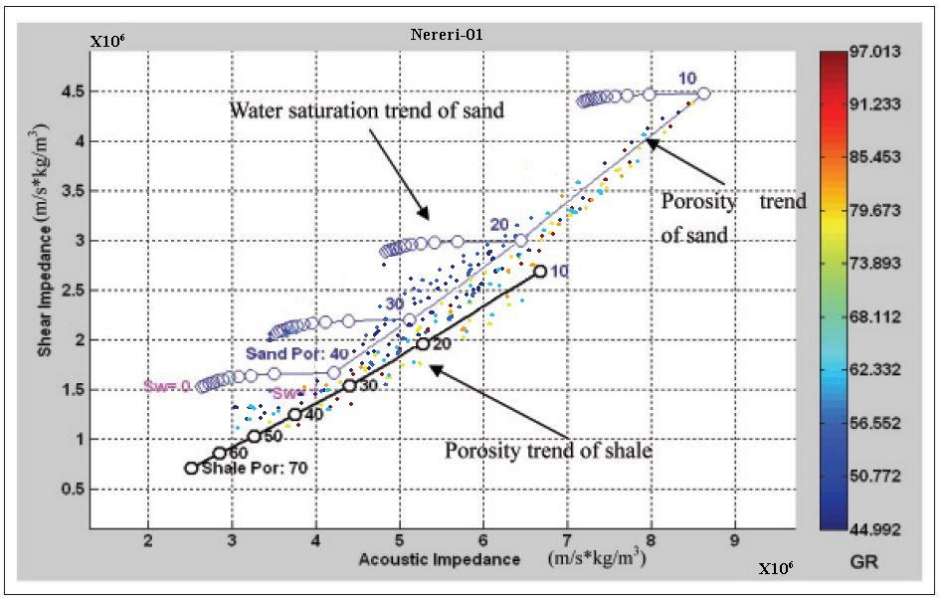
Nereri-01
X10⁶
Shear Impedance (m/s*kg/m³)
Acoustic Impedance (m/s*kg/m³)
X10⁶
GR
97.013
91.233
85.453
79.673
73.893
68.112
62.332
56.552
50.772
44.992
Water saturation trend of sand
Porosity trend of sand
Porosity trend of shale
Sand Por: 40
Shale Por: 70
Sw=1.0
Sw=0
10
20
30
40
50
60

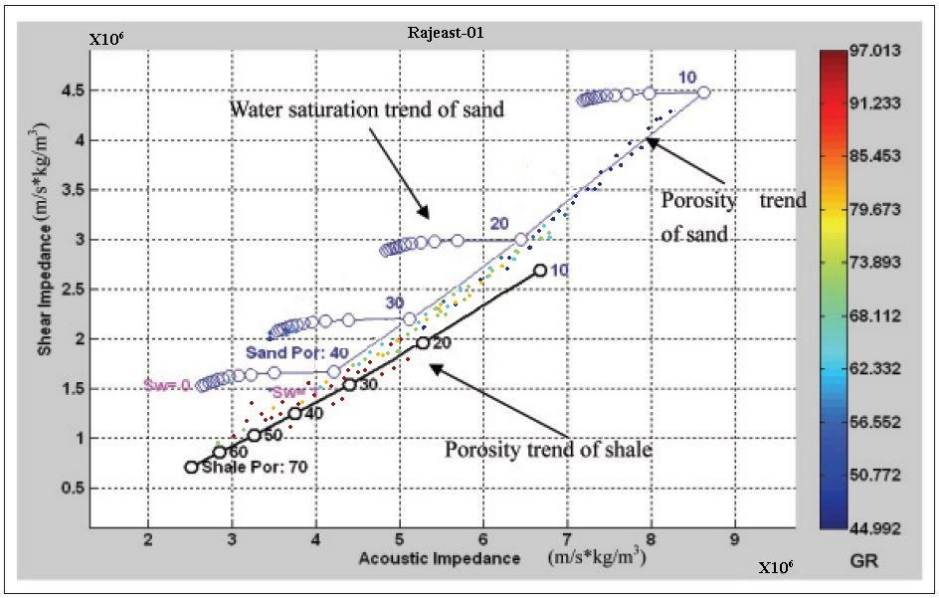
Rajeast-01
X10⁶
Shear Impedance (m/s*kg/m³)
Acoustic Impedance (m/s*kg/m³)
X10⁶
GR
97.013
91.233
85.453
79.673
73.893
68.112
62.332
56.552
50.772
44.992
Water saturation trend of sand
Porosity trend of sand
Porosity trend of shale
Sand Por: 40
Shale Por: 70
Sw=1.0
Sw=0
10
20
30
40
50
60

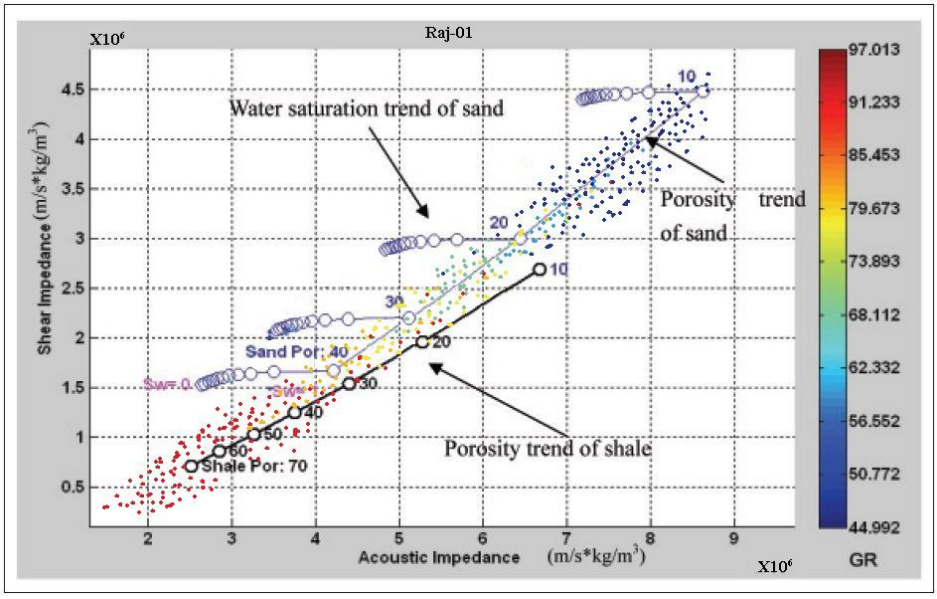

Figure 5.8 Cross plot between acoustic impedance and shear impedance of Sembar Formation

The aim is to analyze petrophysics and rock characteristics of Sembar Formation in all the three wells. Petrophysics results that the shale characteristics of Sembar Formation having higher porosity and fluid contents. The rock physics study predicted elastic rock properties for the lithology characterization.

CHAPTER 6

MEASUREMENTS OF TOC

6.1 Introduction

For the estimation of the hydrocarbon potential in Badin block, it is significant to assess the source rock in terms of total organic carbon (TOC) and level of organic maturity (LOM) by utilizing the geochemical data. However this study utilized the theoretical approach to compute TOC and maturity of organic matter, which is depend on logs, overlay technique to measure the organic maturity. The Sembar Formation show comparatively high values of gamma ray, high sonic transit time, high resistivity with decrease in density as displayed in table 6.3. This method provides the measurable data about TOC and maturity of the source rock where the geochemical data is not existing.

Shale play include high total organic carbon (TOC) content, thermal maturity (R_0 %) with low clay content along with higher brittleness act as key feature. Other important factors are reservoir thickness and gas in place (GIP) (Chopra et al., 2012). Shale gas is term for gas production from fine grained organic rich gas prone rocks also know as unconventional gas resources (Lakatos and Szabo, 2009). The main factors on which source potential estimation depends include total organic content and level of maturity of source rock. These factors are calculated through the geochemical sedimentological methods.

TOC is the amount of carbon present in the rock and is presented as a proportion by weight contained in the rock (Glorioso and Rattia, 2012). TOC is mostly utilized to assess the quality of source rock i.e., utilized in measurement of unconventional reservoirs. Generally TOC and kerogen are strongly linked with shales and silt rich claystone however they can also be exist in many carbonates. TOC

economic shale-gas potential require adequate organic matter to generate good amounts of hydrocarbons; Table. 6.1. shows TOC quality.

Table. 6.1 Total organic carbon (TOC) content quality (Peters and Cassa, 1994)

Quality	**Total Organic Carbon, Weight %**
Poor	**<0.5**
Fair	**0.5 to 1**
Good	**1 to 2**
Very Good	**2 to 4**
Excellent	**>4**

Table. 6.2 as below shows the least values required for viable discovery as reported in different studies.

Table. 2 Values for commercially viable reservoir (Dong et al., 2013)

Parameter	**Minimum Value**
TOC	> 2 %
Ro	> 1 %

The composition of petroleum in a source rock changes values in response to change of temperature and pressure conditions. With increasing temperature/ pressure as increase in depth of burial leads to thermal maturation of the hydrocarbon. The trend is established where the lighter fractions increase as the density of oil decrease in the series from oil, to lighter oil, to wet gas, and finally dry gas. Source rocks are typically composed of fine to very fine grained sediments (Dong et al., 2013). Organic matter (OM) is the main component for identification of source rock which is expressed in terms of TOC.

6.2 Methodology and Process

TOC is the key gauge for the classification of shale gas reservoirs. TOC is typically calculated by the cores, cutting or sidewall cores in the laboratory. Due to the inadequate number of core samples, the experimental results are not continuous nature and it is unfeasible to show the complete portrait of a source rock bed. From

well logs, several methods have been introduced to compute the TOC. In this research work, ΔlogR technique (Passey et al., 1990) is opted for analysis of Badin block because of its reliability.

Passey et al., (1990) presented theoretical method for classification of source rocks and calculation of the total organic carbon content. This technique utilizes the overlaying of a properly scaled porosity log on a resistivity curve. The separation of log curves occurs due to organic-richness of lithology, as displayed in table 3. In organic rich source rocks, this separation in organic-rich intervals is gauged and called Δlog R parameter for TOC calculation. Organic-rich intervals can be recognized by separation of the resistivity and sonic, as well as neutron and density curves (Meyer and Nederlo, 1984; Passey et al., 1990). The ΔlogR separation is related linearly to TOC and is function of maturity. ΔlogR separation can be directly converted to TOC if the LOM is estimated through vitrinite reflectance. LOM is found by using Hood et al. (1975) single scale which synthesizes many current indices of organic maturity based on coal rank. The scale relates LOM to vitrinite reflectance among other indicators as shown in figure, 6.1. LOM is unit less.

The Δ logR linearly separation is related to the TOC content and empirical equation for its calculation is:

$$TOC = (\Delta \log R) \times 10^{(2.297 - 0.1688 \times LOM)} \text{ ----------Eq. 1.}$$

where

TOC = Total organic carbon content measured in wt. %

LOM = Level of maturity.

Table. 6.3 Reference table for source rock identification (Passey et al., 1990).

LOG	**Response**
Gamma ray	>150API(Uranium associated with(OM)
Bulk Density	<2.6
Sonic Transit-Time	>140 µs/ft
Neutron porosity	65-67
Resistivity	Increasing Trend

6.3 Results and Discussions

This study utilized logs of three wells i.e., Nereri-01, Raj-01, Raj East-01, for the classification of source rock potential. This technique is based on unconventional logs analysis. Digital logs values were taken for the interval of Sembar Formation at different depths in all three wells. For application of Passey method, available logs of all three wells were analyzed respectively using Petro Mod 1D module, which is freeware module. Source input values of buried formation time in million years and age was Stratigraphy of Pakistan chart developed by GSP, Pakistan. From these input information, burial history, temperature, thermal conductivity and vitrinite reflectance (R_o) of Sembar Formation were calculated from Petro Mod. For Nereri-01 well, resistivity log verses two porosity logs, i.e., sonic and neutron, were utilized. For the case of Raj East-01, resistivity log verses porosity logs i.e., density, neutron and sonic logs were applied. In Raj-01 well, the only porosity log available for analysis is sonic log.

Because core data is not available therefore, the vitrinite reflectance (R_o) of Sembar Formation was calculated by utilizing the burial history, temperature model and thermal conductivity as shown in figures 6.1.a, 6.1.b, 6.2.a, 6.2.b and 6.3.a, 6.3.b respectively. The vitrinite reflectance of wells is shown in figures 6.5.a, 6.5.b. This R_o was correlated from the Hood (1975) coal rank table to calculate the LOM. Vitrinite reflectance is the representation of maximum paleo-temperature exposure to which sediment has been exposed. Therefore, it is important parameter which presents the maturity of organic material to calibrate the thermal and burial history models.

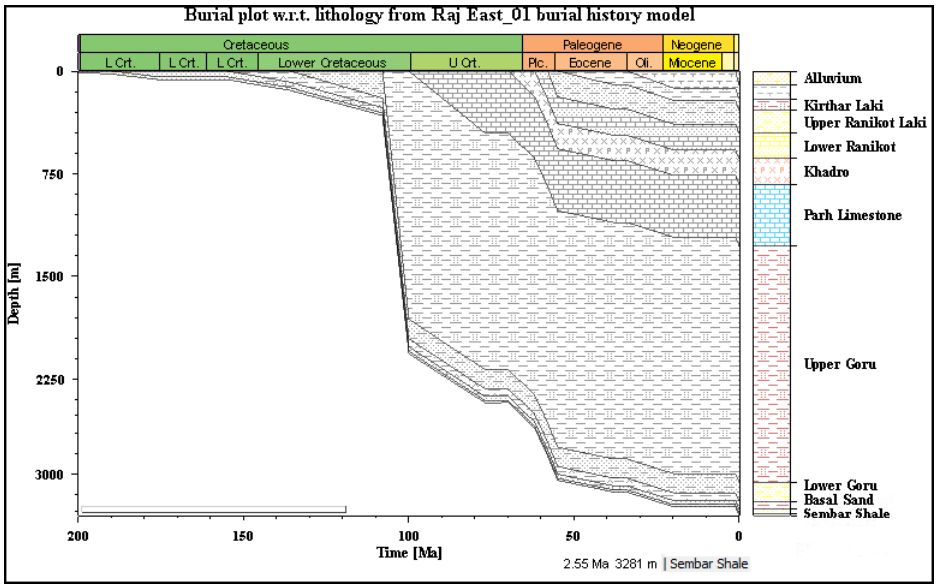

Figure 6.1.a Lithological burial history of Raj East-01

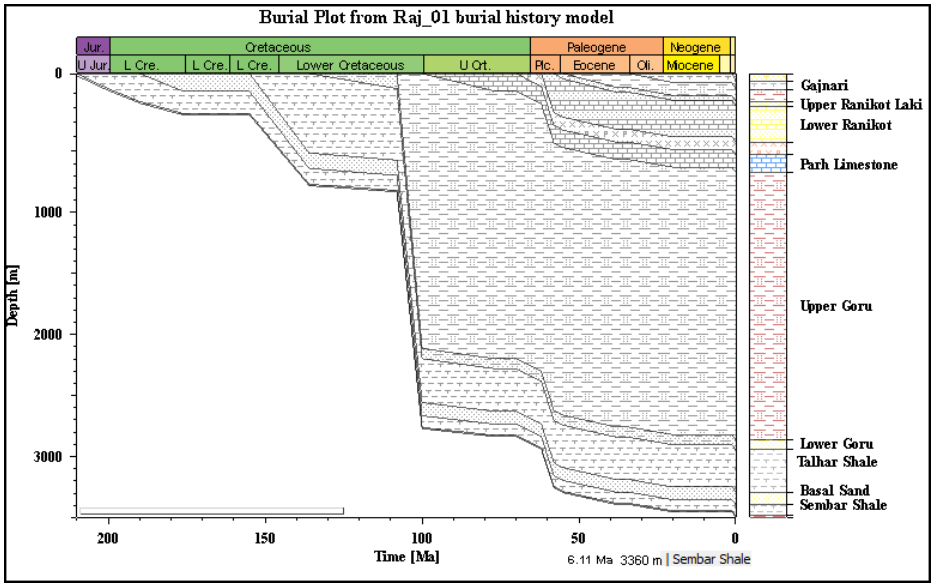

Figure 6.1.b Lithological burial history of Raj-01

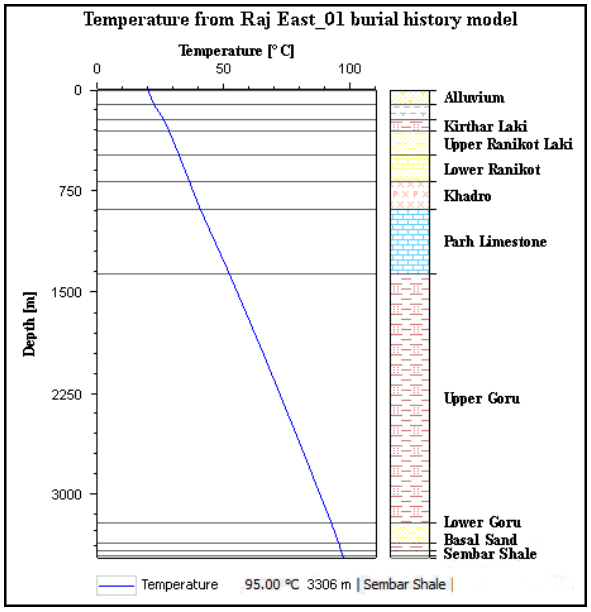

Figure 6.2.a Temperature calculation for Raj East-01

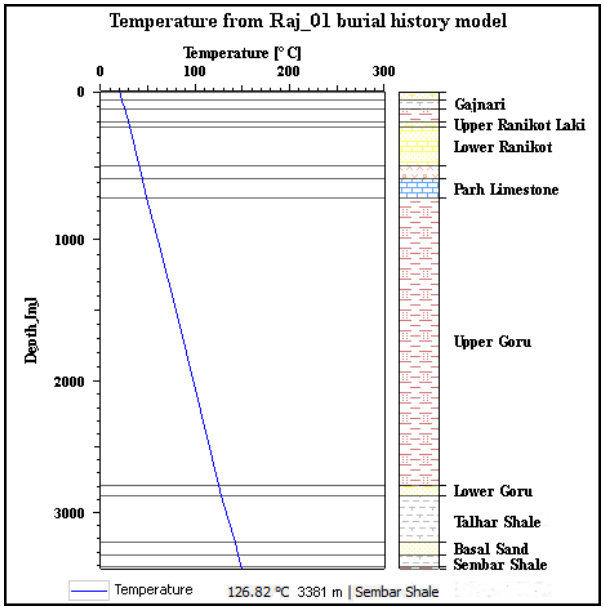

Figure 6.2.b Temperature calculation for Raj-01

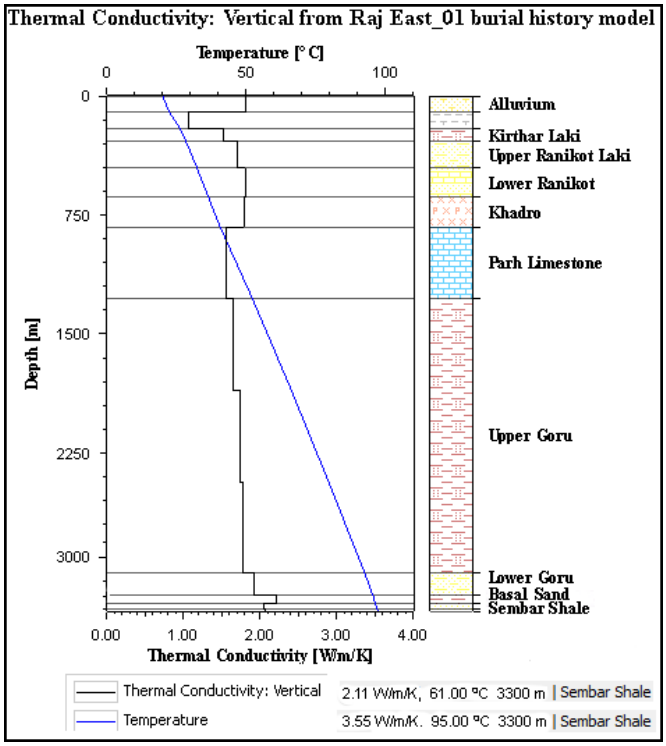

Figure 6.3.a Thermal conductivity calculation for Raj East-01

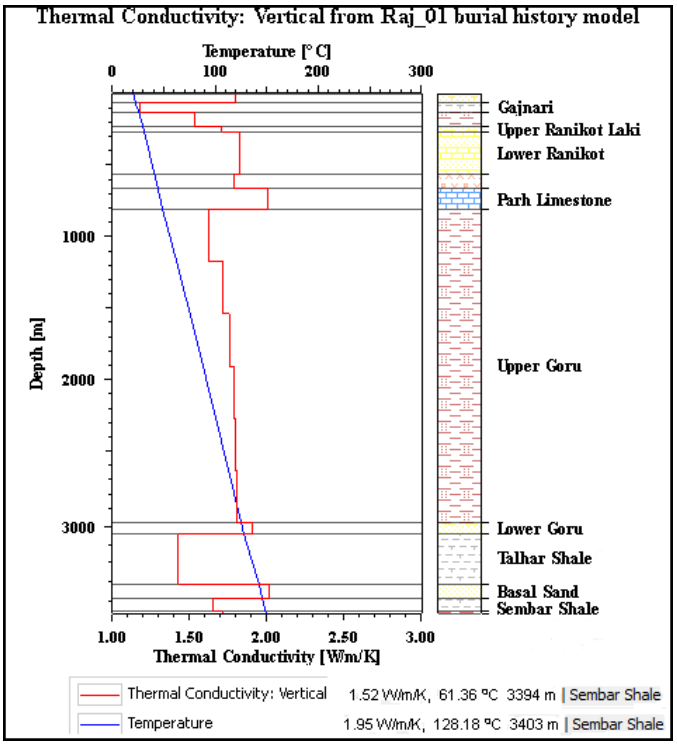

Figure 6.3.b Thermal conductivity calculation for Raj-01

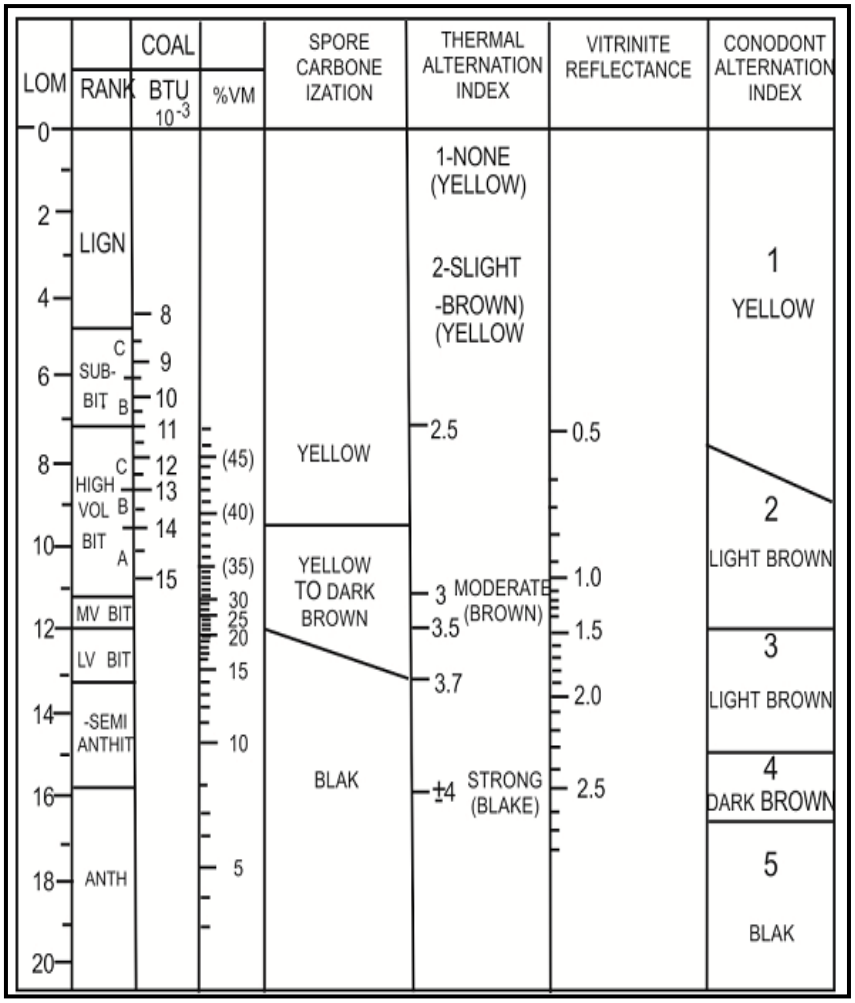

Figure 6.4 Scale for the relation of $\%R_o$ to the thermal maturity indicator i.e., Level of organic maturity (LOM) (Hood, 1975).

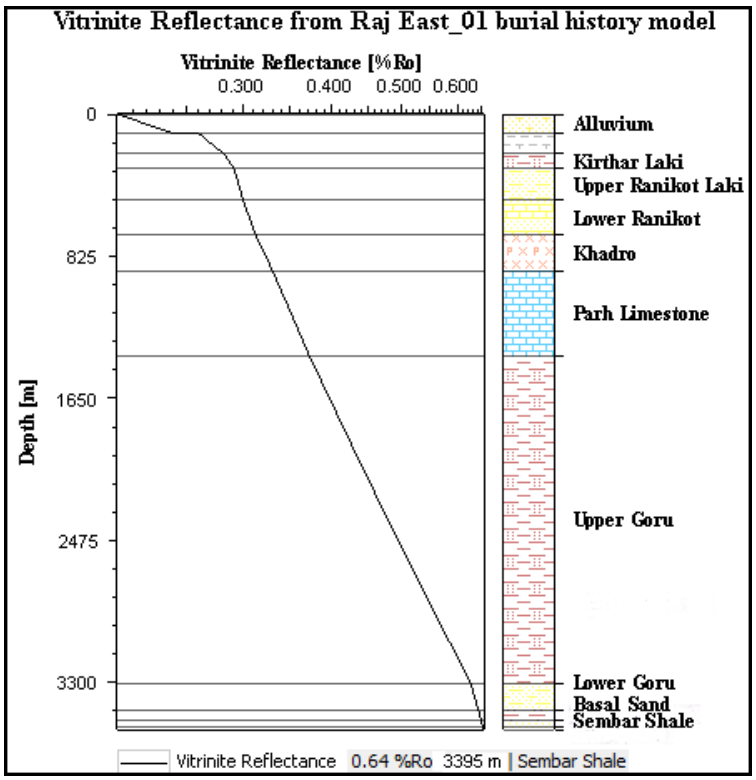

Figure 6.5.a Vitrinite reflectance (R_o) equal to 0.64% for Raj East-01

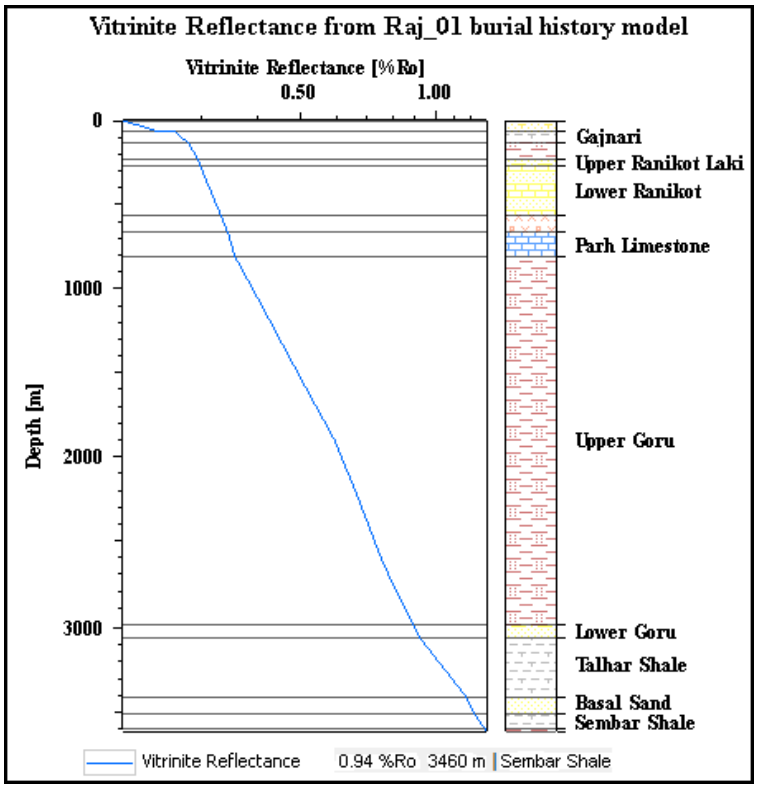

Figure 6.5.b Vitrinite reflectance (R_o) equal to 0.94% for Raj-01

These calculated Ro values of wells are correlated with table as shown in figure 6.4. and corresponding LOM value was noted. The calculated LOM values are 8, 8.5, 10.5 for Nereri-01, Raj East-01, and Raj-01 wells respectively. The values of LOM less than 10 are usually considered being the pre-mature hydrocarbon. Because LOM values of 8, & 9 corresponds to the beginning of maturity for oil prone kerogen type III and an LOM of 12 represents to the onset of over maturity for oil-prone kerogen typeII. (Passey et al.,1990). These LOM values were utilized in Passey et al., 1990 equation along with the standards of separated porosity logs curves from resistivity curve region. The resultant values provide the TOC in % of Sembar Formation.

The separation between overlade curves of the wells are show in figure 6.6.a, 6.6.b, and 6.6.c. respectively. For Raj East-01 this separation is measured at the depth range from 3281m to 3317 m in all three overlaid log curves. While in Raj-01 well, the Sember Shale TOC potential source depth range between 3360m to 3477m. This separation is the ΔlogR and computed at each depth interval. The determined values are presented in Annexure 1, & 2.

For Nereri-01 well, the calculated TOC values (by wt%). For Sembar Formation from DT log ranged from minimum 0.1026 to maximum 11.2133 with average of 3.83. Because of low LOM and TOC values, the potential for shale gas was quite negligible. TOC (by wt%) of Nereri-01well was minimum 0.1184 and maximum 4.34 with average of 1.85 which is calculated by utilizing the sonic and neutron logs along with resistivity curves.

Raj East-01, the TOC values of Sembar Formation is calculated from all the porosity logs. TOC (by wt%) calculated from DT log shows minimum value of 9.85 and maximum value of calculated 16.19. TOC values calculated from RHOB (by wt%) remained between minimum value of 1.56 to maximum 13.63 averaging 4.44. Similarly TOC from NPHI fluctuated between lowest values of 5.37 to highest value of 12.21 with average of 8.527. But due to less LOM index value, it is rate in Kerogen type III and is not feasible to develop economically.

At Raj-01 well, the calculated value of LOM is higher that is 10.5. The TOC value at Raj-01 well is calculated using DT log. The minimum value of TOC comes

out to be 2.78 and maximum value 9.6, with average of 6.75. It can be rated in Kerogen type II and has the potential of exploiting the shale gas.

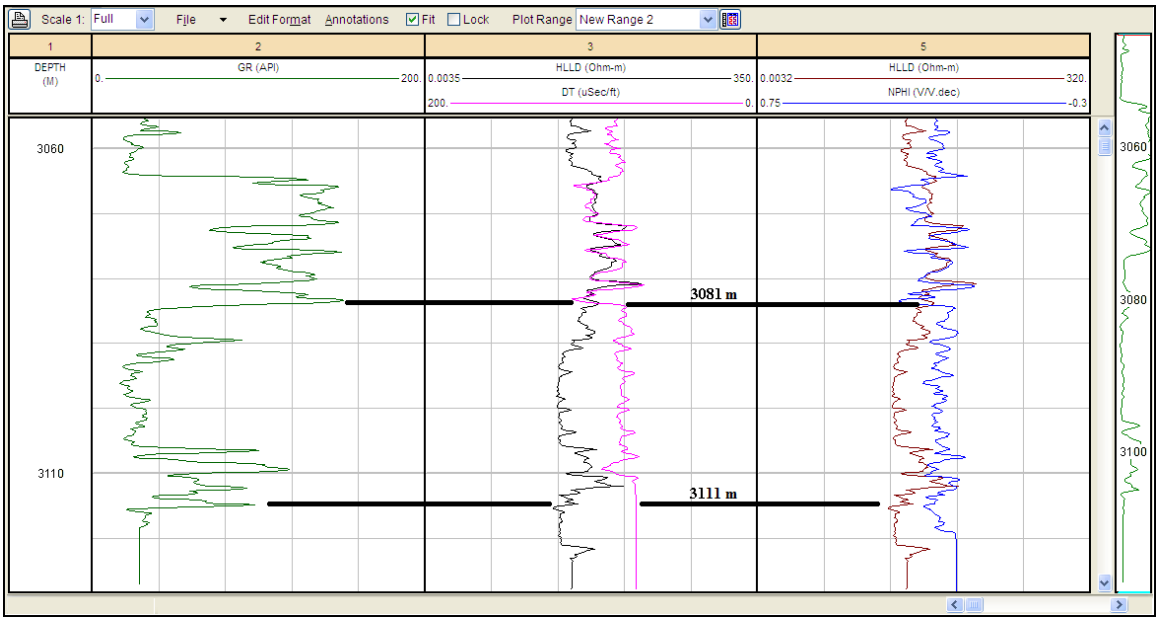

Figure 6.6.a GR and Resistivity verses porosity logs overlain. Resistivity values in Logarithmic scale for Nereri-01well

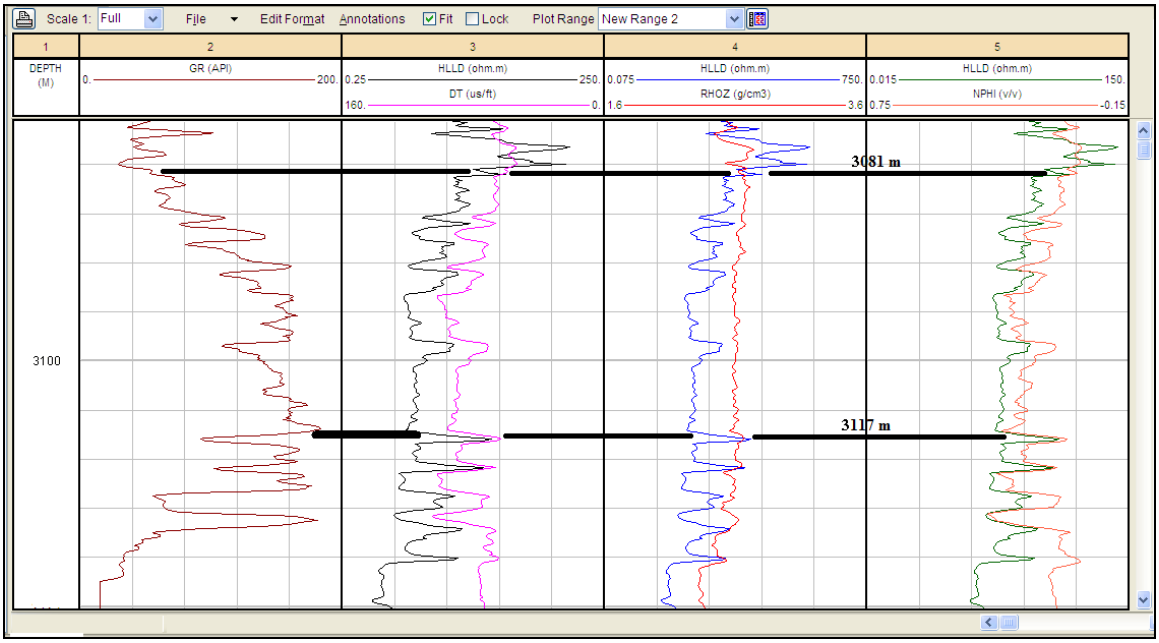

Figure 6.6.b GR and Resistivity verses porosity logs overlain. Resistivity values in Logarithmic scale for Raj East-01well

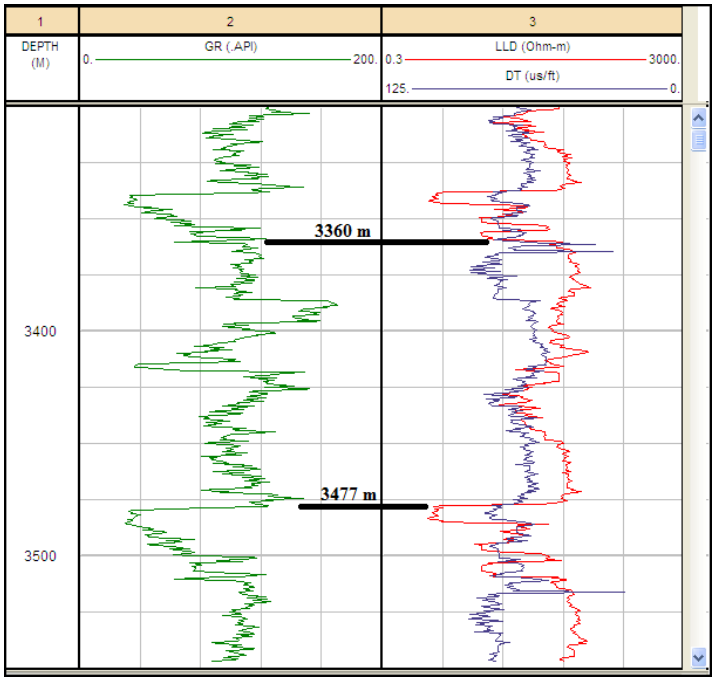

Figure 6.6.c GR and Resistivity verses porosity logs overlain. Resistivity values in Logarithmic scale for Raj-01well

Source rock measuring process was started by using the responses of the logs (gamma ray, density, resistivity neutron and sonic). With amplification of gamma ray (uranium associated with OM), sonic transit time, neutron porosity and resistivity with decrease of density specify enrichment of organic content. On the basis of calculated values for all three wells i.e., Nereri-01, Raj-01, Raj East-01, it is examined that source rock in Badin block has not sufficiently matured to produce hydrocarbon in Nereri-01 and Raj East-01 wells. Only Raj-01 well has potential for shale gas potential because of higher LOM calculated value which is 10.5 and average TOC is 6.75.

CHAPTER 7

ASSESSMENT OF SUBSIDENCE PHENOMENA

7.1 Introduction

Monitoring of earth surface subsidence has been carried out in the different parts of world but the best of authors' knowledge, this phenomenon has not been documented in Pakistan by utilizing remote sensing techniques. For this research, Southern Pakistan region was selected, which also includes Indus River delta. This area has not yet been explored. ENVISAT Interferometric Synthetic Aperture Radar (InSAR) dataset was utilized for quantification of subsidence rate. Computation of localized temporal and spatial subsidence pattern of time period from Jan, 2004 to Dec, 2009 with 20 acquisitions of ascending orbit had been performed. For this vertical surface displacement measurement, InSAR time-series analysis was utilized with Small Baseline Subset (SBAS) interferogram technique application. Total 53 interferograms were formed with relative temporal baseline position of +/- 300m with respect to master acquisition. Subsidence of average 4mm per year was measured in the Badin area with total subsidence of 24 mm over the period of six years. The deformation zone is due to intense extraction of subsurface hydrocarbon. Approximately, Badin block is the source of 90% of Hydrocarbon from Lower Indus Basin. This subsidence hazard may lead to subsurface structural collapse and structural trap displacement. This significant subsidence may also cause serious problems to the surface geomorphology, fresh water and saline water balance.

Land surface subsidence linked with ground fluid-level decline has been recognized as a potential problem for policy makers. Numerous basins in the world have been underwent subsidence because of anthropogenic changes, soil

consolidation, subsurface compaction, tectonic processes and exploitation of fluid resources. Therefore, precise knowledge and modeling of uplifting and subsidence of basin is essential to take significant measures related to planning, managing and monitoring measures. In this study, subsidence measurements are carried out over the Badin area. The monitoring area covers portion of delta of Indus River of Pakistan. For this activity, the Space-based measuring technique of InSAR is utilized because it is one of the important tools for measuring the surface deformation as well as surface subsidence (Ebmeier et al., 2012). It has capability to monitor surface deformation of a few millimeters over large the spatial coverage with the resolutions of a few tens of meters. It has unlocked new possibilities for remote monitoring of different areas of geology and geophysics (Madsen and Zebker, 1998; Smith et al., 2002).The objective of study was to detect possible subsidence rate, which is the sluggish poroelastic process and require the precision level of millimeters. To cover large area, the interferogram of InSAR data over the long period was used.

InSAR technique is widely accepted and permits the estimation of ground motion either vertical or horizontal along the sensor Line-of-Sight (LOS) direction. This formed the interferogram between the co-registered two SAR scenes acquired at different period over the same area (Massonnet and Feigl, 1998; Rosen et al., 2000). SBAS methodology of InSAR technique was applied for the time series analysis. This methodology stands on the combination of multiple small baseline interferograms for increasing the temporal sample rate (Berardino et al., 2002; Lanari et al., 2004; Lee et al., 2006). SBAS technique mostly works with normally multilook, filtered and unwrapped interferograms (Berardino et al., 2002). Total 20 images of ENVISAT Synthetic Aperture Radar (SAR) ascending orbit for the time period between Jan, 2005 and Dec, 2009 were processed. Total 53 interferograms were formed.

This technique measures precisely deformation associated with extraction of fluids, and inter and intra plate movement. The time series analysis used in this study, is an extensional form of the conventional InSAR technique, for mapping surface deformation (Beradino et al., 2002; Ferretti et al., 2000, 2001, 2011, Kampes., 2006). The trend of subsidence in area presents contemporary tectonic deformation in response to over pumping of hydrocarbon resources. Therefore, continuous

monitoring of ground subsidence is the key to assess the level of risk over the Badin area.

7.2 Methodology and Processing

The SBAS technique (Berardino et al., 2002; Werner et al., 2003) presents significant improvements in subsidence measurement while increase in detection of surface motions and enabling easier interpretation. This is obtained through the interferograms inversion with appropriate sequence. The ascending orbit data of 20 images acquired by the ENVISAT along T485 path was used in this subsidence analysis between the time periods of June, 2004 to Dec, 2009. ENVISAT data has resolution of 20-150 meters and provide opportunity of capturing wide image of Badin Area with swath width >100 Km. It has retake image cycle of 35 days. Therefore, ENVISAT provides opportunity for closer and precise cover of subsidence deformation. The European Space Agency is the platform, which provides ENVISAT data for user.

For SBAS processing, selected data pairs were distinguished by spatial and temporal baseline of 350m and five years as displayed in figure 7.1 and 7.2 respectively, this data set was utilized for this time series analysis, which have mitigated decorrelation phenomena. The generated output was in the form of 53 multilook interferograms after connection graphs generation with application of SBAS processing technique. The SRTM digital elevation model (DEM) with 90m (3 arc-second) resolution was used for the topographic corrections and geocoding (Rabus, et al., 2003). Before SBAS time series analysis, ground control points (GCPs) were marketed over stable areas and the unwrapped phases re-flattened to eliminate phase inclining due to orbit inaccuracies. The SBAS preprocessing, processing and co-registration sequence steps are presented in the figure 7.3. These steps were carried out with GMTSAR package (Sandwell, et al., 2011). The usefulness of the SBAS technique is highlighted in the quantitative analysis of displacement measurements. The resultant image was corrected with atmospheric correction and geocoded for shape file output. Time series analysis was applied at the end.

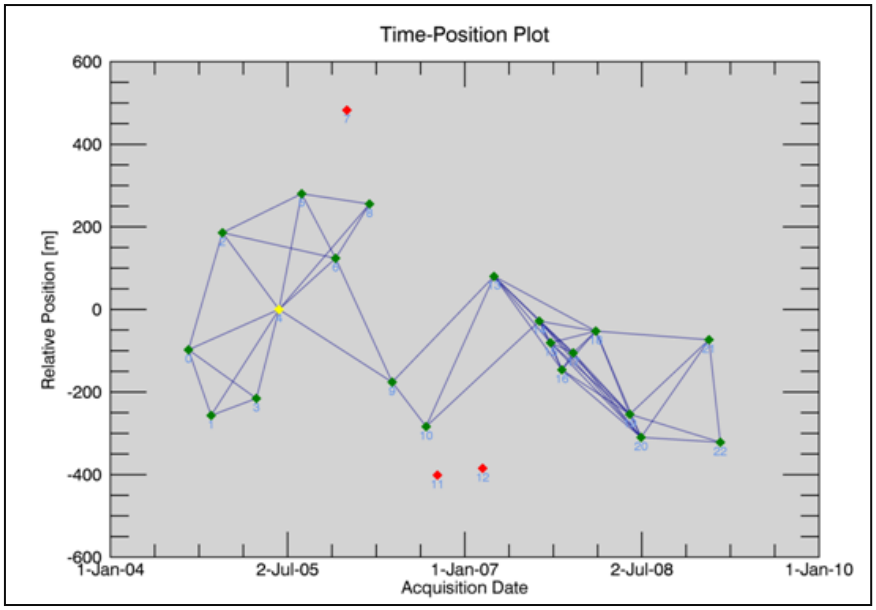

Figure 7.1 Time position plot for InSAR data pairs characterized by spatial and temporal baseline of 350m and 5 years respectively, utilizing SBAS technique.

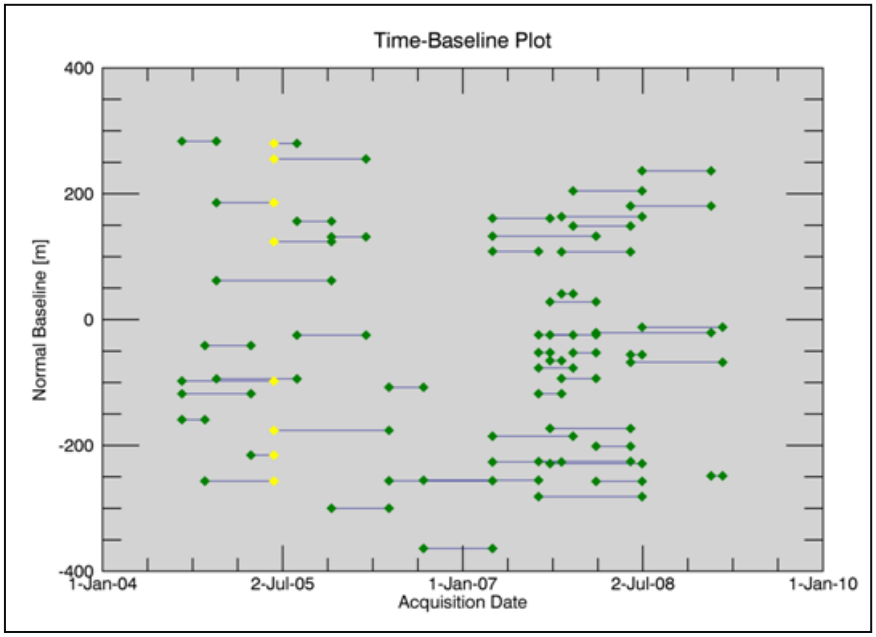

Figure 7.2 Time base line plot for InSAR data pairs characterized by spatial and temporal baseline of 400m and 5 years respectively, utilizing SBAS technique.

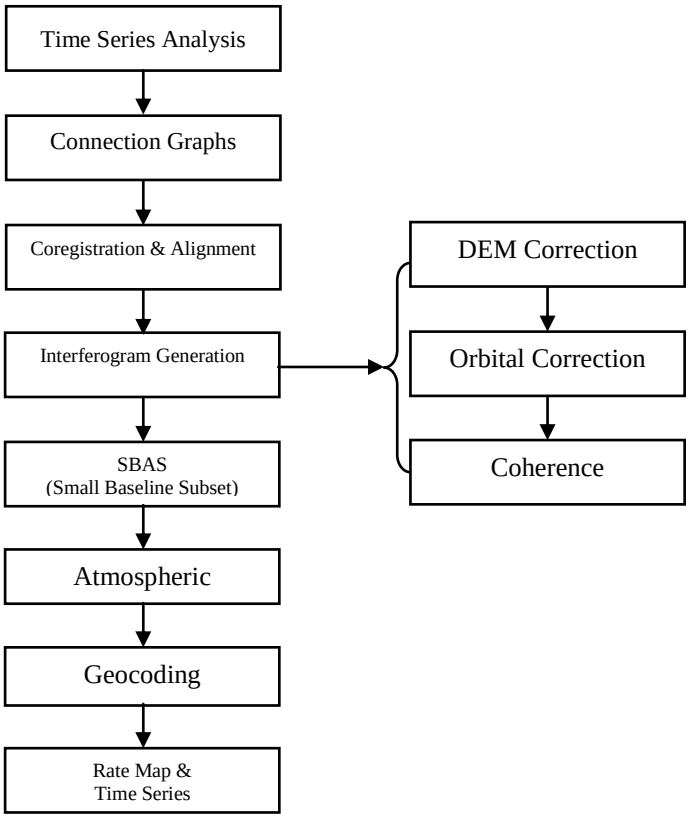

Figure 7.3 Flow chart for InSAR data processing using SBAS technique

7.3 Results and Discussions

The time series InSAR analysis results are shown in SBAS surface subsidence map, which was super imposed on the digital elevation model (DEM) of Badin Area. In this case the subsidence motion shows linear geographical pattern of deformation correspond to motion of region away from the satellite in vertical direction with the deduced consistent mean rate of 4mm per year along the cross section of study area. This subsidence movement is cross validated by EW trending profile graph shown in figure 7.5. The total calculated subsidence was 24 mm for time frame of six years. This subsidence rate map is shown in figure 7.6.

These measurements show continuous land surface subsidence with constant rate. The subsidence is expected to continue with the linear average trend of 4mm per year over the period of coming years. This linear behavior may be due to intense hydrological pumping which create pore gaps leading to subsidence of surface due to over burden pressure. Lacking of vegetation in the study area along with long dry climatic conditions may also be the other reasons.

Hydrocarbon extraction at a single location can influence a much large area of Badin district. It may be due to the compaction and contraction of reservoir. Collocation of this surface subsidence with the over pumping suggests that this attribute is result of this activity.

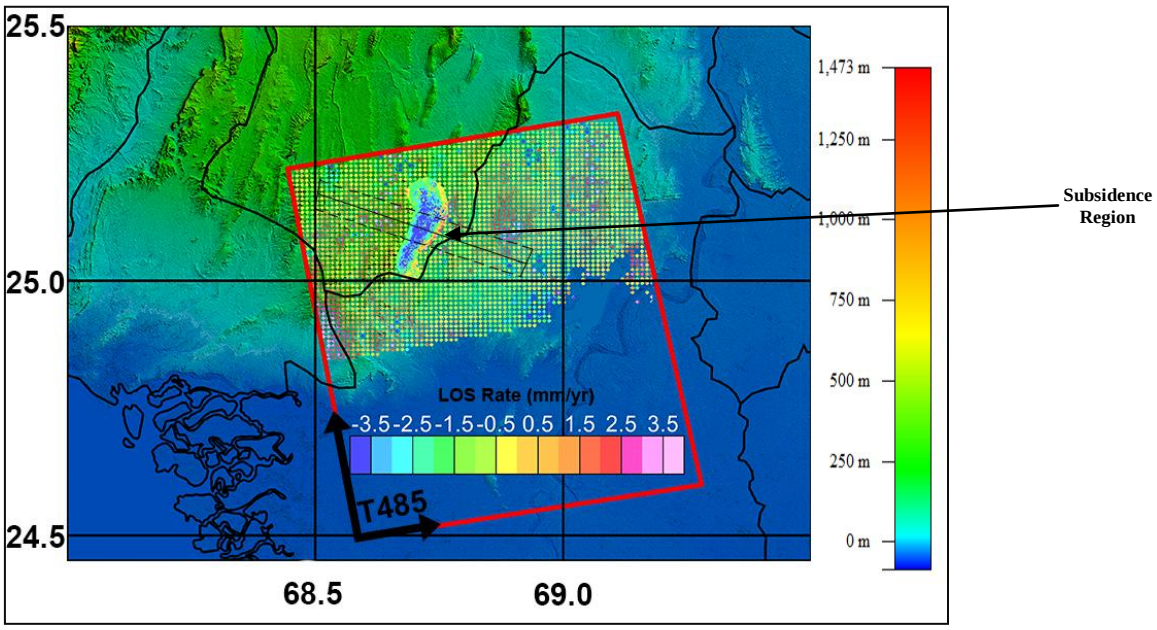

Figure 7.4 The InSAR subsidence model for AOI, Subsidence rate in the map with highlighted region of blue color

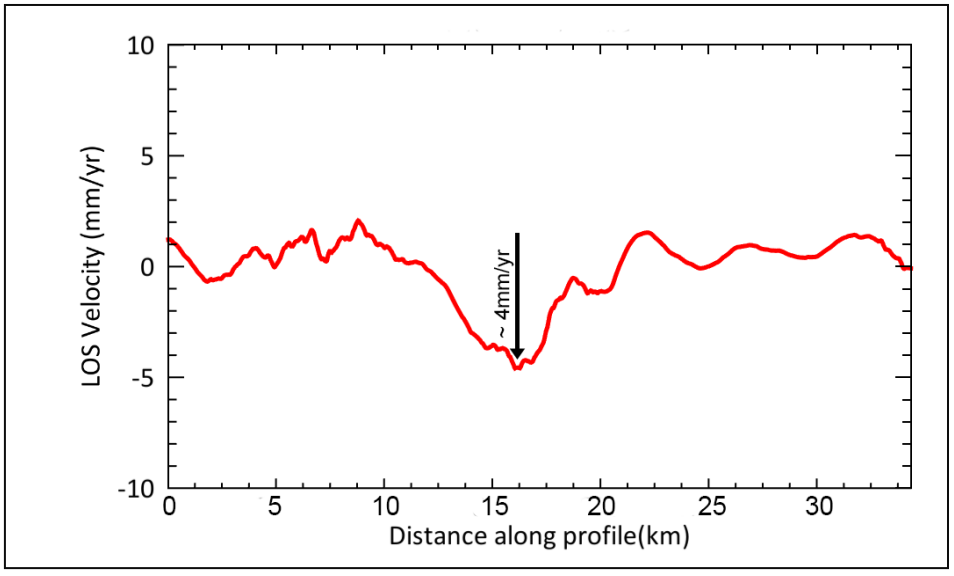

Figure 7.5 Subsidence profile depicting deformation rate along the cross-section of the AOI

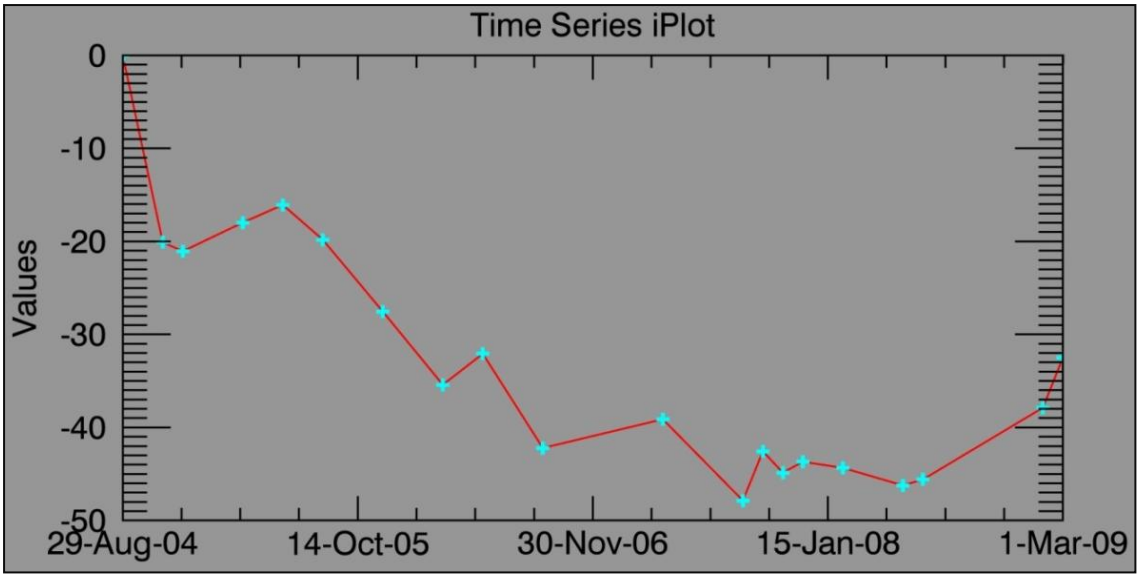

Figure 7.6 Average Time series plot of subsidence of AOI.

The process of land subsidence in outcome of heavy withdrawal of fluid has been monitored in different locations of the world like Arizona and California (USA), Bologna (Italy), Mexico, Ruhrgebiet (Germany), Tokyo (Japan) (Amelung et al., 1999; Galloway et al., 1998; Rahman, 1995; Strozzi et al., 2001, and 2003).

With the increase in hydrocarbon extraction, the average rate of subsidence also increases. The subsidence in the ground level is the result of imbalanced extraction activity, which caused the depletion of fluid and cause vacuum in subsurface. The intense pumping may effect the subsurface structure and reservoir extensions. This may also cause decline and imbalance in pore and hydrostatic head pressures. In conclusion, the hydrocarbon extraction must be controlled and should be managed properly to avoid further subsidence.

7.4 Recommendations

Ground subsidence is major issue related to man-made surface and subsurface activities. InSAR observations help to measure the whole subsidence area at broader scale by giving detailed resolution in space and time. In this high resolution investigation, the rate and pattern of surface subsidence was measured by time series modeling of InSAR data. The obtained results show the active and continuous subsidence with average of 4mm per year in Badin demarked in blue color in figure 7.4. Tectonically, the study area lies in extensional regime with horst and graben

structures, therefore, due to subsidence shallow faults along the structures result in local level subsurface rupture and fracturing. The Subsurface subsidence can be attributed to over pumping of hydrocarbons from Badin field for the time being. This phenomenon of subsidence is localized and restricted to surface layers, but if such activities remain continuous, it would ultimately result in fracturing, reservoirs pore pressure misbalancing, and collapse of structural traps as well in Badin field. This continuous subsidence process may also cause submerging of land to the sea, due to high tides. This will also reduce the drainage capacity.

With subsidence, slower morphological changes may occur in the Badin Area, which are slow changes and may require detailed regular monitoring and investigation. This evaluation will provide insight for policy makers to craft polices accordingly regarding water resource planning and subsidence mitigation measures. Therefore, continues monitoring is very important.

The Badin Area has no GPS instrument observations on ground in order to cross validate the InSAR results. Therefore, it is recommended to have GPS stations for ground base readings. It will help in easy measurements of subsidence rate.

It is clear from this technique, by using time series maps, the land surface deformation correlate with groundwater-level fluctuations in the Badin Area. Therefore, such monitoring will give qualitative and semi-quantitative information for hydrocarbons resource management, with more focus on the subsiding area from where fluid has been pumped with unsustainable rate, thus causing compaction. In the long run, this compaction will be irreversible resulting in forever loss of storage capacity of subsurface. Hydrocarbon dynamics in relation to gravity changes at localized level can be modeled with study of more time span coverage.

CONCLUSIONS

The selected study area was Badin block, which is integral part of the lower Indus basin. With utilization of Geophysical techniques, study area results conclude as following,

1) Sub-surface structure modeling from 2D seismic lines correlates with regional tectonic model of extensional regime with horst and graben structures.
2) From seismic attributes, shale characteristic of Sembar Formation on 2D seismic line is validated.
3) Petrophysics results for Sembar Formation also confirms its shale properties.
4) From Passey Method for TOC measurements, unconventional shale gas potential capacity of Sembar Formation is evaluated. Only Raj-01 has capacity for unconventional shale gas with LOM calculated value which is 10.5 and average TOC is 6.75.
5) Ground subsidence due to over extraction of sub-surface hydrocarbon is measured from ENVISAT InSAR data. The obtained results show the active and continuous subsidence average 4mm per year of study area.

REFERENCES

Adagunodo, T.A., Sunmonu, L.A. and Adabanija, M.A. (2017). Reservoir characterization and seal integrity of Jemir field in Niger Delta, Nigeria. *Journal of African Earth Sciences*, *129*, pp.779-791.

Ahmad, N., Fink, P., Sturrock, S., Mahmood, T. and Ibrahim, M. (2004). Sequence stratigraphy as predictive tool in lower goru fairway, lower and middle Indus platform, Pakistan. *PAPG, ATC*, pp.85-104.

Ahmed, S., Solangi, S.H., Brohi, I.A., Khokhar, Q.D. and LASHARI, R.A. (2014). Study of Stratigraphy and Structural Styles in the Subsurface of Southern Sindh Monocline, Pakistan: Using Seismic and Well Data. *Sindh University Research Journal-SURJ (Science Series)*, *46*(4).

Akinyokun, O.C., Enikanselu, P.A., Adeyemo, A.B. and Adesida, A. (2009). Well Log Interpretation Model for the Determination of Lithology and Fluid: 507–517

Alam, S.M., Wasimuddin, M. and Ahmad, S. (2002). Zaur structure: A complex trap in a poor seismic data area. In *Pakistan: Proceedings of PAPG-SPE Annual Technical Conference, Islamabad* (pp. 147-163).

Amelung, F., Galloway, D.L., Bell, J.W., Zebker, H.A. and Laczniak, R.J. (1999). Sensing the ups and downs of Las Vegas: InSAR reveals structural control of land subsidence and aquifer-system deformation. *Geology*, *27*(6), pp.483-486.

Archie, G. E. (1942). The Electrical Resistivity Log as an Aid in Determining Some Reservoir Characteristics. Society of Petroleum Engineers. doi:10.2118/942054-G

Avseth, P., Mukerji, T. and Mavko, G. (2010). *Quantitative seismic interpretation: Applying rock physics tools to reduce interpretation risk*. Cambridge university press.

Badley, M.E. (1985). Practical seismic interpretation.

Barnes, A.E. (1991). Instantaneous frequency and amplitude at the envelope peak of a constant-phase wavelet. *Geophysics*, *56*(7), pp.1058-1060.

Barnes A.E. (1993). Instantaneous spectral bandwidth and dominant frequency with applications to seismic reflection data, *Geophysics*, 58, pp.419–428.

Berardino, P., Fornaro, G., Lanari, R. and Sansosti, E. (2002). A new algorithm for surface deformation monitoring based on small baseline differential SAR interferograms. *IEEE Transactions on geoscience and remote sensing*, *40*(11), pp.2375-2383.

Bergbauer, S., Mukerji, T. and Hennings, P. (2003). Improving curvature analyses of deformed horizons using scale-dependent filtering techniques. *AAPG bulletin*, *87*(8), pp.1255-1272., http://dx.doi.org/10.1306/0319032001101

Blanford, W. T. (1876). On the geology of Sindh, Rec. Geol. Surv. India., v.9, pp. 8-27.

Bodine, J.H. (1984). Waveform analysis with seismic attributes. In *SEG Technical Program Expanded Abstracts 1984* (pp. 505-509). Society of Exploration Geophysicists.

Bannert, D. and Raza, H.A. (1992). A: The Segmentation of the Indian Plate Pakistan Journal. of Hydrocarbon Research

Brown, A.R. (2001). Understanding seismic attributes. *Geophysics*, *66*(1), pp.47-48.

Buiting, J.J.M. and Bacon, M. (1999). January. Seismic inversion as a vehicle for integration of geophysical, geological and petrophysical information for reservoir characterization: Some North Sea examples. In *Geological Society, London, Petroleum Geology Conference series* (Vol. 5, No. 1, pp. 1271-1280). Geological Society of London.

Bürgmann, R., Rosen, P.A. and Fielding, E.J. (2000). Synthetic aperture radar interferometry to measure Earth's surface topography and its deformation. *Annual review of earth and planetary sciences*, *28*(1), pp.169-209.

Burke, J.A., Campbell Jr, R.L. and Schmidt, A.W. (1969), January. The litho-porosity cross plot a method of determining rock characteristics for computation of log data. In *SPE Illinois Basin Regional Meeting*. Society of Petroleum Engineers.

Cadoret, T., Mavko, G. and Zinszner, B. (1998). Fluid distribution effect on sonic attenuation in partially saturated limestones. *Geophysics*, *63*(1), pp.154-160.

Casu, F., Manzo, M. and Lanari, R. (2006). A quantitative assessment of the SBAS algorithm performance for surface deformation retrieval from DInSAR

data. *Remote Sensing of Environment*, *102*(3-4), pp.195-210., doi:10.1016/j.rse.2006.01.023.

Chaussard, E., Amelung, F., Abidin, H. and Hong, S.H. (2013). Sinking cities in Indonesia: ALOS PALSAR detects rapid subsidence due to groundwater and gas extraction. *Remote Sensing of Environment*, *128*, pp.150-161.

Cheema, M.R. S.M. Raza and H. Ahmad. (1977). Cainozoic. In: Stratigraphy of Pakistan, (Shah, S.M.I., ed.), GSP, Memoir, (12): 56-98.

Chi, X.G. and Han, D.H. (2009). Lithology and fluid differentiation using a rock physics template. *The Leading Edge*, *28*(1), pp.60-65.

Chopra, S. and Marfurt, K.J. (2005). Seismic attributes—A historical perspective. *Geophysics*, *70*(5), pp.3SO-28SO.

Chopra, S. and Marfurt, K.J. (2008). Emerging and future trends in seismic attributes. *The Leading Edge*, *27*(3), pp.298-318.

Chopra, S., Sharma, R.K., Keay, J. and Marfurt, K.J. (2012). Shale gas reservoir characterization workflows. In *SEG Technical Program Expanded Abstracts 2012* (pp. 1-5). Society of Exploration Geophysicists.

Coffeen, J.A. (1986). Seismic exploration fundamentals.

Cohen, L. (1995). *Time-frequency analysis* (Vol. 778). Prentice hall.

Ding, W., Li, C., Li, C., Xu, C., Jiu, K., Zeng, W. and Wu, L. (2012). Fracture development in shale and its relationship to gas accumulation. *Geoscience Frontiers*, *3*(1), pp.97-105.

Dobrin, M.B. and Savit, C.H. (1988). Introduction to Geophysical Prospecting Singapore. *McGrawHill Book Co*.

Dong, Z., Holditch, S. and McVay, D. (2013). Resource evaluation for shale gas reservoirs. *SPE Economics & Management*, *5*(01), pp.5-16.

Ebmeier, S.K., Biggs, J., Mather, T.A., Elliott, J.R., Wadge, G. and Amelung, F. (2012). Measuring large topographic change with InSAR: Lava thicknesses, extrusion rate and subsidence rate at Santiaguito volcano, Guatemala. *Earth and Planetary Science Letters*, *335*, pp.216-225.

Ferretti, A., Fumagalli, A., Novali, F., Prati, C., Rocca, F. and Rucci, A. (2011). A new algorithm for processing interferometric data-stacks: SqueeSAR. *IEEE Transactions on Geoscience and Remote Sensing*, *49*(9), pp.3460-3470.

Ferretti, A., Prati, C. and Rocca, F. (2001). Permanent scatterers in SAR interferometry. *IEEE Transactions on geoscience and remote sensing*, *39*(1), pp.8-20.

Ferretti, A., Prati, C. and Rocca, F. (2000). Nonlinear subsidence rate estimation using permanent scatterers in differential SAR interferometry. *IEEE Transactions on geoscience and remote sensing*, *38*(5), pp.2202-2212.

Fertl, W.H. (1979). Gamma ray spectral data assists in complex formation evaluation. *The Log Analyst*, *20*(05).

Gadallah, M.R. and Fisher, R. (2008). *Exploration geophysics*. Springer Science & Business Media.

Galloway, D.L., Hudnut, K.W., Ingebritsen, S.E., Phillips, S.P., Peltzer, G., Rogez, F. and Rosen, P.A. (1998). Detection of aquifer system compaction and land subsidence using interferometric synthetic aperture radar, Antelope Valley, Mojave Desert, California. *Water Resources Research*, *34*(10), pp.2573-2585.

Gardner, G.H.F., Gardner, L.W. and Gregory, A.R. (1974). Formation velocity and density—The diagnostic basics for stratigraphic traps. *Geophysics*, *39*(6), pp.770-780.

Glorioso, J.C. and Rattia, A. (2012). March. Unconventional reservoirs: basic petrophysical concepts for shale gas. In *SPE/EAGE European Unconventional Resources Conference & Exhibition-From Potential to Production*.

Grieser, W.V. and Bray, J.M. (2007). January. Identification of production potential in unconventional reservoirs. In *Production and Operations Symposium*. Society of Petroleum Engineers.

Guéguen, Y. and Palciauskas, V. (1994). *Introduction to the Physics of Rocks*. Princeton University Press.

Hart, B.S. (2008). Channel detection in 3-D seismic data using sweetness. *AAPG bulletin*, *92*(6), pp.733-742.

Heslop, A. (1974). Gamma-ray log response of shaly sandstones. *The Log Analyst*, *15*(05).

Hood, A.C.C.M., Gutjahr, C.C.M. and Heacock, R.L. (1975). Organic metamorphism and the generation of petroleum. *AAPG bulletin*, *59*(6), pp.986-996.

Hooper, A., Zebker, H., Segall, P. and Kampes, B. (2004). A new method for measuring deformation on volcanoes and other natural terrains using InSAR persistent scatterers. *Geophysical research letters*, *31*(23).

Jones, A. (1960). Reconnaissance Geology of Part of West Pakistan: A Colombo Plan Cooperative Project: Toronto. *Canada, Government of Canada (Hunting Survey Corporation report)*.

Kampes, B.M. (2006). Radar Interferometry: Persistent Scatterer Technique; Springer: Dordrecht, The Netherlands, 211

Katahara, K. (2008). What is shale to a petrophysicist?. *The Leading Edge*, *27*(6), pp.738-741.

Kazmi, A.H. and Jan, M.Q. (1997). Geology and Tectonics of Pakistan Graphic Publishers. *ISBN: 9698375007, 9789698375003*, p.554.

Kearey, P., M. Brooks, M. and I. Hill. (2002). An Introduction to Geophysical Exploration. 3rd Edition. Blackwell Science: Oxford, UK. 281.

Kemal, A., Zaman, A.S.H. and Humayon, M. (1991). November. New directions and strategies for accelerating petroleum exploration and production in Pakistan. In *Proceedings, International Petroleum Seminar, 16-5*

Keys, R.G. and Foster, D.J. eds. (1998). *Comparison of seismic inversion methods on a single real data set*. Society of Exploration Geophysicists.

Khan, M.A. and Raza, H.A. (1986). The role of geothermal gradients in hydrocarbon exploration in Pakistan. *Journal of Petroleum Geology*, *9*(3), pp.245-258.

Kureshy, A.A. (1984). The foraminiferal stratigraphy of Laki formation (Early Eocene) of Pakistan. *Geologie Mediterraneenne*, *11*(1), pp.231-236.

Lakatos I, and Szabo JI. (2009). Role of conventional and unconventional hydrocarbons in 21st century: comparison of resources, reserves, recovery factors and technologies. Society of Petroleum Engineers 2009; SPE-121776-MS.

Lanari, R., Mora, O., Manunta, M., Mallorquí, J.J., Berardino, P. and Sansosti, E. (2004). A small-baseline approach for investigating deformations on full-resolution differential SAR interferograms. *IEEE Transactions on Geoscience and Remote Sensing*, *42*(7), pp.1377-1386.

Lancaster, S. and Whitcombe, D. (2000). Fast-track 'coloured'inversion. In *SEG Technical Program Expanded Abstracts 2000* (pp. 1572-1575). Society of Exploration Geophysicists, http://dx.doi.org/10.1190/1.1815711

Latimer, R.B., Davidson, R. and Van Riel, P. (2000). An interpreter's guide to understanding and working with seismic-derived acoustic impedance data. *The leading edge*, *19*(3), pp.242-256, doi:10.1190/1.1438580

Lee, K., Yoo, D.G., McMechan, G.A., Hwang, N. and Lee, G.H. (2013). A two-dimensional post-stack seismic inversion for acoustic impedance of gas and hydrate bearing deep-water sediments within the continental slope of the Ulleung Basin, east sea, Korea. *TAO: Terrestrial, Atmospheric and Oceanic Sciences*, *24*(3), p.295.

Lee, C.W., Lu, Z., Jung, H.S., Won, J.S. and Dzurisin, D. (2006). Surface deformation of Augustine Volcano, 1992–2005, from multiple-interferogram processing using a refined small baseline subset (SBAS) interferometric synthetic aperture radar (InSAR) approach. *The*, pp.453-465.

Leveaux, J. and Poupon, A. (1971). Evaluation of water saturation in shaly formations. *The Log Analyst*, *12*(04).

Li, Z (Zhongping)., Huang, F., He, X., Zhang, W. and He, Y. (2014). Shale-gas reservoir-prediction study in Daanzhai, Eastern Sichuan Basin. *The Leading Edge*, *33*(5), pp.526-534.

Lisle, R.J. (1994). Detection of zones of abnormal strains in structures using Gaussian curvature analysis. *AAPG bulletin*, *78*(12), pp.1811-1819.

Lopatin, N.V. (1971). Time and temperature as factors in coalification. *Izvestiya Akademii Nauk SSSR, Ser. Geol.*, *3*, pp.95-106.

Madsen, S. N., and H. A. Zebker. (1998). Imaging radar interferometry, in Principles and Applications of Imaging Radar, Manual of Remote Sensing, vol. 2, edited by F. M. Henderson and A. J. Lewis, Wiley, N.Y., pp. 359–380.

Massonnet, D. and Feigl, K.L. (1998). Radar interferometry and its application to changes in the Earth's surface. *Reviews of geophysics*, *36*(4), pp.441-500.

Mavko, G., Mukerji, T. and Dvorkin, J. (2009). *The rock physics handbook: Tools for seismic analysis of porous media*. Cambridge university press.

Memon, A.A., Siddiqui, I. and Memon, A.A. (1999). The role of cretaceous rifts on the occurrence of oil in Sindh, Monocline, Pakistan. In *SPE-PAPG, Annual Technical Conference* (pp. 65-74).

Meyer, B.L. and Nederlof, M.H. (1984). Identification of source rocks on wireline logs by density/resistivity and sonic transit time/resistivity crossplots. *AAPG Bulletin*, *68*(2), pp.121-129.

McQuillin, R., Bacon, M. and Barclay, W. (1984). An introduction to seismic interpretation-Reflection seismics in petroleum exploration.

Memon, A.D., Siddiqui, I. and Memon, A.A. (1999). The role of cretaceous rifts on the occurrence of oil in sindh monocline, Pakistan. In *PAPG ATC-(1999) Conference Proceedings* (pp. 65-74).

Mozzaffar, S. M., Wasimud din, M., Sayeed, S.M., (2002). Zaur Structure , A complex trap in a poor seismic data are. British Petroleum Pakistan, SPE. 2004, no. 2- 8.

Nabi, A., Liu, X., Gong, Z., Pervaiz, K., Ali, A. and Ashraf, S. (2018). Episodic Uplift along a Quaternary Fault, A Signature of Active Deformation in Frontal Part of Karachi Arc, Southern Pakistan. *International Journal of Economic and Environmental Geology*, pp.6-12.

Naeem, M., Jafri, M.K., Moustafa, S.S., AL-Arifi, N.S., Asim, S., Khan, F. and Ahmed, N. (2016). Seismic and well log driven structural and petrophysical analysis of the Lower Goru Formation in the Lower Indus Basin, Pakistan. *Geosciences Journal*, *20*(1), pp.57-75.

Oliveros, R.B. and Radovich, B.J. (1997). Image-processing display techniques applied to seismic instantaneous attributes over the Gorgon gas field, North West Shelf, Australia. In *SEG Technical Program Expanded Abstracts 1997* (pp. 2064-2067). Society of Exploration Geophysicists.

Omudu, M.L., Ebeniro, J.O. and Olotu, S. (2007). Optimizing quantitative interpretation for reservoir characterization: case study onshore Niger Delta.

In *A paper presented at the 31st annual SPE international technical conference and exhibition in Abuja, Nigeria*.

Passey, Q.R., Creaney, S., Kulla, J.B., Moretti, F.J. and Stroud, J.D. (1990). A practical model for organic richness from porosity and resistivity logs. *AAPG bulletin*, *74*(12), pp.1777-1794.

Passey, Q.R., Bohacs, K.M., Esch, W.L., Klimentidis, R. and Sinha, S. (2010). From oil-prone source rock to gas-producing shale reservoir—Geologic and petrophysical characterization of shale-gas reservoirs: Presented at the International Oil and Gas Conference and Exhibition. *Chinese Petroleum Society and Society of Petroleum Engineers (CPS/SPE), SPE-131350*.

Peters, K.E. and Cassa, M.R. (1994). Applied source rock geochemistry: Chapter 5: Part II. Essential elements.

Rabus, B., Eineder, M., Roth, A. and Bamler, R. (2003). The shuttle radar topography mission—a new class of digital elevation models acquired by spaceborne radar. *ISPRS journal of photogrammetry and remote sensing*, *57*(4), pp.241-262.

Raef, A.E. (2001). Seismic modeling and multi attribute analysis – guiding applications of 3D seismic attributes to reservoir characterization. University of Science and Technology, Cracow, Poland.

Rahman, M.H. (1995). Influence of geostructural aspects in land subsidence. *Land subsidence*, pp.83-91.

Raza, H.A., Ali, S.M. and Ahmed, R. (1990). Petroleum geology of Kirthar sub-basin and part of Kutch Basin. *Pakistan Journal of Hydrocarbon Research*, *2*(1), pp.27-73.

Rich, J. (2008). Expanding the applicability of curvature attributes through clarification of ambiguities in derivation and terminology. In *SEG Technical Program Expanded Abstracts 2008* (pp. 884-888). Society of Exploration Geophysicists.

Rickman, R., Mullen, M.J., Petre, J.E., Grieser, W.V. and Kundert, D. (2008). A practical use of shale petrophysics for stimulation design optimization: All shale plays are not clones of the Barnett Shale. In *SPE annual technical conference and exhibition*. Society of Petroleum Engineers. http://dx.doi.org/10.2118/115258.

Roberts, A. (2001). Curvature attributes and their application to 3D interpreted horizons. *First break*, *19*(2), pp.85-100. http://dx.doi.org/10.1046/j.0263-5046.2001.00142.x

Robison, C.R., Smith, M.A. and Royle, R.A. (1999). Organic facies in Cretaceous and Jurassic hydrocarbon source rocks, Southern Indus basin, Pakistan. *International journal of coal geology*, *39*(1-3), pp.205-225.

Rosen, P.A., Hensley, S., Joughin, I.R., Li, F.K., Madsen, S.N., Rodriguez, E. and Goldstein, R.M. (2000). Synthetic aperture radar interferometry. *Proceedings of the IEEE*, *88*(3), pp.333-382.

Russell, B.H. (1988). *Introduction to seismic inversion methods*. Society of Exploration Geophysicists.

Sandwell, D., Mellors, R., Tong, X., Wei, M. and Wessel, P. (2011). Gmtsar: An insar processing system based on generic mapping tools.

Shah, S. M. I., 2009. Stratigraphy of Pakistan: G. S. P. Memoir 22.

Sheikh, R.A., Saqi, M.I. and Jamil, M.A. (2002). Chiltan Limestone at Ziarat Nala Section and its Reservoir Potential in Western Sulaiman and Kirthar Range-An Elementary Appraisal. In *SPE–PAPG, Annual Tech. Conf. Proc., Islamabad* (pp. 80-105).

Sheriff, R.E. (2002). *Encyclopedic dictionary of applied geophysics*. Society of exploration geophysicists.

Sheriff, R.E. and Geldart, L.P. (1995). *Exploration seismology*. Cambridge university press.

Smith, M.L., Ollinger, S.V., Martin, M.E., Aber, J.D., Hallett, R.A. and Goodale, C.L. (2002). Direct estimation of aboveground forest productivity through hyperspectral remote sensing of canopy nitrogen. *Ecological applications*, *12*(5), pp.1286-1302.

Strecker, M.R., Carrapa, B., Hulley, G.E., Scoenbohm, L. and Sobel, E.R. (2004). Erosional control of Plateau evolution in the Central Andes. *Geological Society of America*, *36*(5).

Strozzi, T., Wegmuller, U., Werner, C.L., Wiesmann, A. and Spreckels, V. (2003). JERS SAR interferometry for land subsidence monitoring. *IEEE Transactions on Geoscience and Remote Sensing*, *41*(7), pp.1702-1708.

Strozzi, T., Wegmuller, U., Tosi, L., Bitelli, G. and Spreckels, V. (2001). Land subsidence monitoring with differential SAR interferometry. *Photogrammetric engineering and remote sensing*, *67*(11), pp.1261-1270.

Subrahmanyam, D. and Rao, P.H. (2008). Seismic attributes–A review. In *7th international conference & exposition on petroleum geophysics, Hyderabad* (pp. 398-404).

Taner, M.T. (2001). Seismic attributes: Canadian Society of Exploration Geophysicists Recorder.

Taner, M.T. and Sheriff, R.E. (1977). Application of amplitude, frequency, and other attributes to stratigraphic and hydrocarbon determination: Section 2. Application of seismic reflection configuration to stratigraphic interpretation.

Vernik, L. and Liu, X. (1997). Velocity anisotropy in shales: A petrophysical study. *Geophysics*, *62*(2), pp.521-532, doi:10.1190/1.1444162.

Wandrey, C.J., Law, B.E. and Shah, H.A. (2004). *Sembar Goru/Ghazij composite total petroleum system, Indus and Sulaiman-Kirthar geologic provinces, Pakistan and India* (No. 2208-C).

Werner, C., Wegmuller, U., Strozzi, T. and Wiesmann, A. (2003). July. Interferometric point target analysis for deformation mapping. In *IGARSS 2003. 2003 IEEE International Geoscience and Remote Sensing Symposium. Proceedings (IEEE Cat. No. 03CH37477)* (Vol. 7, pp. 4362-4364). IEEE.

White, R.E. (1991). Properties of instantaneous seismic attributes. *The Leading Edge*, *10*(7), pp.26-32.

Yilmaz, Ö. (2001). *Seismic data analysis: Processing, inversion, and interpretation of seismic data*. Society of exploration geophysicists.

Zaigham, N.A. and Mallick, K.A. (2000). Prospect of hydrocarbon associated with fossil-rift structures of the southern Indus basin, Pakistan. *AAPG bulletin*, *84*(11), pp.1833-1848.

Zehnder, A. T. (2012). Fracture Mechanics, Springer, DOI: 10.1007/978-94-007-2595-9.

ANNEXURE

Well name = Nereri-01

DT-base = 98.2 µs/ft or 322.194 µs/m

LLD-base = 0.665 ohm-m

NPHI-base = 0.246

LLD-base = 1.36 ohm-m

Table 6.4 Δlog R calculation for Nereri-01 Well (limited illustration due to space constraint)

DEPTH	GR	LLD	DT (us/ft)	NPHI	DT (us/m)	Dlog(DT)	TOC (%)(DT)
3081.549	31.3147	0.3408	85.8994	0.1875	281.84	0.16	1.44
3082.049	31.7648	0.3577	85.0388	0.1625	279.01	0.17	1.48
3082.549	49.3398	0.3189	84.8386	0.1619	278.36	0.11	1.00
3083.049	28.216	0.3252	81.4878	0.1862	267.36	0.05	0.48
3083.549	18.5206	0.285	83.3703	0.1907	273.54	0.04	0.31
3084.049	22.8603	0.3232	83.1543	0.1769	272.83	0.09	0.76
3086.924	21.2368	0.2785	82.3049	0.1879	270.04	0.00	0.03
3087.049	22.0536	0.2838	82.1751	0.1816	269.62	0.01	0.08
3087.549	23.271	0.2848	81.8025	0.1821	268.39	0.00	0.03
3088.049	19.8792	0.284	82.0234	0.1568	269.12	0.01	0.06
3088.549	31.4089	0.3702	77.6598	0.1663	254.80	0.03	0.31
3088.924	33.2318	0.3337	78.7988	0.1566	258.54	0.01	0.11
3089.049	30.2189	0.3133	80.282	0.1653	263.41	0.01	0.13
3089.549	23.1018	0.2947	83.4179	0.1905	273.69	0.05	0.45
3090.049	29.5504	0.3648	78.942	0.1857	259.01	0.05	0.48
3090.549	32.431	0.3286	81.4446	0.1693	267.22	0.06	0.52
3091.049	30.4626	0.3009	84.0964	0.1996	275.92	0.07	0.65
3091.549	32.8428	0.3066	83.8093	0.1922	274.98	0.08	0.67
3092.049	28.0478	0.3136	82.5584	0.1852	270.87	0.06	0.53
3092.549	28.9322	0.3267	81.804	0.1979	268.40	0.06	0.56
3093.049	25.8204	0.3278	82.43	0.1777	270.45	0.08	0.68
3093.549	26.0902	0.4583	74.9703	0.187	245.98	0.07	0.65
3094.049	24.5989	0.3656	77.6551	0.1464	254.79	0.03	0.26
3094.549	20.2649	0.309	82.0686	0.1644	269.27	0.04	0.39
3095.049	22.3376	0.3435	82.7693	0.1864	271.57	0.10	0.92

3095.549	23.7691	0.3484	83.2514	0.1758	273.15	0.12	1.06
3096.049	46.5884	0.6259	78.5885	0.1529	257.85	0.28	2.49
3096.549	99.8986	0.9485	80.5891	0.1612	264.41	0.50	4.44
3097.049	42.0295	0.6757	76.4554	0.183	250.85	0.27	2.40
3097.549	25.2299	1.0516	72.683	0.0938	238.47	0.39	3.43
3098.049	54.0852	0.9491	82.3328	0.1646	270.13	0.54	4.75
3098.549	93.0244	1.1041	88.1019	0.2021	289.06	0.72	6.35
3099.049	105.1305	1.1881	90.7677	0.201	297.81	0.80	7.10
3099.549	116.3169	1.0827	90.4596	0.1897	296.80	0.76	6.69
3100.049	64.2874	0.514	85.3435	0.2017	280.01	0.33	2.92
3100.549	50.8993	1.457	74.424	0.1876	244.19	0.56	4.99
3101.049	64.0816	1.5575	74.7996	0.1126	245.42	0.60	5.32
3101.549	61.4884	1.6167	73.9535	0.1468	242.64	0.60	5.31
3102.049	78.2558	3.3048	73.7533	0.1273	241.98	0.91	8.02
3102.549	78.279	0.596	73.6631	0.1335	241.69	0.16	1.43
3103.049	63.3755	0.7879	73.3847	0.1822	240.78	0.28	2.45
3103.549	36.7059	0.4332	73.2769	0.1999	240.42	0.02	0.13
3104.049	52.5484	0.5665	73.2812	0.1906	240.44	0.13	1.16
3104.549	68.7182	0.5195	73.2812	0.1902	240.44	0.09	0.83
3104.674	76.5315	0.6267	73.2812	0.1905	240.44	0.18	1.55
3111.174	28.3966	0.4367	73.2812	0.1232	240.44	0.02	0.17
3111.549	28.3966	1.0161	73.2812	0.1233	240.44	0.39	3.41
3111.799	28.3966	1.1339	73.2812	0.1233	240.44	0.43	3.83
3111.924	28.3966	0.9721	73.2812	0.1232	240.44	0.37	3.24

Well name = Raj-01

DT-base = 65 µs/ft or 213.265 µs/m

LLD-base = 0.234 ohm-m

Table 6.5 Δlog R calculation for Raj_01 Well (limited illustration due to space constraint)

DEPTH	GR	LLD	DT (us/ft)	DT (us/m)	Dlog(DT)	TOC (%)(DT)
3360	80.58	47.84	72.02	236.30	2.45	7.30
3361	105.99	70.67	51.66	169.50	2.21	6.59
3362	107.65	58.58	72.47	237.77	2.55	7.59
3363	114.32	61.12	72.29	237.18	2.56	7.63
3364	119.1	98.68	70.83	232.39	2.74	8.17
3365	112.06	106.72	77.43	254.05	2.91	8.66
3366	116.95	85.45	84.61	277.61	2.95	8.80
3367	123.2	84.39	80.68	264.71	2.87	8.55
3368	113.27	97.21	77.6	254.61	2.87	8.55
3369	111.69	93.59	85.28	279.80	3.01	8.96
3370	100.45	120.57	74.42	244.17	2.90	8.64
3371	106.2	110.67	83.07	272.55	3.04	9.04
3372	105.29	119.2	81.33	266.84	3.03	9.03
3373	105.49	122.86	81.74	268.19	3.05	9.10
3374	107.75	124.5	87.51	287.12	3.18	9.46
3375	118.92	104.08	80.39	263.76	2.96	8.80
3376	116.38	92.55	80.95	265.60	2.92	8.69
3377	116.56	100.3	75.1	246.40	2.83	8.44
3378	105.58	113.96	76.14	249.82	2.91	8.67
3379	101.34	131.94	76.53	251.09	2.98	8.88
3380	103.65	155.86	79.24	259.99	3.11	9.26
3381	104.55	92.34	76.09	249.65	2.82	8.39
3382	112.69	89.57	77.13	253.06	2.83	8.42
3383	106.59	105.29	76.7	251.65	2.89	8.60
3384	110.03	104.11	78.78	258.48	2.92	8.71
3385	98.21	72.91	79.15	259.69	2.78	8.27
3386	91.5	77.23	77.31	253.65	2.76	8.23
3387	164.43	67.06	62.83	206.15	2.41	7.19
3388	170.24	62.32	64.3	210.97	2.41	7.18

3389	165.81	73.74	64.55	211.79	2.49	7.41
3390	150.06	53.28	66.24	217.33	2.38	7.09
3391	142.07	70.5	63.08	206.97	2.44	7.27
3392	157.65	69.39	60.26	197.71	2.38	7.08
3393	142.77	62.67	64	209.98	2.41	7.17
3394	141.04	66	62.94	206.51	2.41	7.17
3395	151.21	60.41	66.01	216.58	2.43	7.24
3396	145.42	60.81	59.11	193.94	2.30	6.84
3397	97	64.09	63.75	209.16	2.41	7.19
3398	93.51	51.49	63.98	209.92	2.32	6.92
3399	112.51	54.21	62.48	205.00	2.31	6.89
3400	122.58	52.76	61.71	202.47	2.29	6.81
3401	127.6	69.75	62.11	203.78	2.42	7.20
3402	117.81	89.24	61.39	201.42	2.51	7.47
3403	108.14	84.48	62.31	204.44	2.50	7.46
3404	100.02	54.58	61.94	203.23	2.31	6.87
3405	93.08	51.75	60.59	198.80	2.26	6.72
3406	82.82	75.63	59.88	196.47	2.41	7.17
3407	90.96	75.14	60.09	197.16	2.41	7.17
3408	89.48	102.76	58.26	191.15	2.51	7.47
3409	79.61	154.15	56.62	185.77	2.65	7.90
3410	66.6	126.72	58.82	192.99	2.61	7.77
3411	70.18	94.13	56.16	184.26	2.43	7.23
3412	93.64	60.43	57.2	187.67	2.26	6.72
3413	97.22	42.38	57.08	187.28	2.10	6.25
3414	62.32	52.62	57.48	188.59	2.20	6.56
3415	37.02	62.42	59.73	195.97	2.32	6.91
3416	39.46	49.74	58.76	192.79	2.20	6.56
3417	55.13	18.6	64.79	212.58	1.90	5.65
3418	142.73	67.06	63.4	208.02	2.43	7.22
3419	125.74	66.04	60.72	199.22	2.36	7.04
3420	100.52	65.78	64.19	210.61	2.43	7.25
3421	122.56	65.96	68.39	224.39	2.52	7.50
3422	130.55	65.78	69.14	226.85	2.53	7.54
3423	120.4	43	67.72	222.19	2.32	6.91
3424	134.9	22.24	66.26	217.40	2.00	5.97
3425	132.16	35.76	63.25	207.52	2.15	6.40
3426	143.5	24.44	70.77	232.20	2.13	6.36
3427	114.21	14.2	72.65	238.36	1.94	5.77
3428	126.64	10.93	76.53	251.09	1.90	5.66
3429	116.23	21.12	70.37	230.88	2.06	6.14
3430	109.5	24.37	79.54	260.97	2.31	6.88

3431	119.92	27	74.52	244.50	2.25	6.71
3432	103.66	12.62	80.79	265.07	2.05	6.10
3433	95.71	10.23	78.92	258.94	1.92	5.72
3434	101.51	33.25	66	216.55	2.17	6.47
3435	113.03	21.34	72.19	236.86	2.10	6.27
3436	93.92	17.33	68.83	225.83	1.95	5.80
3437	97.79	30.11	71.27	233.84	2.23	6.66
3438	81.34	33.43	69.14	226.85	2.24	6.66
3439	82.25	20.63	65.94	216.35	1.96	5.85
3440	93.77	23.13	71.62	234.99	2.13	6.34
3441	89.16	23.58	69.91	229.37	2.10	6.26
3442	82.94	28.05	63.16	207.23	2.04	6.08
3443	109.56	26.66	68.1	223.44	2.12	6.31
3444	113.55	39.61	71.73	235.35	2.36	7.04
3445	114.52	43.25	65.53	215.00	2.28	6.78
3446	105	43.91	65.48	214.84	2.28	6.80
3447	98.78	41.5	68.77	225.63	2.32	6.92
3448	94.86	42.18	62.61	205.42	2.21	6.58
3449	123.33	70.21	61.65	202.27	2.41	7.18
3450	88.87	77.27	64.9	212.94	2.52	7.50
3451	108.14	64.9	65.75	215.73	2.46	7.32
3452	97.85	66.93	67.57	221.70	2.51	7.47
3453	100.95	91.47	62.9	206.37	2.55	7.59
3454	114.63	79.02	64.27	210.87	2.51	7.49
3455	103.12	81.75	66.33	217.63	2.57	7.65
3456	88.9	76.7	65.74	215.69	2.53	7.54
3457	87.72	74.7	65.37	214.48	2.51	7.48
3458	95.75	94.69	61.81	202.80	2.54	7.57
3459	83.95	92.46	60.82	199.55	2.51	7.48
3460	111.42	83.45	64.14	210.44	2.54	7.55
3461	119.04	84.1	64.08	210.25	2.54	7.56
3462	95.83	88.23	64.41	211.33	2.56	7.64
3463	106.58	71.5	61.56	201.98	2.42	7.20
3464	111.37	84.91	63.94	209.79	2.54	7.56
3465	106.88	84.19	65.34	214.38	2.56	7.63
3466	111.76	89.57	64.7	212.28	2.58	7.67
3467	127.48	85.5	64.28	210.90	2.55	7.59
3468	112.82	84.73	62.42	204.80	2.51	7.47
3469	105.76	85.15	64.6	211.95	2.55	7.60
3470	85.5	103.82	61.27	201.03	2.57	7.66
3471	95.47	130.57	62.03	203.52	2.69	8.00
3472	98.71	96.45	67.21	220.52	2.66	7.92
3473	130.27	73.22	67.78	222.39	2.55	7.60
3474	133.45	70.61	67.76	222.32	2.53	7.55
3475	119.53	77.31	69.68	228.62	2.61	7.78

3476	108.91	64.22	67.38	221.07	2.49	7.40